# EXPLORING EXTRACELLULAR VESICLES-BASED THERAPEUTICS FOR AMYOTROPHIC LATERAL SCLEROSIS

by

#### JINGHUI GAO

(Under the Direction of Yao Yao)

#### **ABSTRACT**

Amyotrophic lateral sclerosis (ALS) is a devastating neuromuscular disease characterized by motor neuron degeneration and muscle atrophy, with no effective treatments. Given its complex pathology, my research explores extracellular vesicle (EV)based therapies to target multiple disease mechanisms in both central and peripheral systems. While skeletal muscle was traditionally considered a secondary consequence of motor neuron loss, emerging evidence suggests it actively contributes to ALS progression via retrograde signaling to the central nervous system. This dissertation establishes skeletal muscle as a viable therapeutic target and investigates EVs from regenerating skeletal muscle and neural progenitor cells (NPCs) as a novel intervention. In the first study, I examined NPC-derived EVs (NPC-EVs) as a neuroprotective therapy, demonstrating their ability to enhance motor neuron survival, reduce oxidative stress, and suppress inflammatory NF-kB signaling in ALS models. These findings highlight NPC-EVs as a safer, cell-free alternative to stem cell transplantation. The second study focused on EVs from regenerating skeletal muscle 14 days post-injury (CTXD14SkM-EVs) as a muscle-targeted ALS therapy. Results showed CTXD14SkM-EVs enhanced

muscle regeneration, shifted macrophage polarization toward an anti-inflammatory (M2) phenotype, and suppressed NF-kB signaling, preserving muscle mass. Recognizing skeletal muscle's active role in ALS progression, my third study examined the therapeutic potential of EVs from day 3 post-injury regenerating skeletal muscle (CTXSkM-EVs), fibro/adipogenic progenitors (CTXFAP-EVs), and NPC-EVs to maximize therapeutic benefits. Skeletal muscle actively secretes EVs during early regeneration to initiate muscle repair, making them promising candidates. CTXSkM-EVs, representing total muscle-derived EVs, and CTXFAP-EVs, derived from mesenchymal FAPs, promoted myogenesis in atrophic muscle cells, suggesting potential benefits for other musclewasting diseases. Additionally, these EVs improved ALS-like motor neuron viability and mitochondrial function, suggesting a role in reducing oxidative stress and preserving cellular energy homeostasis. Beyond individual applications, we introduced a novel mixed EV therapy, combining NPC-EVs with CTXSkM-EVs or CTXFAP-EVs to simultaneously target ALS pathology. In vivo, this therapy mitigated muscle atrophy, promoted regeneration, and suppressed NF-kB signaling in ALS-affected muscle and spinal cord. These findings provide the first evidence that regenerative muscle-derived EVs, particularly when combined with NPC-EVs, offer a promising dual-targeted ALS therapy.

INDEX WORDS: Regenerating Skeletal Muscle, Neural Progenitor Cells, Extracellular Vesicles, Amyotrophic Lateral Sclerosis

# EXPLORING EXTRACELLULAR VESICLES-BASED THERAPEUTICS FOR AMYOTROPHIC LATERAL SCLEROSIS

by

#### JINGHUI GAO

B.S., University of Camerino, Italy, 2014

M.S., University of Southern California, U.S., 2017

A Dissertation Submitted to the Graduate Faculty of The University of Georgia in Partial Fulfillment of the Requirements for the Degree

DOCTOR OF PHILOSOPHY

ATHENS, GEORGIA 2025

© 2025

Jinghui Gao

All Rights Reserved

# EXPLORING EXTRACELLULAR VESICLES-BASED THERAPEUTICS FOR AMYOTROPHIC LATERAL SCLEROSIS

by

JINGHUI GAO

Major Professor: Yao Yao Committee: Steven S

Steven Stice Nadja Zeltner Jarrod Call Ross Marklein

Electronic Version Approved:

Ron Walcott Vice Provost for Graduate Education and Dean of the Graduate School The University of Georgia May 2025

## **DEDICATION**

To my grandparents, parents, and my husband, Tienan Li—your unwavering love, support, and belief in me have been my greatest strength throughout this journey. This achievement is as much yours as it is mine.

#### **ACKNOWLEDGEMENTS**

I would like to express my gratitude to my mentor, Dr. Yao Yao, for giving me the opportunity to join her team and contribute to such meaningful research projects. Her support and guidance have been instrumental in shaping my scientific journey. Yao always empowers us to explore our own interests and research directions. She is always willing to provide support for our research endeavours, encouraging curiosity, critical thinking, and innovation. Her generosity in sharing her experiences and insights has been invaluable, not only in refining my scientific thinking but also in cultivating essential qualities that extend beyond research. I am grateful for her mentorship, which has profoundly facilitated my growth over the past four years. Furthermore, I would like to sincerely thank my committee members, Dr. Steven Stice, Dr. Nadja Zeltner, Dr. Jarrod Call, and Dr. Ross Marklein for their invaluable time, insights and support throughout this journey. Their guidance and expertise have been instrumental in shaping my research and scientific thinking. I deeply appreciate their thoughtful feedback, constructive discussions, and encouragement, which have challenged me to grow both intellectually and professionally. I am grateful for their dedication and for being part of my Ph.D. journey.

I would also like to extend my thank to my colleague, Yaochao Zheng, for his technical support throughout this journey. His assistance is very valuable in helping me overcome various challenges. A special thank you to my undergraduate student, Aria Sikal, who has worked with me for nearly three years. Her dedication, responsibility, and

consistent contributions have been instrumental in supporting my projects. I feel incredibly fortune to have had such as dependable and committed undergraduate student by my side throughout this journey. Furthermore, I want to thank Rachel Hankin for her kindness and thoughtfulness during our collaboration. Her meticulous approach to developing experiments has left a lasting impression on me, and I truly appreciate her thoroughness and dedication. I would also like to thank Elijah Sterling, whose willingness to help and easygoing nature have made working together an enjoyable experience. His support and positive attitude have been greatly appreciated.

Outside of our lab, I deeply grateful for the help and support from the members of the Stice lab, Call lab, Marklein lab, Zeltner lab, Karumbaiah lab, Liu lab, West lab, Mortensen lab and Easley lab throughout my Ph.D. journey. The collaborative and supportive atmosphere among graduate students has been truly inspiring, and I feel fortunate to have been part of such a generous research community. I sincerely appreciate the kindness, willingness to help, and insightful discussions that have contributed to my research and personal growth. Thank you all for fostering an environment where learning, collaboration, and success are shared.

Lastly, I would like to thank the staff of the Animal and Dairy Science Department for their consistent assistance and support throughout my Ph.D. journey. Their kindness, patience, and willingness to help have contributed to creating an efficient and well-organized environment. Thank you all for your continued support in ensuring our success.

## TABLE OF CONTENTS

	Page
ACKNOWLEDGEMENTS	v
LIST OF TABLES	x
LIST OF FIGURES	xi
CHAPTER	
1 INTRODUCTION AND LITERA	ATURE REVIEW1
1.1 Introduction	2
1.2 Muscle Satellite Cells	5
1.3 Inflammation	9
1.4 Neuromuscular Junction	າ 13
1.5 Mitochondria	
1.6 Conclusions	
2 HUMAN NEURAL PROGENIT	OR CELL-DERIVED EXTRACELLULAR
VESICLES PROTECT AGAIN	ST AMYOTROPHIC LATERAL SCLEROSIS'S
DISEASE PATHOLOGIES	19
2.1 Introduction	20
2.2 Results	23
2.3 Discussion	28
2.4 Methods	

3	EXTRACELLULAR VESICLES FROM REGENERATING SKELETAL	
	MUSCLE MITIGATE MUSCLE ATROPHY IN AN AMYOTROPHIC LATE	RAL
	SCLEROSIS MOUSE MODEL	37
	3.1 Introduction	38
	3.2 Results	41
	3.3 Discussion	52
	3.4 Materials and Methods	55
4	SYNERGIZED THERAPEUTIC EFFICACIES OF EXTRACELLULAR	
	VESICLES FROM REGENERATING SKELETAL MUSCLE AND NEURA	L
	STEM CELLS IN AN ALS MOUSE MODEL	62
	4.1 Introduction	64
	4.2 Results	66
	4.3 Discussion	84
	4.4 Materials and Methods	86
5	PROTOCOL FOR THE ISOLATION OF MOUSE FIBRO/ADIPOGENIC	
	PROGENITORS USING MAGNETIC ACTIVATED CELL SORTING	94
	5.1 Background	96
	5.2 Preparation of muscle digestion media, FAPs growth media and	
	gelatin-coated plate	96
	5.3 Step-by-Step method details	97
	5.4 Key resources table	. 109
6	SUMMARY AND CONCLUSIONS	. 112
	6.1 NPC-FV Mitigate the ALS's Pathological Phenotynes	112

REFERENC	ES	. 120
	Muscle Atrophy	. 117
	FAP-Derived EVs, and NSC-Derived EVs in Mitigating ALS-Associated	b
	6.3 Synergistic Effects of Regenerating Skeletal Muscle-Derived EVs,	
	Stage Mitigate ALS-Associated Muscle Atrophy	. 114
	6.2 Regenerating Skeletal Muscle-derived EVs at the Anti-Inflammator	У

## LIST OF TABLES

	Page
Table 1: Key Resource	109
Table 2: Wash Solution (WS)	110
Table 3: Digest Mix Solutions	111
Table 4: Growth Media (GM)	111

## LIST OF FIGURES

Page		
Figure 1.1: Dynamic interplay of skeletal muscle and nerves in response to therapeutics		
targeting skeletal muscles in ALS		
Figure 2.1: NPC-EVs treatment modulates the inflammatory NF-κB pathway		
Figure 3.1: Isolation and characterization of CTXD14SkM-EVs 42		
Figure 3.2: CTXD14SkM-EVs Promote Myoblast Differentiation in a cellular muscle		
atrophy model induced by proinflammatory cytokine TNF-α		
Figure 3.3: CTXD14SkM-EVs Alleviate Muscle Atrophy in SOD1 <sup>G93A</sup> Mice		
Figure 3.4: CTXD14SkM-EVs Promote Muscle Regeneration in SOD1 <sup>G93A</sup> Mice 47		
Figure 3.5: CTXD14SkM-EVs Enhance M2 Macrophage Polarization in ALS-affected		
Skeletal Muscle		
Figure 3.6: CTXD14SkM-EVs Suppress NF-κB Pathway Activation in the Skeletal		
Muscle of SOD1 <sup>G93A</sup> Mice51		
Supplement 3.1: Transcription levels of M2 macrophage polarization-associated		
markers		
Figure 4.1: Isolation and Characterization of CTXSkM-EVs and CTXFAP-EVs 68		
Figure 4.2: CTXSkM-EVs and CTXFAP-EVs Enhance C2C12 Differentiation in the		
Presence of Pro-Inflammatory Cytokine TNF-α		
Figure 4.3: CTXSkM-EVs and CTXFAP-EVs Alleviate Mitochondrial Dysfunction in an		
ALS-like Motor Neuron In Vitro Model		

Figure 4.4: CTXSkM-EVs and CTXFAP-EVs Mitigate Muscle Atrophy in SOD1 <sup>G93A</sup> Mice
76
Figure 4.5: CTXSkM-EVs and CTXFAP-EVs Downregulate the Activated NF-κB
Pathway in Muscle80
Figure 4.6: Effects of EV Treatment on the Activated NF-κB Pathway in the Spinal Cord
82
Figure 5.1: Extraction of hindlimb skeletal muscles from adult mice. Mouse skeletal
muscle dissection98
Figure 5.2: Mechanical and enzymatic dissociation of skeletal muscle to release single
cells
Figure 5.3: MACS isolation of FAPs
Figure 5.4: Immunofluorescent staining of MACS-sorted FAPs 106

# CHAPTER 1 INTRODUCTION AND LITERATURE REVIEW<sup>1</sup>

<sup>&</sup>lt;sup>1</sup> Gao, J., Sterling, E., Hankin, R., Sikal, A., Yao, Y. Therapeutics Targeting Skeletal Muscle in Amyotrophic Lateral Sclerosis. 2024. *Biomolecules*. Reprinted here with permission of the publisher.

#### **Abstract**

Amyotrophic lateral sclerosis (ALS) is a complex neuromuscular disease characterized by progressive motor neuron degeneration, neuromuscular junction dismantling, and muscle wasting. The pathological and therapeutic studies of ALS have long been neurocentric. However, recent insights have highlighted the significance of peripheral tissue, particularly skeletal muscle, in disease pathology and treatment. This is evidenced by restricted ALS-like muscle atrophy, which can retrogradely induce neuromuscular junction and motor neuron degeneration. Moreover, therapeutics targeting skeletal muscles can effectively decelerate disease progression by modulating muscle satellite cells for muscle repair, suppressing inflammation, and promoting the recovery or regeneration of the neuromuscular junction. This review summarizes and discusses therapeutic strategies targeting skeletal muscles for ALS treatment. It aims to provide a comprehensive reference for the development of novel therapeutics targeting skeletal muscles, potentially ameliorating the progression of ALS.

#### 1.1 Introduction

Amyotrophic lateral sclerosis (ALS) is a devastating neuromuscular disorder characterized by progressive degeneration of motor neurons (MNs) and severe muscle atrophy. Most ALS cases are sporadic, and a minority of cases (5–10%) are familial [1]. Over 30 genes have been identified as being linked to ALS [2], with the most prevalent mutations found in *SOD1* (Cu/Zn superoxide dismutase 1), *C9ORF72* (chromosome 9 open reading frame 72), *TARDBP* (TAR DNA-binding protein 43; *TDP-43*), and *FUS* (fused in sarcoma) [3]. ALS patients endure progressive muscle wasting, which gradually impairs their ability to move, speak, eat, and breathe. Typically, patients succumb to

respiratory failure within 2 to 5 years after diagnosis [4,5]. No efficacious therapies have been developed, mainly due to an elusive pathogenic mechanism underlying this multisystemic disorder. Multiple cell types, such as motor neurons and glial cells in the central nervous system (CNS) and Schwann cells and skeletal muscle in peripheral tissues, collectively orchestrate the onset and progression of the disease [6–9]. Moreover, defects in cellular structure, physiology, and metabolism interact and reinforce each other, making it difficult to pinpoint a primary pathogenic mechanism and develop effective therapeutics [6–9]. Current FDA-approved medications, such as the glutamate antagonist Riluzole, the free radical scavenger Edaravone, or the endoplasmic reticulum stress and mitochondrial dysfunction mitigator Relyvrio, only extend patients' lives for a few months, with no capacity to reverse nerve damage or muscle atrophy [10–12].

In ALS, muscle atrophy has traditionally been viewed as a secondary consequence of MN degeneration and denervation [13]. However, distinct pathologies within the skeletal muscle, such as fiber necrosis, inflammation, and myopathic features, have been documented in ALS muscles [14–16], suggesting that skeletal muscle atrophy in ALS may not solely result from denervation. Furthermore, studies of ALS patients have indicated that skeletal muscle plays an early and active role in the development of ALS [17,18]. Defects in skeletal muscle and the neuromuscular junction (NMJ) can occur before MN degeneration and the onset of clinical symptoms in ALS animal models and patients [19,20,21]. Skeletal muscle-restricted expression of an ALS-associated mutated protein (a G93A mutant form of human superoxide dismutase type 1 (SOD1)) causes motor neuron degeneration and a fatal ALS-like syndrome in transgenic mice [22,23,24,25]. All these observations suggest that ALS can be a distal axonopathy. These findings have

brought renewed attention to the 'dying-back' hypothesis for ALS, where a retrograde pathogenic signaling cascade that originates in the peripheral tissues, such as skeletal muscles, can trigger the degeneration of MNs in the CNS [17,18]. Intriguingly, evidence of distal axonopathy has also surfaced in other neurodegenerative diseases, such as Parkinson's disease and Alzheimer's disease, suggesting that targeting peripheral tissues may be an effective therapeutic strategy for a range of neurodegenerative disorders, including ALS [26,27,28]. This review aims to provide a comprehensive summary of studies on therapies that target skeletal muscle and their impact on muscle satellite cells (MuSCs), inflammation, and the NMJ, which are essential components of ALS pathogenesis.

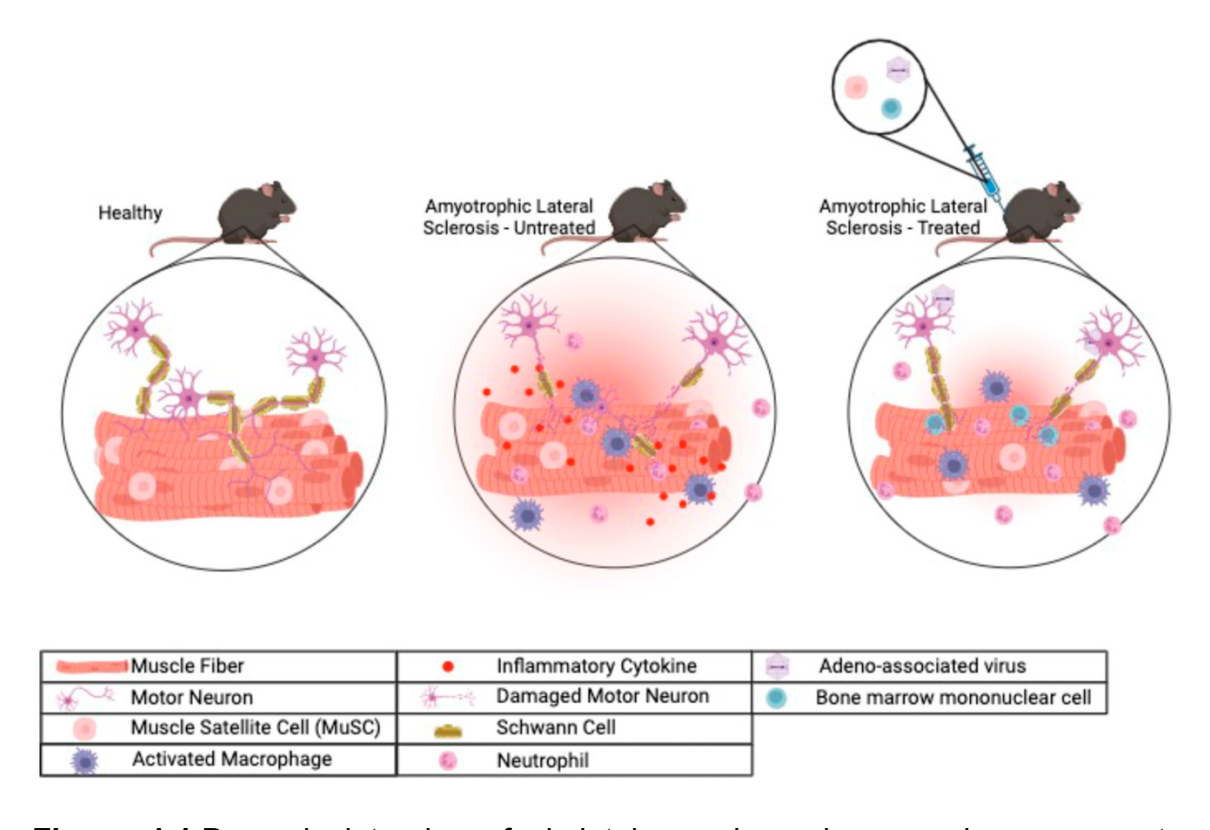


**Figure 1.1** Dynamic interplay of skeletal muscle and nerves in response to therapeutics targeting skeletal muscles in ALS. In a healthy state, motor neurons are wrapped with Schwann cells to form the myelin sheath, aiding in neural signaling towards

the NMJ and ultimately reaching the muscle fibers. In ALS, significant damage is evident in muscle fibers and Schwann cells, often accompanied by the presence of activated macrophages and neutrophils, releasing inflammatory cytokines within the skeletal muscle and the surrounding NMJ. This inflammatory milieu may signal back to the central nervous system and aggravate motor neuron degeneration. In response to therapeutics targeting skeletal muscle in ALS, such as stem cell transplantation or adeno-associated virus (AAV)-based gene therapies, a profound reduction in muscle inflammation is observed, which is paralleled by muscle regeneration and NMJ recovery, leading to neuroprotection and regeneration.

#### 1.2 Muscle Satellite Cells

Skeletal muscle regeneration is a well-coordinated process of myogenesis that relies on MuSCs activation, proliferation, fusion, and differentiation [29]. Quiescent MuSCs are activated in response to acute injury, muscle denervation, or exercise stimuli. Once activated, MuSCs enter the cell cycle for proliferation, followed by differentiation into myoblasts and fusion with existing myofibers to repair and regenerate muscle fibers. The orderly process of myogenesis is tightly regulated by a family of transcription factors known as the myogenic regulatory factors (MRFs). They are crucial for regulating the gene expression essential for specifying the skeletal muscle lineage and controlling myogenic differentiation [30]. MuSCs express specific MRFs depending on their state. In their quiescent state, they express the MRF family member *Pax7* (a paired box family transcription factor) and myogenic factor 5 (*Myf5*) [31,32]. Upon activation, MuSCs quickly enter the cell cycle and begin to express another MRF member, *MyoD* (myogenic differentiation 1) [33]. The co-expression of both *Pax7* and *MyoD* indicates that these

stem cells have shifted active state. As activated MuSCs to an proliferate, Pax7 expression is downregulated, while MyoD and/or Myf5 expression persists. During differentiation, another MRF, myogenin (MyoG; Myf4), is expressed and is essential for the differentiation of MuSCs into multinucleated myotubes, making myogenin a marker for the onset of myogenic differentiation [33]. Besides muscle regeneration, MuSCs also help maintain the structure and activity of the NMJ [34,35]. Depletion of MuSCs results in impaired myofiber/NMJ connectivity and inefficient reinnervation of the NMJ [34].

In ALS, the activity and function of MuSCs are altered. Pradat and colleagues isolated MuSCs from the deltoid muscle biopsies of ALS patients and observed that these cells proliferated at a similar rate to those from healthy controls [36]. However, the myoblasts derived from ALS patients displayed a senescent-like morphology, with increased senescence markers, including senescent-associated (SA)-βGal and p16 expression. In addition, MuSCs derived from ALS patients were unable to fully differentiate in vitro, which was evidenced by the abnormal morphology of the myotubes and reduced expression of MHC isoforms [36]. In another study, Scaramozza and colleagues observed that myoblasts derived from the vastus lateralis muscle of ALS patients exhibited a higher proliferation rate than those of control cultures [37]. Additionally, these ALS-derived myoblasts displayed significantly higher transcription levels of MyoD compared to controls, while maintaining similar levels of Pax7. Ultrastructural assays revealed that ALS myoblasts had an altered morphology characterized by a large number of vacuoles. Furthermore, differentiating ALS myoblasts displayed lower expression levels of Myf4 compared to controls [37]. Studies by both Pradat and Scaramozza suggest that myoblasts derived from ALS patients are unable to fully differentiate into myotubes to achieve efficient muscle regeneration. Mitochondrial bioenergetics failure was observed in satellite cells isolated from the early presymptomatic stage (p55) of an established ALS mouse model carrying human mutated SOD1 (G93A) genes [38]. Dysfunctional mitochondria accelerate the accumulation of reactive oxygen species and other DNA-damaging factors. These factors may contribute to the susceptibility of MuSCs to degeneration following the activation of the repair system [37]. Although further research is necessary to elucidate the mechanisms underlying the compromised muscle regeneration mediated by MuSCs in ALS, these cells could represent a potential therapeutic target for the disease.

#### 1.2.1 Therapeutic Targets on MuSCs

Recently, researchers have explored the purinergic P2X receptor 7 (P2XR7), a family member of purinergic ionotropic receptors, as a therapeutic target for ALS, aiming to promote muscle regeneration. For example, Fabbrizio and colleagues found that activation of P2XR7 was able to reduce muscle atrophy in ALS mice [39]. Activation of P2XR7 through intramuscular administration of the P2XR7 agonist 2'(3')-O-(4-benzoylbenzoyl) adenosine 5-triphosphate (BzATP) into the tibialis anterior (TA), gastrocnemius medialis (GCM), and quadriceps (QC) of SOD1 (G93A) mice enhances the pro-regenerative activity of infiltrating macrophages and improves the motor performance of ALS mice by promoting the activation and differentiation of MuSCs [40]. BzATP-treated muscle exhibited a larger muscle fiber cross-sectional area and higher expression levels of myogenic factors (*MyoD* and *MyoG*) in the QC muscle compared to controls. Primary satellite cells isolated from BzATP-treated mice also showed increased

proliferation rates and fusion index during differentiation. A serial of in vitro evaluations confirmed that BzATP promotes satellite cell proliferation and differentiation, which were mediated by the activation of P2XR7. Additionally, supplements of BzATP resulted in decreased glycogen synthase kinase 3 (GSK3) activation and increased extracellular signal-regulated kinase 1/2 (ERK1/2) phosphorylation in the skeletal muscle of SOD1 (G93A) mice, suggesting the involvement of pro-survival/regenerative pathways. In addition, activation of P2XR7 by BzATP increased the recruitment of CD11b+ cells (macrophages) in the skeletal muscles of SOD1 (G93A) mice, particularly at the disease onset stage. Histological analysis revealed an increase in Macrophage 2 (M2) while CD206<sup>+</sup> macrophages BzATP-treated mice, in Macrophage (M1)iNOS+ macrophages showed no significant difference compared to controls, suggesting a correlation between P2XR7 activation and M2 polarization. At the onset of the disease, BzATP treatment led to downregulation of pro-inflammatory cytokines like insulin-like growth factor-1 (IGF-1) and Tumor Necrosis Factor α (TNF-α) while increasing the antiinflammatory cytokine interleukin 10 (IL-10), indicating a shift towards an antiinflammatory milieu favoring muscle regeneration [39]. Other studies have shown that activating P2X7 benefits the peripheral nervous system (PNS) by promoting Schwann cell proliferation after sciatic nerve injury and facilitating myogenesis and the formation of the NMJ [39,41].

In addition to P2XR7, mouse insulin-like growth factor (mlgf)-1 isoform, previously implicated in the anabolism of muscle and nerve tissues, has shown promising potential as a muscle-focused ALS treatment [42]. Dobrowolny and colleagues found that the skeletal muscle-restricted expression of mlgf-1 enhanced MuSC activity and fiber

maturation [42]. Transgenic mlgf-1 expression also stabilized the NMJ, reduced spinal cord inflammation, improved MN survival, and ultimately prolonged the lifespan of mice carrying the ALS-associated SOD1 (G93A) mutation [42]. These studies highlight the potential of targeting MuSCs for ALS therapies.

#### 1.3 Inflammation

Neuroinflammation has been recognized as one of the key mediators of ALS pathogenesis. Zamiri and colleagues identified immunological dysregulation as a central contributor to disease progression in sporadic ALS, making it a potential therapeutic target [43]. They observed infiltration of immune cells such as IL-17A and granzymepositive cytotoxic T lymphocytes (CTLs), IL-17A-positive mast cells, and inflammatory macrophages into the brain and spinal cord. Early elevation in inflammatory cytokines (IL-12A, IFN-y, TNF-α), granzymes, and transcription factors (STAT3, STAT4) in peripheral blood mononuclear cells (PBMCs) was also observed. Upregulation of autoimmunityassociated cytokines (IL-23A, IL-17B) and chemokines (CXCL9, CXCL10) in PBMCs was detected, attracting CTLs and monocytes into the CNS. Furthermore, systemic inflammation in ALS is also driven by changes in T-cell regulation. In ALS patients, inhibitory co-receptors like CTLA4 (cytotoxic T lymphocyte-associated protein 4) and PD-1 (programmed cell death protein-1) decrease, while stimulatory co-receptors like OX40 and GITR increase. CTLA4 gradually decreases over time, while LAG3 initially increases but sharply declines around 40 months post-onset. Conversely, OX40 and GITR significantly upregulate in the same time frame. Longersurviving patients exhibit increased FOXP3 activity, a key regulator of regulatory T cells (Tregs), aiding immune response regulation. In addition, proteomic analysis revealed

heightened expression of granzymes, kinases, cell adhesion, and apoptotic proteins in the natural killer (NK) cells of an ALS patient compared to their healthy twin. Investigations into therapeutic interventions for sporadic ALS patients revealed that dimethyl fumarate (DMF) and the cGAS/STING pathway inhibitor H-151 downregulate granzymes and proinflammatory cytokines (IL-1β, IL-6, IL-15, IL-23A, IFN-γ), promoting a pro-resolution macrophage phenotype. Additionally, anti-inflammatory eicosanoid epoxyeicosatrienoic acids (EETs) from arachidonic acid synergize with DMF. DMF and H-151 emerge as promising drugs that target inflammation and autoimmunity in sporadic ALS by modulating the NFκB and cGAS/STING pathways [43].

Dysregulated inflammatory processes in the skeletal muscle also play a significant role in ALS pathology [15]. For healthy muscles, when muscle injury occurs, resident and recruited mast cells, neutrophils, and other immune cells contribute to creating a proinflammatory environment through the secretion of pro-inflammatory cytokines, such as TNF- $\alpha$ , interferon- $\gamma$  (IFN- $\gamma$ ), and interleukin-1 $\beta$  (IL-1 $\beta$ ). This process recruits macrophages, derived from monocytes in the bone marrow, to the site of muscle injury at approximately two days post-injury. During muscle regeneration, the macrophages undergo a transition from the M1 (pro-inflammatory) to the M2 (anti-inflammatory) phase. In the early stage of muscle regeneration, M1 macrophages predominate, promoting the proliferation of MuSCs by secreting large amounts of cytokines such as TNF- $\alpha$ , IL-1 $\beta$ , IGF-1, interleukin-6 (IL-6), and IFN- $\gamma$  [44]. As the number of MuSCs reaches its peak, the pro-inflammatory (M1) microenvironment transitions into the anti-inflammatory state (M2), facilitating the differentiation of MuSCs and the maturation of newly formed myofibers. M2 macrophages establish this anti-inflammatory environment by producing anti-

inflammatory cytokines, such as interleukin-4 (IL-4), interleukin-10 (IL-10), and interleukin-13 (IL-13), and suppressing the local inflammatory response at the injury site. Simultaneously, M2 macrophages facilitate the differentiation of MuSCs into myotubes, thereby contributing to the later stages of myogenesis and regeneration through secreting various growth factors, such as GDF3 [45,46]. This transition from the pro-inflammatory to the anti-inflammatory macrophage phenotype during muscle regeneration is crucial to maintaining a favorable regeneration microenvironment.

In the ALS in vivo model, inflammation gradually worsens as the disease advances from the late pre-symptomatic stage to the symptomatic and late disease states in the limb muscles. This inflammation is particularly prominent near the postsynaptic region of the NMJ [47]. Elevated inflammasome activation has been implicated in skeletal muscle pathology in ALS, as evidenced by macrophage infiltration and increased levels of caspase-1 and IL-1β in both the SOD1 (G93A) mouse model and sporadic ALS patients [48]. Furthermore, the elevated levels of these proteins in the skeletal muscle of presymptomatic SOD1 (G93A) mice indicate an early activation of innate immunity in the pathogenesis of ALS [48]. In addition, during muscle regeneration, elevated IL-1β levels correlate with an accumulation of activated macrophages, leading to impaired regeneration [49]. Prolonged inflammation disrupts the microenvironment of cells within the skeletal muscle, upsets the delicate equilibrium between protein synthesis and degeneration, and affects components like the myosin heavy chain, the major contractile protein required to sustain muscle contraction [50]. This disruption is achieved through the activation of various inflammatory signaling pathways, including but not limited to the NF-κB (nuclear factor-κB), JAK/STAT (Janus-activated kinase/signal transducer and

activator of transcription), and p38 MAPK (mitogen-activated protein kinase) pathways [51]. Therefore, modulating inflammation in ALS skeletal muscle may facilitate tissue regeneration and ameliorate disease progression.

#### 1.3.1 Therapeutic Targets for Anti-Inflammation

During muscle regeneration, macrophages are the dominant immune cells recruited within the damaged tissue and directly interplay with MuSCs to orchestrate their fate through different secretory cues [45]. Intramuscular injection of the anti-inflammatory factor IL-10 into SOD1 (G93A) mice has been shown to counteract skeletal muscle atrophy by facilitating macrophage polarization and MuSCs differentiation [52]. Upon IL-10 administration, protein levels of MyoD and MyoG were significantly increased in the MuSCs, indicating a promotive role in facilitating the transition from the proliferative stage to the differentiation stage [53]. IL-10, as a potent immunomodulatory factor, can induce the shift of M1 macrophages to M2, which is crucial for muscle growth and regeneration. The study found that IL-10 treatment increased CD11b<sup>+</sup> cell density in the TA muscle, suggesting a potential influence on macrophage proliferation. In vitro, SOD1 (G93A) macrophages showed a 2.7-fold increase in proliferation with IL-10 treatment, which was reversed upon IL-10 blockage. In C57-SOD1 (G93A) mice, IL-10 reduced M1 iNOS<sup>+</sup> macrophages while increasing their M2 CD206<sup>+</sup> counterparts in the quadriceps muscle. Histological and RNA lysate analyses confirmed the decreased expression of pro-inflammatory cytokines (TNFα and IL1-β) with IL-10 treatment, indicating an antiinflammatory effect. The study further investigated the influence of IL-10 on the interaction between macrophages and MuSCs in damaged skeletal muscle. The administration of IL-10 enhanced the migration of macrophages towards MuSCs in vitro, even in the

absence of M2 polarization. This effect was further boosted when IL-10 was combined with IL-4, indicating enhanced macrophage–MuSCs crosstalk. Eventually, the immunomodulation and anti-inflammation mediated by IL-10 led to the preservation of MNs, improving motor performance and extending the lifespan of SOD1 (G93A) mice [52].

Trolese and colleagues also demonstrated that boosting the peripheral immune response by utilizing an intramuscular injection of the scAAV9 vector packed with *Mcp1* (monocyte chemoattractant protein-1) improved motor functions in SOD1 (G93A) mice [54]. *Mcp1* is a key chemokine that regulates the migration and infiltration of monocytes/macrophages. This intervention, in turn, triggered the differentiation of myogenic progenitors and facilitated muscle re-innervation, ultimately leading to improved muscle strength and a delay in disease onset. The study also revealed that the fluorescent protein-tagged scAAV9 vector spread retrogradely from the injected muscles alongside the motor unit, eventually transducing the soma of MNs [54]. The induction of *Mcp1* in the motor unit protected MNs in the spinal cord by decreasing neuroinflammation, as indicated by decreased pro-inflammatory markers, such as IL-1β [54]. Together, these studies suggest that the direct modulation of inflammation in skeletal muscle not only stimulates muscle regeneration but also preserves the NMJ and enhances motor function in an ALS mouse model.

#### 1.4 Neuromuscular Junction

Given the early pathological changes that occur at the NMJ prior to the onset of ALS clinical symptoms, the NMJ is emerging as a promising therapeutic target for ALS treatment. The NMJ directly links the nervous and muscular systems and enables communication between the MNs and skeletal muscle fibers [55]. It comprises three

essential elements: the presynaptic motor nerve terminal, the perisynaptic Schwann cells (SCs), and the postsynaptic plasma membrane of the muscle fiber [56,57]. Upon the arrival of the action potential, calcium enters the presynaptic terminal, promoting the release of the neurotransmitter acetylcholine (ACh) into the extracellular space. The ACh then binds to tightly clustered ACh receptors (AChRs) on the muscle tissue, initiating the muscle action potential that ultimately leads to muscle contraction [58]. The malfunction of the NMJ disrupts muscle contraction, highlighting its central role in neuromuscular disorders [58]. In support of the distal axonopathy theory of ALS, pathological changes in the NMJ were reported to occur before MN degeneration and the onset of clinical symptoms [7,59,60]. Studies have revealed deficiencies in NMJ formation, fidelity, stability, and fatigability across all ALS NMJ models [61]. Additionally, there is a significant decrease in the innervated endplate area and increased fragmentation of the NMJ in ALS [61].

### 1.4.1 Therapeutic Targets for the NMJ

To ameliorate NMJ and MN defects in ALS patients, Barrientos and colleagues injected bone marrow mononuclear cells (BMMCs) into the skeletal muscle in a phase I/II clinical trial [62]. The results revealed a significant increase in the compound muscle action potential (CMAP), which was indicated by the D50 index, within the treatment group, suggesting that BMMCs have the potential to ameliorate NMJ damage in ALS [62]. In another study, human umbilical cord blood-derived mesenchymal stem cells (hUCB-MSCs) were repeatedly intramuscularly injected into the limbs of SOD1 (G93A) mice [63]. The treated group exhibited a significant enlargement of the NMJ endplate area compared to the vehicle-treated group. Implanted hUCB-MSCs also ameliorated muscle

atrophy by inhibiting reactive oxidative species generation and activating AMPKregulated protein synthesis. As a result, the transplantation of hUCB-MSCs improved motor function and extended survival in an ALS mouse model [63]. In addition, there are other treatments that combine stem cells with neurotrophic factors, such as glial-derived neurotrophic factors (GDNFs) and vascular endothelial growth factor (VEGF), to target the NMJ and muscle atrophy in an ALS animal model [64,65]. GDNFs and VEGF have also been shown to protect motor neurons in ALS models [66,67]. Intramuscular injection of human mesenchymal stem cells (hMSCs) engineered to express GDNF and/or VEGF led to a significant improvement in innervated endplates, as indicated by increased AChR cluster formation in an ALS animal model [64]. This protective effect extended to MNs in the spinal cord, resulting in an overall increase in the survival of SOD1 (G93A) rats [64]. In another study, overexpression of neurequlin (NRG-1), a neurotrophic factor that supports axonal and neuromuscular development and maintenance, within the skeletal muscle contributed to NMJ maintenance and improved redox homeostasis in the muscle of SOD1 (G93A) mice [68,69,70,71]. This also led to decreased glial reactivity and enhanced MN survival in the spinal cord [71]. Therefore, neurotrophic factors in conjunction with stem cells may serve as a valuable therapeutic target for ALS, as demonstrated by their ability to ameliorate both NMJ and MN phenotypes.

In addition, gene therapy for ALS has also been successfully administered in an ALS mouse model by intramuscular injection of AAV to express human Dok-7, a crucial muscle protein involved in NMJ formation [72]. This treatment effectively reduced muscle denervation and improved motor function [72]. Nonetheless, the perceived safety of the direct administration of gene editing-based therapy into humans warrants further studies

to ensure that there are no short- and long-term side effects. Overall, these studies show promising results for targeting the NMJ as a treatment for ALS.

#### 1.5 Mitochondria

Mitochondria, which support various essential cellular processes, including energy production, calcium storage, and lipid synthesis, are vital for cell viability and maintenance of life. In ALS patients, both sporadic and familial cases exhibit similar mitochondrial abnormalities in the spinal cord and muscles, as characterized by defects in morphology, quantity, and disposition. These abnormalities are accompanied by defects in the respiratory chain complex and increased oxidative stress [73]. Research by Bernardini et al. (2013) utilizing microarray technology identified significant alterations in mitochondrial network gene expressions in ALS, which are crucial for oxidative phosphorylation and ATP synthesis in muscle tissues [74]. Further studies using multigene gRT-PCR revealed a downregulation of genes responsible for mitochondrial biogenesis and dynamics, indicating a pervasive mitochondrial dysfunction in ALS [75]. Defective mitochondrial respiratory function, a primary source of reactive oxygen species (ROS) production, can lead to elevated intracellular ROS levels. Alleviated ROS and the resulting oxidative stress play a role in the pathogenesis of ALS, potentially leading to the formation of the unfolded protein aggregates that are invariably found in ALS motor neurons [76]. Halter B observed that the accumulation of ROS in skeletal muscles occurs at the asymptomatic stage in SOD1 (G93A) mice [77]. Similarly, Méndez-López I and Scaricamazza S found that mitochondrial dysfunction in the skeletal muscles of SOD1 (G93A) mice occurs before clinical symptoms appear [38,78]. These studies suggest that mitochondria and the resulting oxidative stress may contribute to the onset and progression of ALS.

#### 1.5.1 Therapeutic Targets for Mitochondrial Dysfunction and Oxidative Stress

Edaravone (MCI-186, 3-methyl-1 phenyl-2-pyrazolin-5-one), first described as a free radical scavenger, has been approved for treating ALS since 2015 in several countries, including Japan, South Korea, the United States, and Canada [79]. Edaravone treatment of rats with cerebral infarction significantly boosts the expression of Nrf2 (nuclear factor erythroid 2-related factor-2), a key stimulator of antioxidant activities that defend against oxidative stress [80]. Nrf2 activation, triggered by inflammation or injury, leads to its translocation from the cytoplasm to the nucleus, where it binds to antioxidant response elements in the promoter regions of various detoxifying enzymes, such as HO-1 (heme oxygenase-1) and NQO1 (NAD(P)H quinone oxidoreductase-1), thereby protecting cells from oxidative damage [81]. Additionally, Honokiol has demonstrated the ability to reduce cellular oxidative stress by enhancing the synthesis of glutathione (GSH) and activating the Nrf2 antioxidant response element (ARE) pathway. It also improves mitochondrial efficiency and morphology, promoting mitochondrial dynamics in SOD1(G93A) cells. Notably, Honokiol extends the lifespan and enhances the motor function of SOD1(G93A) transgenic mice when administered daily from disease onset to the end stage [82]. ALCAT1 (acyl-CoA:lysocardiolipin acyltransferase 1), an acyltransferase associated with mitochondrial dysfunction in age-related diseases, has been found to have increased expression in the skeletal muscle of SOD1(G93A) mice. Targeted deletion of ALCAT1 and pharmacological inhibition of this enzyme can prevent the aggregation of SOD1 (G93A) protein and mitochondrial dysfunction. These interventions may help to attenuate motor neuron dysfunction, skeletal muscle atrophy, and neuronal inflammation in SOD1 (G93A) mice [83]. Sodium butyrate has been shown

to improve mitochondrial respiration and alleviate disease progression in ALS models [84,85,86]. Additionally, it promotes MuSCs renewability and increases the expression of *Cxcl12*, which aids in axon attraction. Supplementation with sodium butyrate also resulted in reduced NMJ loss in the hindlimb and diaphragm muscles of SOD1 (G93A) mice [87]. These studies suggest that alleviating mitochondrial dysfunction and oxidative stress could significantly improve disease symptoms and influence the progression of ALS in cellular and animal models.

#### 1.6 Conclusions

As a multisystem disorder, ALS underscores the critical yet often overlooked involvement of skeletal muscle in the onset and progression of the disease. The dysregulation of MuSCs activation and differentiation, chronic inflammation, and dismantling of the NMJ collectively shape retrograde signaling that may contribute significantly to MN degeneration and exacerbate ALS syndromes. These skeletal musclerelated defects represent therapeutic targets with the potential to delay or even reverse the progression of the disease. This review has summarized therapies targeting MuSCs, inflammation, and the NMJ within the skeletal muscle as potential treatments for ALS. These therapies have exhibited numerous beneficial effects, including the reduction in inflammation and mitochondria defects and the amelioration of muscle and motor functions. These improvements led to extended lifespan in ALS in vivo models, supporting the critical roles of skeletal muscles in understanding and treating ALS. These findings further demonstrate the intricate interplay between multiple tissues and cell types in the complexity of ALS, which will aid in identifying novel pathogenic mechanisms and innovative therapeutic targets for the treatment of ALS.

#### CHAPTER 2

# HUMAN NEURAL PROGENITOR CELL-DERIVED EXTRACELLULAR VESICLES PROTECT AGAINST AMYOTROPHIC LATERAL SCLEROSIS'S DISEASE PATHOLOGIES<sup>2</sup>

<sup>2</sup>Gao, J., Hankin, R., Sterling, E., Sikal, A., Heo, J., Call, J., Daga, K., Marklein, R., Zheng, Y., Yousuf, H., Yao, Y. Human Neural Progenitor Cell-derived Extracellular Vesicles protect against Amyotrophic Lateral Sclerosis's disease pathologies. To be submitted to a peer-reviewed journal.

<sup>\*:</sup> Co-First Author

#### Abstract

Human neural stem cells (NSCs) have demonstrated neuroprotective and regenerative potential in Amyotrophic lateral sclerosis (ALS) models, yet safety and ethical concerns limit their clinical application. Recent studies have highlighted NSCderived extracellular vesicles (NSC-EVs) as a promising alternative. In this study, we investigated the therapeutic potential of neural progenitor cell-derived extracellular vesicles (NPC-EVs) in ALS. NPC-EVs significantly enhanced the cell viability and proliferation of ALS-like motor neurons under oxidative stress by reducing reactive oxygen species (ROS) levels, indicating strong antioxidative effects. Additionally, NPC-EVs mitigated inflammatory cytokine TNF-α-induced morphological changes in microglia, suggesting their role in modulating neuroinflammation. In vivo, NPC-EVs exhibited superior uptake efficiency in the central nervous system compared to HEK-EVs and modulated inflammatory NF-κB signaling in an ALS mice model (SOD1<sup>G93A</sup> mice) following intravenous administration. These findings suggest that NPC-EVs possess neuroprotective, antioxidative, and anti-inflammatory properties, making them a promising therapeutic strategy for ALS. Further studies and evaluations are necessary to optimize dosing, administration timing, and long-term efficacy to advance their clinical translation.

#### 2.1 Introduction

Amyotrophic lateral sclerosis (ALS) is a fatal neurodegenerative disease characterized by the progressive degeneration of motor neurons in the spinal cord, brainstem, and motor cortex, as well as skeletal muscle atrophy. Approximately 90% of ALS cases are sporadic, while the remaining 10% are familial and associated with

inherited genetic mutations [1]. Despite advancements in understanding the disease, ALS remains incurable. Current FDA-approved therapies include the glutamate antagonist riluzole, the antioxidant edaravone, and the SOD1 antisense oligonucleotide gene therapy tofersen [2-4]. However, these treatments provide only modest benefits, extending survival by two to six months. The limited success of these therapies reflects the multifactorial nature of ALS pathology, which involves interrelated processes such as neuroinflammation, mitochondrial dysfunction, and elevated oxidative stress [5, 6]. These mechanisms contribute to motor neuron degeneration in both sporadic and familial ALS, underscoring the complexity of the disease. The failure of clinical trials targeting single pathological pathways underscores the necessity of adopting a more comprehensive therapeutic strategy. Given the clinical and molecular heterogeneity of ALS, interventions designed to simultaneously target multiple interconnected pathological mechanisms hold greater promise for improving treatment outcomes.

Stem cell therapy is widely regarded as a promising therapeutic approach capable of addressing multiple pathological mechanisms. Numerous preclinical studies have demonstrated its potential to treat Amyotrophic Lateral Sclerosis (ALS) [7]. Specifically, the administration of neural stem cells (NSCs) has shown beneficial effects in various preclinical models [8-11]. However, significant safety and ethical concerns surrounding stem cell therapy have constrained its clinical application in human patients [12]. As an alternative, recent research has increasingly focused on extracellular vesicles (EVs). EVs are nanosized vesicles that serve as intercellular communicators by transporting bioactive molecules, such as proteins, lipids, and nucleic acids, from source cells to recipient cells, thereby modulating their function [13]. EVs derived from neural stem cells (NSC-EVs)

have demonstrated therapeutic potential in preclinical models of neurodegenerative diseases, including Alzheimer's disease, Parkinson's disease, and stroke [14-17]. These findings suggest that EVs could offer a safer and more ethically acceptable alternative to direct stem cell transplantation for treating ALS and other neurological conditions.

In this study, we explored the therapeutic potential of EVs derived from neural progenitor cells (NPC-EVs) for addressing ALS-relevant phenotypes in both in vitro and in vivo models. Our results demonstrated that NPC-EVs exert significant beneficial effects on ALS-like motor neuron models, enhancing cell viability and proliferation under oxidative stress conditions. Notably, NPC-EVs effectively mitigated oxidative stress in ALS-like motor neuron cells, suggesting a potential role in supporting mitochondrial function. Moreover, NPC-EVs promoted anti-inflammatory phenotypes in human microglia treated with the pro-inflammatory cytokine TNF- $\alpha$ , simulating the inflammatory environment of the central nervous system in ALS. Compared to extracellular vesicles derived from non-neuronal cells (HEK-EVs), NPC-EVs exhibited a unique ability to cross the blood-brain barrier via intravenous administration. This finding indicates that NPC-EVs may be taken up by central nervous system cells, such as motor neurons and microglia, to deliver their therapeutic effects directly. In addition to these properties, NPC-EVs were found to modulate the pro-inflammatory NF-kB pathway, a critical driver of motor neuron degeneration and disease progression in ALS. Collectively, these findings underscore the therapeutic potential of NPC-EVs as a promising avenue for ALS treatment.

#### 2.2 Results

#### 2.2.1 Extracellular vesicle characterization

This study investigated the therapeutic potential of EVs derived from human neural progenitor cells (NPC-EVs) in ALS-affected models. To highlight the significance of the cellular source of EVs, EVs derived from human embryonic kidney cells (HEK-EVs) were included as a control. The isolated EVs were first characterized using specific EV markers. Western blot analysis confirmed the presence of EV markers CD81 in the NPC-EV sample, while the intracellular marker Tubulin was not detected. Transmission electron microscopy further validated the presence of EVs, revealing their typical morphology and size. The size distribution and particle concentration of the EV samples were analysed using nanoflow cytometry, which measured mean particle sizes of 76.4 ± 4.7 nm for NPC-EVs and 79.6 ± 4.2 nm for HEK-EVs. To verify the purity of the EV population, MemGlow dye, a fluorogenic membrane probe, was used to label the lipid bilayer. The results demonstrated high EV purity, with values of 74.4 ± 13.2% for NPC-EVs and 72.2 ± 14.5% for HEK-EVs, with no significant difference observed between the two groups. To assess whether NPC-EVs can be taken up into the central nervous system, we conducted a biodistribution study and compared their distribution with EVs derived from a non-neural source, HEK-EVs. Equal amounts of NPC-EVs or HEK-EVs dyed with carboxyfluorescein succinimidyl ester (CFSE), a fluorescent dye that covalently binds to free amines, were intravenously injected into wild-type mice. The fluorescence in the brain, heart, liver, spleen, lungs, and kidney was visualized using IVIS imaging after 90 minutes. For both types of EVs, the majority of the EVs were visualized in the brain and liver. Intriguingly, a

higher fluorescence signal was seen in the brain for NPC-EVs, suggesting that these EVs may have a higher natural biodistribution to the brain than HEK-EVs.

# 2.2.2 NPC-EVs protect against hydrogen peroxide-induced phenotypes in SOD1<sup>G93A</sup> NSC-34 cells

Hydrogen peroxide (H<sub>2</sub>O<sub>2</sub>) can induce cell death and other ALS-relevant phenotypes in mouse motor neuron-like NSC-34 cells, a commonly used in vitro model of ALS [18-21]. Our team member Rachel Hankin and I optimized NSC-34 cells in vitro model that under the H<sub>2</sub>O<sub>2</sub> - induced oxidative stress to mimic the ALS-related degeneration. Meanwhile, we optimized the dosage of NPC-EVs for the treatment. Then, Rachel Hankin repeated confirmed the therapeutic efficacy of NPC-EVs on NSC-34 cells treated with H<sub>2</sub>O<sub>2</sub>, where the NSC-34 cells have a stable expression of wild-type human SOD1 or mutated human SOD1 (here referred to as SOD1WT or SOD1G93A, respectively). Treatment with 30 ng/uL of H<sub>2</sub>O<sub>2</sub> caused a significant decrease in cell viability in SOD1<sup>G93A</sup> cells (6.2 ± 2.7 %). Cell viability was significantly increased when the cells were treated with NPC-EVs under oxidative stress induced by H<sub>2</sub>O<sub>2</sub>, with higher NPC-EVs concentrations leading to a greater effect. The highest concentration of NPC-EVs (2.5 x 10<sup>9</sup> particles) increased cell viability to 94.1 ± 12.8 % and was not significantly different from the SOD1WT cells. Treatment with HEK-EVs at the same concentration only increased cell viability to 46.1 ± 22.6 %. This indicates that NPC-EVs have a greater beneficial effect on the viability of ALS-like motor neurons compare to non-neural source HEK-EVs. We then tested whether NPC-EV treatment would attenuate H<sub>2</sub>O<sub>2</sub>-induced decreases in cell proliferation. Treatment with NPC-EVs significantly increased the

percentage of proliferating SOD1<sup>G93A</sup> cells under  $H_2O_2$  treatment, while HEK-EV treatment did not significantly enhance cell proliferation in these cells.

Since mitochondrial dysfunction, increased oxidative stress, and increased levels of reactive oxygen species (ROS) are a main pathological feature of ALS [22, 23]. We wanted to test whether NPC-EV treatment could attenuate mitochondrial dysfunction in the SOD1<sup>G93A</sup> cells. It has been reported that H<sub>2</sub>O<sub>2</sub> treatment increases ROS levels in NSC-34 cells [19]. Our team member Rachel Hankin found that when SOD1<sup>G93A</sup> cells were treated with 30 ng/uL of H<sub>2</sub>O<sub>2</sub>, ROS levels significantly increased. NPC-EV treatment reduced ROS levels by more than 90%, bringing them to levels not significantly different from those in SOD1WT cells. In contrast, HEK-EVs treatment at the same concentration reduced ROS levels by approximately 50% compared to the H<sub>2</sub>O<sub>2</sub>-treated cells. These results suggest that NPC-EV treatment has a significant beneficial effect on reducing mitochondrial ROS level, potentially improving mitochondrial function. Furthermore, NPC-EVs demonstrated a greater protective effect than HEK-EVs, indicating that NPC-EVs may contain specific functional biomolecules beneficial to ALSlike motor neurons or may exhibit higher uptake efficiency in motor neurons compared to HEK-EVs. These in vitro experiments have been repeated three times to validate their reliability and reproducibility.

# 2.2.3 NPC-EVs treatment modulates microglia morphologies under inflammatory cytokine

During the early stages of the disease, the immune system is protective by providing anti-inflammatory agents that support dying motor neurons. However, as the disease progresses, the immune response shifts toward a pro-inflammatory and cytotoxic

state, significantly accelerating disease progression [24-26]. Microglia, the primary immune cells of the central nervous system, are actively involved in ALS pathology and contribute to disease progression [27]. Upon stimulation of the immortalized human microglia cell line with inflammatory cytokine TNF-α (5 ng/mL), previous study has reported significant morphological changes, including increased perimeter and major axis length [28]. These changes reflect the characteristic enlargement of microglia in response to TNF-α. Our team member Rachel Hankin performed treatment with NPC-EVs effectively prevented this cytokine-induced morphological shift by inhibiting the increase in cell size, as reflected by reductions in both area and perimeter. With concurrent NPC-EV treatment, microglia exhibited a smaller morphology, with higher NPC-EV concentrations producing greater effects. Overall, the composite morphology score, assessed using principal component 1, indicates that NPC-EV-treated groups shift toward the morphology of unstimulated microglia, suggesting a protective effect against inflammatory TNF-α-induced morphological alterations.

#### 2.2.4 NPC-EVs treatment modulates the inflammatory NF-κB pathway

Aberrant activation of NF-κB signaling in the ALS-affected spinal cord is a critical driver of chronic inflammation and motor neuron degeneration [27, 29]. Targeting NF-κB signaling represents a promising therapeutic strategy for attenuating inflammation and mitigating ALS disease progression. To assess the impact of NPC-EV treatment on NF-κB signaling in the spinal cord of an ALS mice model, we used SOD1<sup>G93A</sup> mice, a transgenic mouse line extensively utilized in ALS preclinical research. These mice effectively recapitulate several key pathological features of ALS, including motor neuron degeneration, muscle atrophy, and reduced lifespan, all of which are observed in human

ALS patients [30, 31]. We performed western blot analysis to quantify the expression of total NF-κB, its active phosphorylated format NF-κB (pNF-κB), and the loading control Vinculin across three experimental groups: wild-type (WT) mice, PBS-treated SOD1<sup>G93A</sup> mice, and NPC-EVs treated SOD1<sup>G93A</sup> mice. The results indicate that total NF-κB protein levels were significant elevated in the spinal cord of SOD1<sup>G93A</sup> mice compared to WT mice, suggesting a heightened inflammatory state in ALS-affected spinal cord. Notably, NPC-EV treatment markedly downregulated NF-κB protein levels (Figure 2.1A, B). Although statistical analysis did not show significant difference in pNF-κB levels between the NPC-EVs and PBS group, the data still revealed a decreasing trend. Overall, these results suggest the NPC-EV treatment has the potential to module the inflammatory NF-κB pathway.

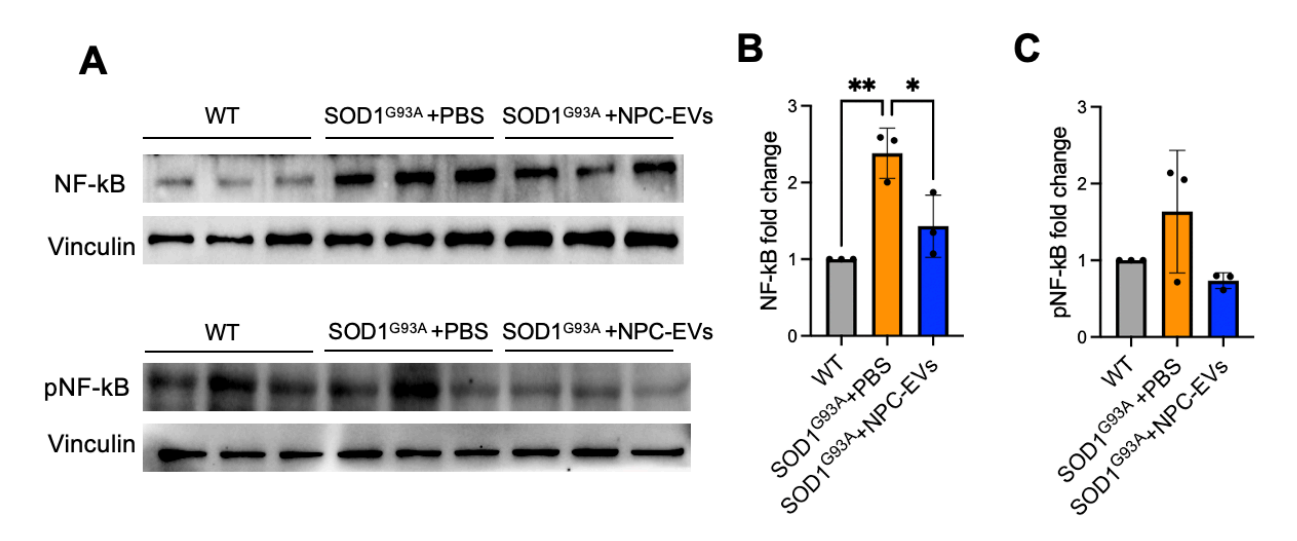


Figure 2.1 NPC-EVs treatment modulates the inflammatory NF-κB pathway. (A) Western blot analysis of NF-κB, pNF-κB, and Vinculin proteins for three groups: WT mice (n=3), SOD1<sup>G93A</sup> mice with PBS treatment (n=3), and SOD1<sup>G93A</sup> mice with NPC-EV treatment (n=3). (B) Quantification of NF-κB protein levels among the three groups using Image J, statistical analysis by one-way ANOVA. (C) Quantification of pNF-κB protein

levels among the three groups using Image J, statistical analysis by one-way ANOVA. \*  $P \le 0.05$ , \*\* $P \le 0.005$ .

#### 2.3 Discussion

The therapeutic potential of human NSCs has been extensively explored in both preclinical studies using ALS animal models and in clinical trials, including phase 1 and phase 2 trials [32-36]. In these studies, transplantation of human NSCs into the spinal cord of ALS mouse models has demonstrated the ability to ameliorate several pathological processes, including delaying disease onset, prolonging survival, preserving neuromuscular function, and reducing astrogliosis and inflammation [32, 33, 36]. In clinical trials with ALS patients, human NSC transplantation has been evaluated for safety and feasibility [34, 35]. These findings suggest that NSCs possess both neuroprotective and regenerative capabilities for ALS. The potential therapeutic mechanisms may include the replacement of damaged neurons, modulation of the disease microenvironment, and secretion of neuroprotective factors that help delay or prevent motor neuron degeneration. However, significant safety and ethical concerns surrounding the stem cell transplantation have constrained its clinical application in human patients [12].

Recent research has shifted focus toward NSC-EVs, which have demonstrated therapeutic potential in various neurodegenerative disease models, including Parkinson's disease, Alzheimer's disease, and stroke [14, 15, 17]. In these models, NSC-EVs administration has been associated with significant therapeutic benefits, particularly in reducing neuroinflammation and mitigating disease-associated pathological phenotypes. Given that neuroinflammation is a critical driver of ALS progression, characterized by glial activation and the release of pro-inflammatory cytokines that exacerbate motor neuron

degeneration. In this study, we explored the neuroprotective efficacy of NPC-EVs in both in vitro and in vivo ALS models. Our findings demonstrate that NPC-EVs significantly enhanced the survival and proliferation of ALS-like motor neurons (NSC-34 SOD1 G93A cells) under oxidative stress induced by H<sub>2</sub>O<sub>2</sub> treatment. Additionally, NPC-EVs exhibited strong therapeutic potential in mitigating mitochondrial dysfunction by reducing ROS levels, indicating a robust antioxidative effect. Beyond their protective effects on ALS-like motor neurons, NPC-EVs also attenuated TNF-α-induced morphological changes in microglia, further emphasizing their therapeutic role in addressing the multifaceted pathology of ALS. Moreover, NPC-EVs demonstrated higher uptake efficiency in the central nervous system compared to HEK-EVs, suggesting their potential to effectively deliver therapeutic effects to the brain. Following non-invasive intravenous administration of NPC-EVs in an ALS mouse model (SOD1<sup>G93A</sup> mice), we observed their modulatory effects on inflammatory NF-kB protein levels. This suggests that NPC-EVs may play a role in attenuating neuroinflammation, potentially contributing to neuroprotection in ALS. Overall, these findings provide compelling evidence for the neuroprotective, antioxidative, and anti-inflammatory properties of NPC-EVs, supporting their promise as a novel therapeutic approach for ALS. To advance the translational potential of NPC-EVs for clinical applications, further studies are required to optimize dosage, timing, and frequency of EV administration, as well as to elucidate the molecular mechanisms underlying their therapeutic effects. Additionally, future studies should evaluate the impact of NPC-EV treatment on disease onset and lifespan in ALS preclinical models to better understand their long-term therapeutic potential.

#### 2.4 Methods

#### 2.4.1 Cell Culture

ReNcell CX human neural progenitor cells (NPCs) were purchased from Millipore Sigma (Cat#SCC007). Before culture, plates were coated with 20 µg/mL of natural mouse laminin (Gibco, Cat#23017015) for at least 4 hours at 37°C. NPCs were cultured in Modified Dulbecco's Eagle Medium (DMEM)/Nutrient Mixture F-12 (Gibco, Cat#11320033) supplemented with 10% fetal bovine serum (FBS, Neuromics, Cat#FBS002, Lot#218H19), 1% penicillin/streptomycin (Gibco, Cat#15070-063), 2 µg/mL heparin (STEMCELL Technologies, Cat#07980) 1X B27 (Thermo Fisher Scientific, Cat#17504044), 20 ng/mL of EGF (Millipore Sigma, Cat#GF144) and fibroblast growth factor 2 (FGF-2) (Millipore Sigma, Cat#GF003). Human embryonic kidney (HEK293T) cells and HEK293T cells were cultured in DMEM high glucose (Gibco, Cat#11965118) supplemented with 10% FBS and 1% penicillin/streptomycin. NSC-34 cells, a mouse motor neuron-like cell line [37]. They were stably transfected with the wild-type superoxide dismutase 1 (SOD1) protein (SOD1WT) or a mutated SOD1 protein (SOD1G93A) fused to GFP under a doxycycline-controlled promoter. The NSC-34 cells were cultured in DMEM/Nutrient Mixture F-12 supplemented with 10% FBS and 1% penicillin/streptomycin. C20 human microglia cells were generously provided by the Marklein Lab at the University of Georgia. The cells were cultured in DMEM/Nutrient Mixture F-12 supplemented with 10% FBS, 1% penicillin/streptomycin, and 0.2% normocin (InvivoGen, Cat#ant-nr-1). When thawing the C20 cells, the media was additionally supplemented with 1% N2 Supplement (Gibco, Cat#17502048) and 1 µM dexamethasone (Millipore Sigma, Cat#D4902). All cell lines were grown in a 5% CO<sub>2</sub> atmosphere at 37°C.

#### 2.4.2 Extracellular Vesicle Isolation

For EVs collection, the culture media was replaced with media not containing FBS to prevent external EVs contamination. Conditioned media was collected every 24 hours for a total of 48 hours. Conditioned media was centrifuged at 1000 rpm for 10 minutes at  $4^{\circ}$ C to pellet cells and large cell debris. The supernatant was frozen at -20°C until the EV isolation occurred. Conditioned media was thawed overnight at  $4^{\circ}$ C and centrifuged at  $1000 \times g$  for 30 minutes at  $4^{\circ}$ C. The supernatant was macro-ultracentrifuged at  $133,000 \times g$  for 2 hours at  $4^{\circ}$ C to pellet the EVs. Then, the EV pellet was washed with 1 mL of cold PBS and micro-ultracentrifuged at  $100,000 \times g$  for 1 hour at  $4^{\circ}$ C. The final EV pellet was resuspended in cold PBS and stored at  $-80^{\circ}$ C until use. The size and concentration of the isolated EVs were determined by nano-flow cytometry using the Flow NanoAnalyzer (NanoFCM Inc., Xiamen. China). In addition, the morphology of NPC-EVs and HEK-EVs was identified by transmission electron microscopy (TEM) (JEM-1011, JEOL, Japan)

#### 2.4.3 MemGlow assessment

The EVs were stained with 2 nM MemGlow 488 (Cytoskeleton, Cat#MG01), a fluorogenic membrane probe, to quantify the percentage of particles with a lipid membrane for 10 minutes. The fluorescence was measured using the Flow NanoAnalyzer.

#### 2.4.4 Animal model & Treatment

Transgenic mice (B6SJL-TgN[SOD1\*G93A]1Gur), which express a high copy number of the mutant human SOD1 gene containing the Gly93Ala substitution, were acquired from Jackson Laboratories (Bar Harbor, ME, USA). Mice were housed under standard conditions with free access to food and water, and all experimental protocols were approved by the institutional animal care and use committee. At approximately

postnatal day 21 (P21), genotyping was performed on each mouse to confirm the presence of the SOD1<sup>G93A</sup> mutation. DNA was extracted from ear tissue samples. Polymerase chain reaction (PCR) was then conducted using specific primers to amplify the region of interest, confirming the genetic status of the transgenic mice. The successful identification of the mutation allowed for the inclusion of these mice in subsequent experimental procedures. Mice received an intravenous injection of NPC-EVs, resuspended in 100 μL of PBS, with a dosage ranging from 1.8 × 10<sup>9</sup> to 1.2 ×10<sup>10</sup> EVs. Control group mice were injected with an equivalent volume of PBS. Each group consisted of four mice. Treatment commenced at 61 days of age, approximately coinciding with the onset of disease progression. The treatments were administered weekly for four consecutive weeks. At 120 days of age, corresponding to the late-symptomatic stage of the disease, tissue samples were collected for analysis.

#### 2.4.5 Cell Viability

NSC-34 SOD1<sup>WT</sup> or SOD1<sup>G93A</sup> cells were seeded into a black, clear-bottom 96-well plate (15,000 cells/well) and incubated for 24 hours at 37°C. After 24 hours, the cells were treated with 2 μg/mL of doxycycline hyclate (STEMCELL Technologies, Vancouver, BC) for 24 hours. The cells were treated with 30 ng/μL of hydrogen peroxide (Millipore Sigma) and NPC-EVs (5 x 10<sup>8</sup> EVs, 1 x 10<sup>9</sup> EVs, or 2.5 x 10<sup>9</sup> EVs) or HEK-EVs (2.5 x 10<sup>9</sup> EVs) for 4 hours at 37°C. The cell viability was evaluated using the Cell Counting Kit-8 (CCK8; Dojindo Molecular Technologies, Rockville, MD) following the manufacturer's instructions. The CCK8 reagent was added to each well for 1 hour at 37°C, and the absorbance at 450 nm was measured using a plate reader. Data is represented as the

average of three technical replicate wells for three separate experiments, normalized as the percent change of SOD1<sup>WT</sup>.

#### 2.4.6 Cell Proliferation

NSC-34 SOD1<sup>WT</sup> or SOD1<sup>G93A</sup> cells were seeded into a 12-well plate (200,000 cells/well) and incubated for 24 hours at 37°C. After 24 hours, the cells were treated with 2 μg/mL of doxycycline hyclate (STEMCELL Technologies, Cat#100-1047) for 24 hours. The cells were treated with 30 ng/μL of hydrogen peroxide (Millipore Sigma, Cat#H1009) and 3.0 x 10<sup>10</sup> NPC-EVs or HEK-EVs for 4 hours at 37°C. The proliferation was assessed using the Click-&-Go EdU 594 Flow Cytometry Kit (Click Chemistry Tools, Cat#1389) following the manufacturer's instructions. The EdU fluorescence was measured using the Quanteon flow cytometer (Agilent). The percentage of the population containing EdU-positive cells was quantified using FlowJo software, where the negative control was set to have less than 1% of EdU-positive cells. Data is shown as the percent of cell proliferation of the total population for three separate experiments, normalized to SOD1<sup>WT</sup>.

#### 2.4.7 Reactive Oxygen Species

NSC-34 SOD1<sup>WT</sup> or SOD1<sup>G93A</sup> cells were seeded into a 96-well plate (15,000 cells/well) and incubated for 24 hours at 37°C. After 24 hours, the cells were treated with 2 μg/mL of doxycycline hyclate (STEMCELL Technologies, Cat#100-1047) for 24 hours. The cells were treated with 30 ng/μL of hydrogen peroxide (H<sub>2</sub>O<sub>2</sub>) (Millipore Sigma, Cat#H1009) and 2.5 x 10<sup>9</sup> NPC-EVs or HEK-EVs for 4 hours at 37°C. The cells were dyed with 500 nM MitoSOX Red (Thermo Fisher Scientific, Cat#M36008) in HBSS for 20 minutes at 37°C following the manufacturer's instructions. After thorough washing, the fluorescence was measured using the Quanteon flow cytometer (Agilent). Data analysis

and compensation were performed using FlowJo software. For compensation, NSC-34 SOD1<sup>WT</sup> cells were used as a control. The fluorescence values of three technical replicates from three separate experiments were min-max normalized. The data is shown as the average normalized value from each experiment for each group.

#### 2.4.8 Microglia Morphology Assay

Based on a previously established assay [28], the morphology of stimulated human microglia cells was evaluated before and after NPC-EV treatment to represent their potential to modulate neuroinflammation. Briefly, C20 human microglia cells were seeded into a black, clear-bottom 96-well plate (480 cells/well) coated with poly-D-lysine hydrobromide (Millipore Sigma, Cat#P7280) and incubated for 24 hours. After 24 hours, cells were stimulated with 5 ng/mL tumor necrosis factor-alpha (TNF-α, Sino Biological, Cat#10602-HNAE) and 5 ng/mL interferon-gamma (IFN-y, Gibco, Cat#PHC4033). Various concentrations of NPC-EVs were added: 1 x 10<sup>9</sup> EVs, 1 x 10<sup>8</sup> EVs, or 1 x 10<sup>7</sup> EVs. After 24 hours, cells were fixed with 4% PFA solution for 20 minutes, followed by thorough washing. Fixed cells were stained with 1.5 µg/mL Wheat Germ Agglutinin, Alex Fluor<sup>™</sup> 555 Conjugate (WGA, Invitrogen, Cat#W32464), 8.25 nM Phalloidin/AlexaFluor 568 conjugate (Invitrogen, Cat#A12380), and 10 µg/mL Hoechst (Invitrogen, Cat#H3570), diluted in 1X HBSS, 1% (w/v) bovine serum albumin (BSA, Sigma-Aldrich, Cat#A9418), and 0.1% of 0.22 µm-filtered Triton, for 30 minutes. The wells were washed 3 times with 1X HBSS and images using a 10X objective using BioTek Cytation5 (Aglilent) automated microscope. Thirty-six total images were captured for each well, with 6 technical replicate wells used for all groups in each experiment. Single-cell morphological analysis was performed using Cell Profiler. Data is represented as the median of the cell area or cell

perimeter or as a principal component analysis (PCA) combining 21 previously established cellular and nuclear features to assess overall microglia morphology changes [28].

#### 2.4.9 Western blot

Following the experiment, proteins were extracted from mouse spinal cord samples using RIPA lysis buffer (EMD Millipore Corp, Cat#20-188) supplemented with proteinase inhibitors (Thermo Scientific Cat#1861281). The expression levels of each protein were assessed by subjecting 5 µg of whole cell lysate to 10% SDS-PAGE. Following electrophoresis, the proteins were transferred onto a nitrocellulose membrane (BIO-RAD, Cat#1620174). The membrane was then blocked with a buffer containing Tris-Buffered Saline (TBS) with 0.1% Tween 20 (TBS-T) and 5% bovine serum albumin (BSA) for 60 minutes to prevent nonspecific binding. Subsequently, the membrane was probed overnight at 4°C with a specific primary antibody diluted in 5% BSA in TBS-T. Antibodies used included mouse anti-CD81 (Proteintech, Cat#66866-1), rabbit anti-Tubulin (Cell Signaling, Cat#2148S), rabbit anti-NF-kappaB p65 (cell signaling, 8242T, 1:1000), rabbit anti-P-NF-kappaB p65 (S536) (Cell signaling, 3033T, 1:1000), and rabbit anti-Vinculin (Cell Signaling Technology, Cat#13901). After primary antibody incubation, the membrane was washed three times with TBS-T to remove unbound antibodies. Next, the membrane was incubated with HRP-linked anti-rabbit IgG secondary antibody (PROMEGA, W401S, 1:10,000) or HRP-conjugated anti-Mouse IgG (Cell Signaling, Cat#7076S) for 1 hour at room temperature. Thereafter, the membrane was washed three times with TBS-T to remove excess secondary antibody. Finally, protein bands were

visualized using BIO-RAD ChemiDoc<sup>™</sup> MP Imaging System imager. The band density was quantified using image analysis software ImageJ.

#### 2.4.10 Statistical Analysis

All data were analysed using GraphPad Prism version 10.0 (GraphPad Software). Comparisons between several groups were performed using one-way ANOVA followed by Tukey's post-hoc test for multiple comparisons. Results are expressed as the mean  $\pm$  standard error of the mean (SEM). Statistical significance was defined as \* P  $\leq$  0.005, \*\*\* p < 0.0001, \*\*\*\*  $P \leq 0.0001$ .

#### CHAPTER 3

# EXREACELLULAR VESICLES FROM REGENERATING SKELETAL MUSCLE MITIGATE MUSCLE ATROPHY IN AN AMYOTROPHIC LATERAL SCLEROSIS MOUSE MODEL<sup>3</sup>

\_

<sup>&</sup>lt;sup>3</sup> Gao, J., Sikal, A., Hankin, R., Zheng, Y., Sterling, E., Chan, K., & Yao, Y. Extracellular Vesicles from Regenerating Skeletal Muscle Mitigate Muscle Atrophy in an Amyotrophic Lateral Sclerosis Mouse Model. 2025. *Cells*. Reprinted here with permission of the publisher.

#### **Abstract**

Amyotrophic lateral sclerosis (ALS) is a devastating neuromuscular disease characterized by progressive motor neuron degeneration and muscle atrophy, with no effective treatments available. Chronic inflammation, which impairs muscle regeneration and promotes proteolysis, is a key contributor to ALS-related muscle atrophy and a promising therapeutic target. Here, we applied extracellular vesicles (EVs) derived from regenerating skeletal muscles 14 days post-acute injury (CTXD14SkM-EVs), which possess a unique anti-inflammatory profile, to target muscle defects in ALS. We found that CTXD14SkM-EVs enhanced myoblast differentiation and fusion in a cellular musclewasting model induced by pro-inflammatory cytokine tumor necrosis factor alpha. Intramuscular administration of these EVs into an ALS mouse model mitigated muscle atrophy by promoting muscle regeneration, shifting macrophage polarization from proinflammatory M1 to anti-inflammatory M2 state, and suppressing the aberrant Nuclear Factor Kappa B (NF-kB) signaling, a key driver of muscle protein degradation. These results underscore the therapeutic potential of regenerating muscle-derived EVs for combating muscle atrophy in ALS.

#### 3.1 Introduction

Amyotrophic lateral sclerosis (ALS) is a debilitating neuromuscular disease characterized by the progressive degeneration of motor neurons in the spinal cord and brain, accompanied by severe skeletal muscle atrophy [38]. ALS patients experience rapid muscle wasting, and the majority succumb to the disease within 2-5 years of diagnosis, primarily due to respiratory failure. The annual incidence of ALS ranges from 1 to 2.6 cases per 100,000 persons, with a prevalence of approximately 11.8 per 100,000

in the United States [39, 40]. Despite extensive research, effective therapeutic options for ALS remain unavailable. Emerging studies indicate that skeletal muscle defects in ALS, beyond being a consequence of motor neuron loss, can retrogradely impair motor neuron health. This bidirectional role contributes to disease progression, positioning skeletal muscle as an accessible and promising therapeutic target [41].

Dysregulated inflammation in ALS-affected skeletal muscle is a significant pathological factor that disrupts the local cellular microenvironment and destabilizes the balance between protein synthesis and degradation [42, 43]. Aberrant activation of inflammatory signaling pathways, including the Nuclear Factor Kappa B (NF-kB) pathway, drives this imbalance by promoting muscle protein breakdown and accelerating muscle wasting [44, 45]. Furthermore, chronic inflammation hampers muscle regeneration by impairing the regenerative capacity of muscle stem cells and promoting fibrosis and fat infiltration. Notably, sustained inflammation prevents the transition of macrophages from a pro-inflammatory (M1 macrophage) to an anti-inflammatory (M2 macrophage) phenotype. Instead, macrophages adopt a hybrid profile that is unable to effectively clear damaged tissue debris, inhibits angiogenesis, and suppresses muscle stem cell activity necessary for tissue repair. Moreover, these macrophages may release profibrotic factors, such as transforming growth factor-beta (TGF-β), which exacerbate pathological fibrosis [46]. Intramuscular administration of the anti-inflammatory cytokine IL-10 has been shown to reduce muscle atrophy in ALS mice by facilitating macrophage polarization and activating muscle stem cells [47]. In this study, we investigate a therapeutic strategy targeting the inflammatory microenvironment in ALS-afflicted skeletal muscle, with the

goal of mitigating muscle degradation and promoting regeneration as a potential treatment for ALS.

Skeletal muscle possesses an intrinsic ability to regenerate in response to acute injuries. This process is well-coordinated, involving several interrelated and time-sensitive phases, such as necrosis of injured muscle cells, inflammation, regeneration, maturation, and ultimately, functional recovery. A single intramuscular injection of the snake venom toxin cardiotoxin (CTX) is widely used to induce acute skeletal muscle regeneration in mice and a distinctive anti-inflammatory environment emerges by day 14 post-injection (CTXD14SkM) [48]. At this stage, coordinated interactions among various cell types actively support muscle repair. Predominant among these are anti-inflammatory M2 macrophages, which secrete cytokines such as IL-10 and growth factors that drive muscle stem cell differentiation and the maturation of new myofibers [49, 50]. Furthermore, M2 macrophages aid in resolving inflammation by suppressing the pro-inflammatory signaling that predominates in the initial phases of injury [51].

EVs, essential mediators of intercellular communication, inherit bioactive molecules such as proteins and nucleic acids from their parent cells. This enables them to mirror the functional characteristics of their cells of origin, facilitating diverse biological effects [52]. EVs secreted by cells within the anti-inflammatory milieu of CTXD14SkM, including M2 macrophages and other immune cells, myogenic progenitor cells, and regenerating myofibers, are likely enriched with factors possessing anti-inflammatory properties. Therefore, in this study, we isolate CTXD14SkM-EVs and assess their therapeutic potential in mitigating inflammation and promoting muscle regeneration and repair in an ALS mouse model.

Here, we showed that CTXD14SkM-EVs enhance myoblast differentiation and fusion in a muscle atrophy cellular model induced by the pro-inflammatory cytokine TNF-α, highlighting their anti-inflammatory and myogenesis-promoting potential. Furthermore, intramuscular administration of CTXD14SkM-EVs effectively mitigated muscle atrophy and increased muscle fiber size in a well-established ALS mouse model with denervated muscle atrophy. Notably, EV-treated mice exhibited an increased number of regenerating myofibers, accompanied by elevated expression of key myogenic regulatory factors, indicating active muscle regeneration. Additionally, EV treatment facilitated a shift in macrophage polarization from the pro-inflammatory M1 state to the anti-inflammatory M2 state and suppressed activation of the pro-inflammatory NF-κB signaling pathway observed in ALS-afflicted skeletal muscles. These findings underscore the therapeutic potential of EVs derived from regenerating muscle in alleviating inflammation and enhancing muscle regeneration, offering a promising strategy for treating muscle atrophy associated with ALS.

#### 3.2 Results

#### 3.2.1 Isolation and characterization of CTXD14SkM-EVs

To isolate and enrich CTXD14SkM-EVs, skeletal muscle from 3-month-old wild-type mice were dissected 14 days after acute injury induced by intramuscular injection of CTX. The muscles underwent enzymatic dissociation, filtration, and sequential ultracentrifugation (Figure 3.1A). Nanoflow cytometry was used to assess the concentration and size distribution of these isolated EVs, confirming a size range of 50-200 nm, consistent with reported extracellular vesicles, particularly exosomes (Figure 3.1B). These isolate EVs were then treated with MemGlow dye to label the lipid bilayer,

and nanoflow cytometry-based analysis revealed that around 90% of the particles are fluorescent and lipid-enclosed structures, indicating the high-purity of these EV samples (Figure 3.1C). In addition, the morphological integrity and size of CTXD14SkM-EVs were further identified by TEM (Figure 3.1D).

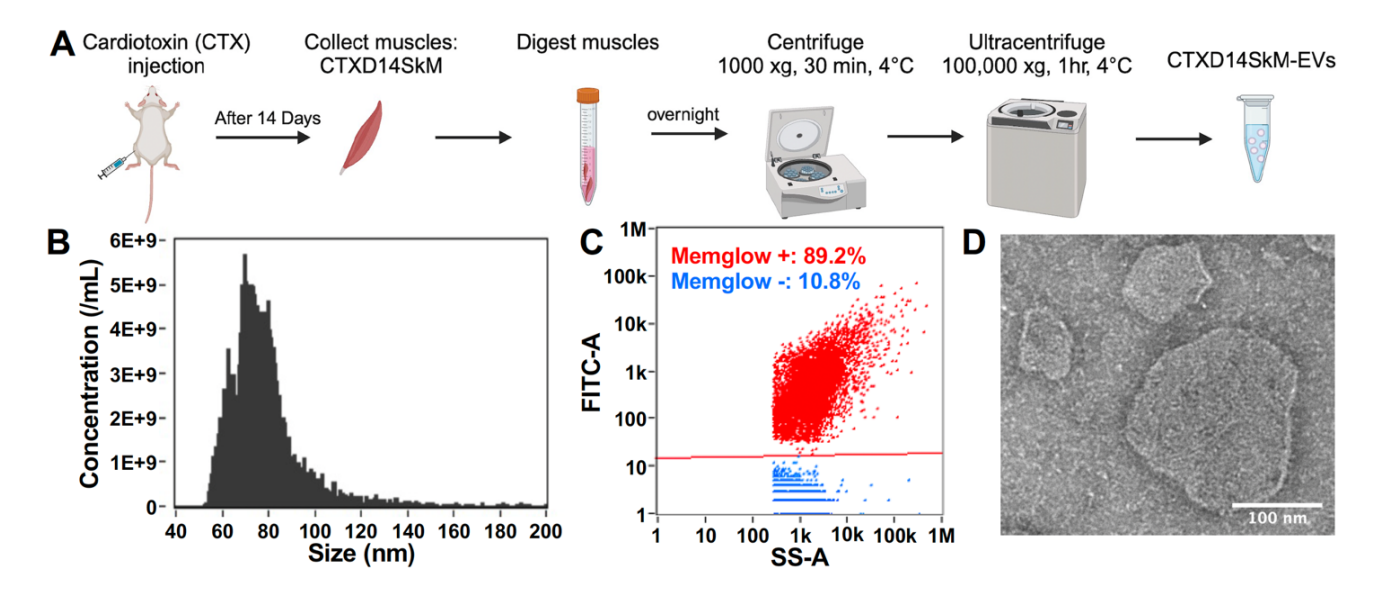
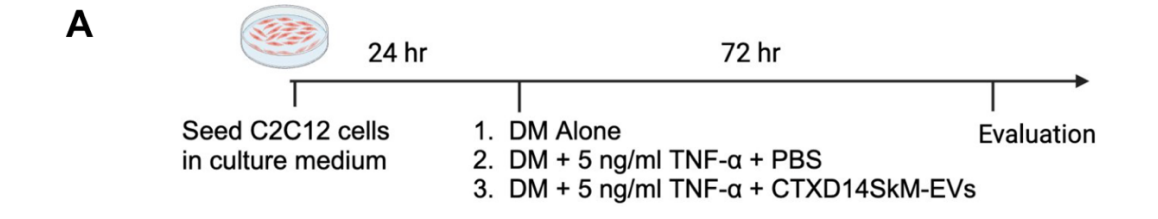


Figure 3.1 Isolation and characterization of CTXD14SkM-EVs. (A) Schematic overview of the isolation process for CTXD14SkM-EVs. (B) Size distribution of EVs. This evaluation performed by Rachel Hankin (C) Memglow staining of EVs: red dots represent the MemGlow-positive population, blue dots represent the MemGlow-negative population. This evaluation performed by Rachel Hankin. (D) Contrast image of CTXD14SkM-EVs sample. Scale bar: 100 μm. This evaluation performed by Yaochao Zheng.

# 3.2.2 CTXD14SkM-EVs promote myoblast differentiation in a cellular muscle atrophy model induced by proinflammatory cytokine TNF-α.

To investigate the therapeutic potential of CTXD14SkM-EVs in mitigating muscle atrophy, we employed a well-established myotube atrophy model using C2C12 myoblasts. This model was induced by TNF-α, a pro-inflammatory cytokine elevated in

ALS and other muscle-wasting disorders. TNF-α is known to impair myogenic differentiation and activate catabolic pathways, including the ubiquitin-proteasome system and NF-kB signaling, leading to the downregulation of essential myogenic markers such as MyoD and myogenin, while promoting the degradation of muscle structural proteins [53-55]. Thus, TNF-α-induced muscle atrophy models are widely used to study muscle degeneration and evaluate therapeutic interventions. In this study, TNFα was administered during C2C12 myoblasts differentiation to inhibit myogenic progression and induce an atrophic state. To assess the protective effects of CTXD14SkM-EVs, these EVs were added concurrently with TNF-α. After 72 hours of treatment, myotubes were immunostained for myosin heavy chain (MHC), a hallmark of mature muscle fibers (Figure 3.2A, B). Our results showed that TNF-α treatment markedly reduced both myoblast differentiation and fusion indices, consistent with its known atrophic effects. Strikingly, CTXD14SkM-EVs treatment significantly rescued both indices under TNF-α-induced condition, indicating a protective effect on myogenic differentiation and myotube formation. These findings highlight the potential of CTXD14SkM-EVs as a therapeutic approach to combat inflammation-driven muscle atrophy (Figure 3.2C, D).



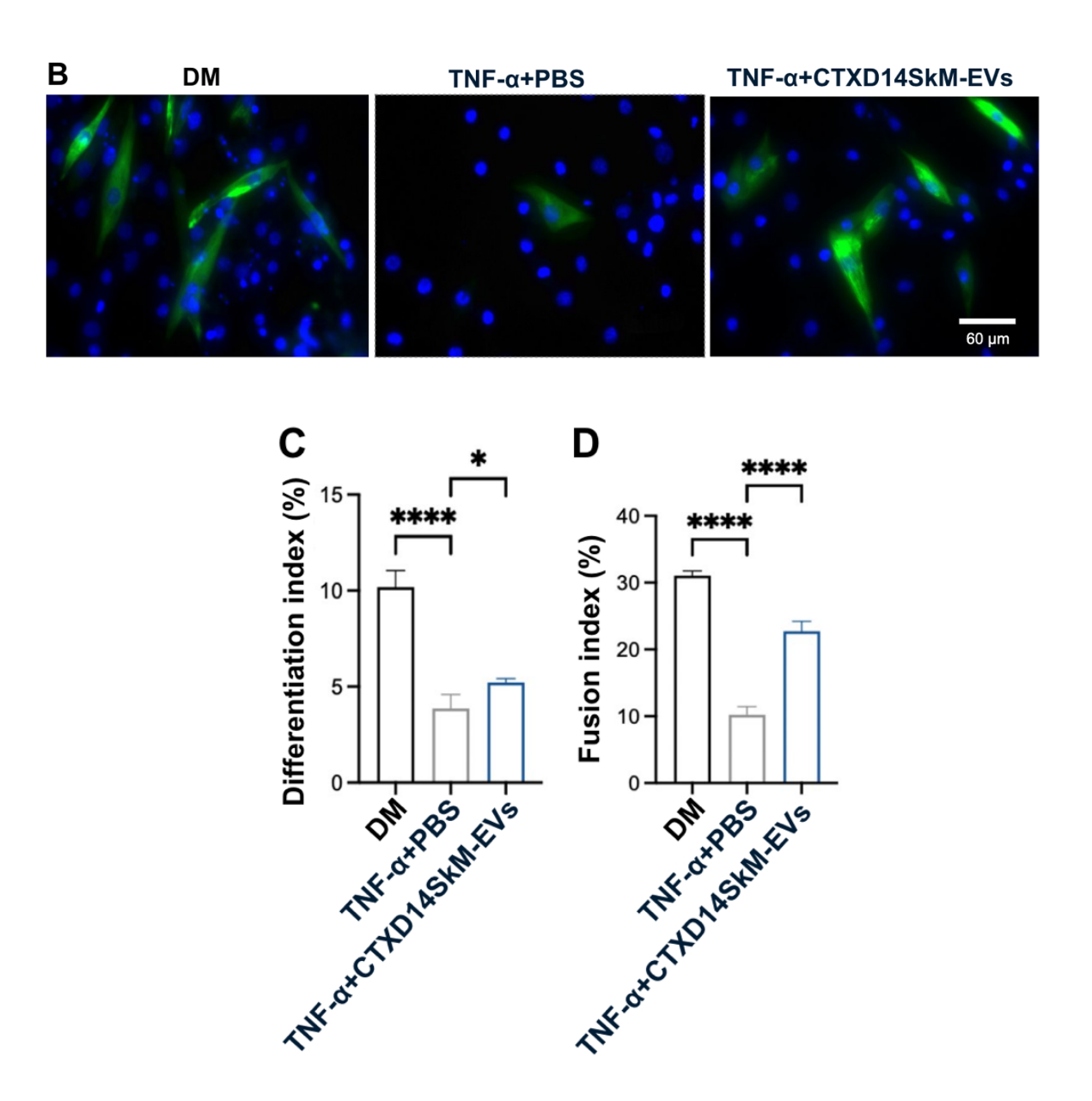


Figure 3.2 CTXD14SkM-EVs Promote Myoblast Differentiation in a cellular muscle atrophy model induced by proinflammatory cytokine TNF-α. (A) Schematic overview of C2C12 differentiation. (B) Immunostaining of MHC (green) and DAPI (blue) of in three groups: differentiation medium only, differentiation medium with 5 ng/mL TNF-α and PBS, differentiation medium with 5 ng/mL TNF-α and CTXD14SkM-EVs. Scale bar: 60 μm. (C) Differentiation index calculated as (number of MHC+ cells/total number of nuclei). (D) The Fusion index calculated as (number of nuclei in MHC+ cells with ≥2 nuclei/total number

of nuclei). The in vitro experiments were repeated three times, and data are reported as means  $\pm$  SEM. \* P  $\leq$  0.05, \*\*\*\* p < 0.0001 by One-way ANOVA.

#### 3.2.3 CTXD14SkM-EVs Alleviate ALS-related Muscle Atrophy in vivo

To assess the therapeutic effects of CTXD14SkM-EVs on mitigating inflammationdriven muscle atrophy in vivo, we utilized a well-established ALS mouse model expressing the human SOD1 protein with the pathogenic missense mutation G93A (SOD1<sup>G93A</sup>) [56]. The SOD1<sup>G93A</sup> mice recapitulate ALS-related muscle atrophy, accompanied by inflammation and impaired muscle regeneration. CTXD14SkM-EVs were intramuscularly injected into the tibialis anterior (TA) and gastrocnemius (GAS) muscles of one limb in SOD1<sup>G93A</sup> mice, while the contralateral limb received PBS as a control. The treatment began at the pre-symptomatic stage (postnatal day 66, P66) and continued weekly until muscle tissues were collected at the late symptomatic stage (P119) for analysis (Figure 3.3A). First, the muscle weight-to-body weight ratios for the TA and GAS muscles were evaluated. Notably, both the TA and GAS muscles treated with CTXD14SkM-EVs exhibited significantly increased muscle weights compared to their PBS-treated counterparts (Figure 3.3B, C). Hematoxylin and eosin (H&E) staining of TA muscle fibres revealed that, as expected, SOD1 G93A mice had smaller muscle fibre crosssectional areas (CSA) compared to wild-type mice. In contrast, the CTXD14SkM-EVs treated group showed increased muscle fibre size and abundant centrally located myonuclei compared to PBS-treated SOD1<sup>G93A</sup> mice (Figure 3.3D). To further investigate CSA distribution, immunostaining for Laminin, a myofiber basement member marker, was performed. TA muscles from the CTXD14SkM-EV-treated group exhibited a reduced proportion of small CSA myofibers and an increased proportion of larger CSA myofibers

compared to the PBS-treated control group (Figure 3.4A, B). The average CSA was significantly greater in the CTXD14SkM-EVs-treated group than in the PBS-treated group (Figure 3.4C, D), indicating that CTXD14SkM-EVs may mitigate muscle atrophy in SOD1<sup>G93A</sup> mice. Furthermore, the percentage of myofibers with centralized nuclei, an indicator of active regeneration, was significantly higher in the CTXD14SkM-EVs-treated group compared to the PBS-treated group, suggesting that CTXD14SkM-EVs may promote muscle stem cell-mediated regeneration (Figure 3.4E). Additionally, the protein level of Myogenin, a myogenic marker linked to the differentiation commitment of muscle stem cells, showed an increasing trend in the EV-treated group TA muscle group, supporting the regenerative potential of CTXD14SkM-EVs (Figure 3.4F, G).

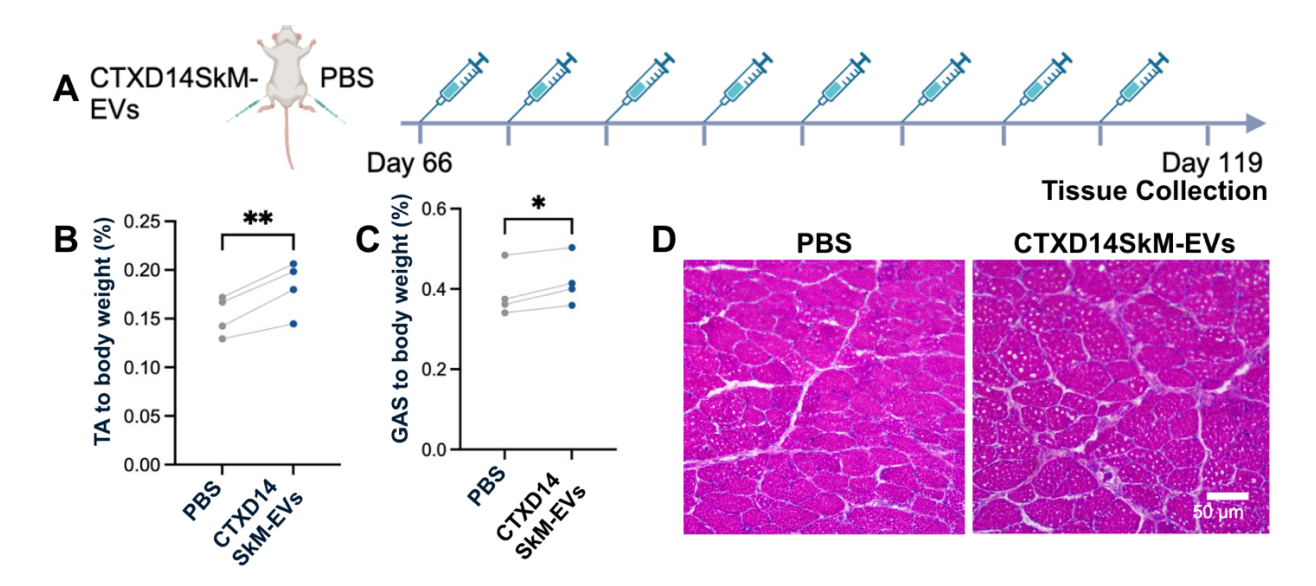
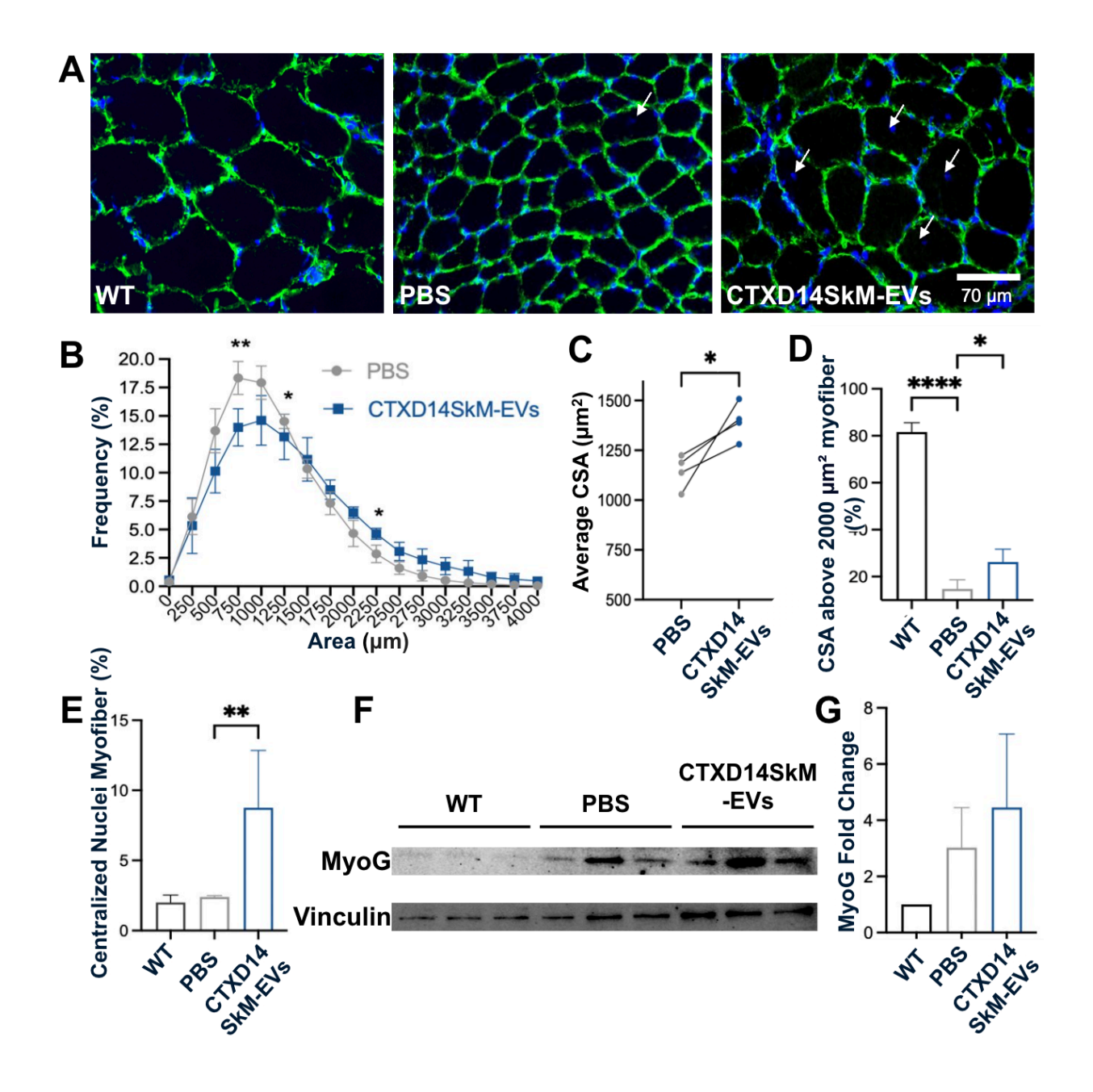


Figure 3.3 CTXD14SkM-EVs Alleviate Muscle Atrophy in SOD1<sup>G93A</sup> Mice. (A) Schematic overview of CTXD14SkM-EVs and PBS treatment in SOD1<sup>G93A</sup> mice. (B) TA muscle weight to body weight ratio (n=4). Paired Student's t-test. \*\*P  $\leq$  0.005. (C) GAS muscle weight to body weight ratio (n=4). Paired Student's t-test. \* P  $\leq$  0.05. (D) H&E staining of TA muscle in two groups: SOD1<sup>G93A</sup> muscle treated with PBS and SOD1<sup>G93A</sup> muscle treated with CTXD14SkM-EVs. Scale bar: 50  $\mu$ m.



**Figure 3.4** CTXD14SkM-EVs Promote Muscle Regeneration in SOD1<sup>G93A</sup> Mice. (A) Immunostaining of Laminin (green) and DAPI (blue) in the three groups: WT muscle (n=3), PBS (n=4), CTXD14SkM-EVs (n=4). Scale bar: 70 μm. White arrows indicate the centralized nuclei. CSA were measured by ImageJ software. (B) Myofiber size distribution in two groups: PBS (gray, n=4) and CTXD14SkM-EVs (blue, n=4). (C) Comparison of

average CSA between PBS and CTXD14SkM-EVs treated groups, analysed by paired Student's t-test. (D) Comparison of the percentage of CSA above 2000  $\mu$ m<sup>2</sup> of among the three groups, analyzed by one-way ANOVA. (E) Percentage of myofibers with central nuclei to total myofibers, analyzed by one-Way ANOVA. (F) Western blot analysis of Myogenin and Vinculin protein levels in WT (n=3), PBS (n=3), and CTXD14SkM-EVs (n=3) groups. (G) Myogenin and Vinculin protein levels among the three groups were quantified using ImageJ software. The protein fold change was evaluated by normalizing Myogenin levels to the housekeeping protein Vinculin. The results were analyzed by one-way ANOVA. \* P  $\leq$  0.05, \*\*P  $\leq$  0.005, \*\*\*\* p < 0.0001.

# 3.2.4 CTXD14SkM-EVs Enhance M2 Macrophage Polarization in ALS-affected Skeletal Muscle

Given the anti-inflammatory microenvironment predominantly driven by M2 macrophages in the skeletal muscles 14 days post-acute injury (CTXD14SkM), we hypothesized that EVs derived from CTXD14SkM would inherit the capacity to promote macrophage polarization towards an anti-inflammatory and pro-regenerative state [48, 50]. To test this hypothesis, we performed immunostaining for M1 and M2 macrophage markers in the GAS muscles of SOD1<sup>G93A</sup> mice treated with either CTXD14SkM-EV or PBS (Figure 3.5A). The results showed that CTXD14SkM-EV treatment significantly increased the proportion of M2 macrophages (CD206+/CD11b+) while reducing the presence of M1 macrophages (iNOS+/CD11b+) compared to PBS treatment (Figure 3.5B, C). These findings indicate that CTXD14SkM-EVs effectively promote the polarization of macrophages toward a pro-regenerative M2 phenotype.

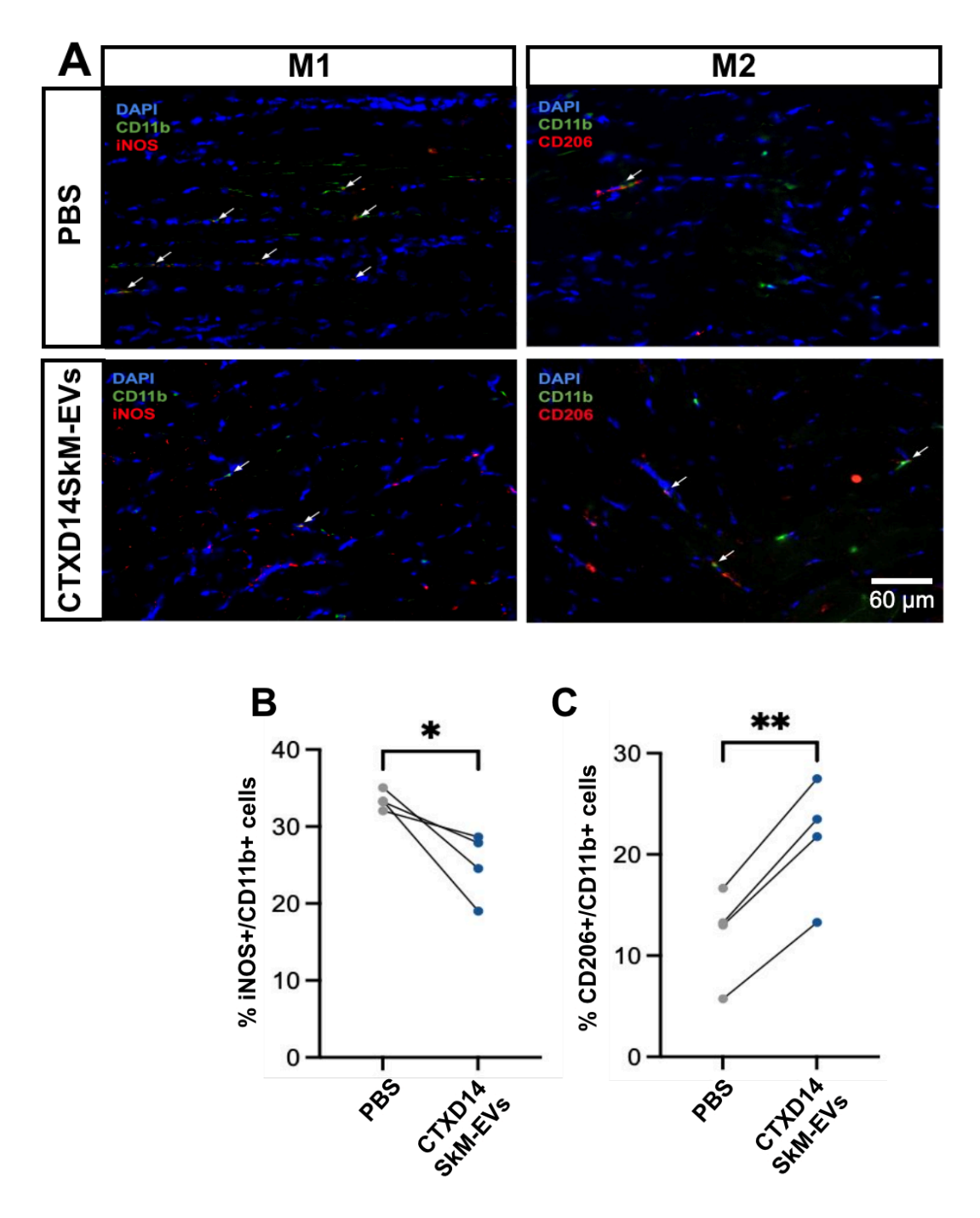
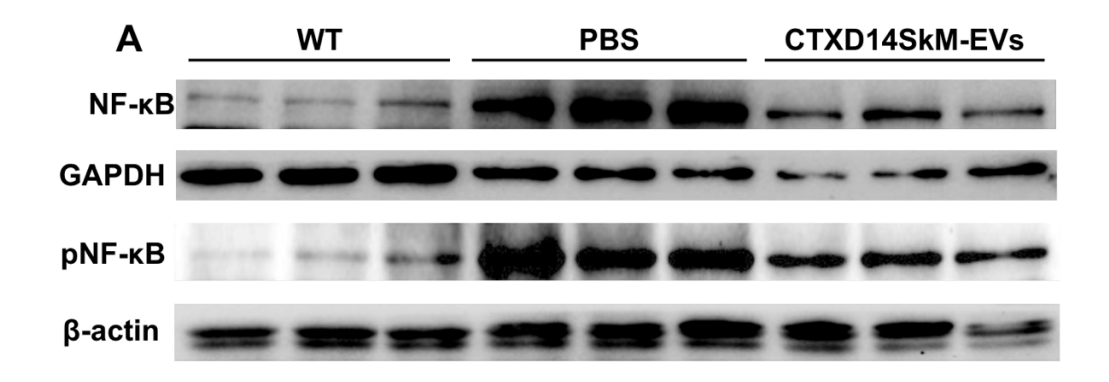


**Figure 3.5** CTXD14SkM-EVs Enhance M2 Macrophage Polarization in ALS-affected Skeletal Muscle. (A) Immunostaining of CD11b (green), iNOS (red), CD206 (red), and DAPI (blue) in GAS muscle sections from PBS (n=4) and CTXD14SkM-EVs (n=4) groups. Scale bar: 60 μm (B) Comparison of the percentage of M1 macrophage

(iNOS+/CD11b+) between the PBS and CTXD14SkM-EVs groups, analysed by paired Student's t-test. (C) Comparison of the percentage of M2 macrophage (CD206+/CD11b+) between the PBS and CTXD14SkM-EVs groups, analysed by paired Student's t-test. \* P  $\leq 0.05$ , \*\*P  $\leq 0.005$ .

# 3.2.5 CTXD14SkM-EVs Suppress NF-κB Pathway Activation in the Skeletal Muscle of ALS Mice

To assess the impact of CTXD14SkM-EVs treatment on NF-κB signaling in the TA muscle of SOD1<sup>G93A</sup> mice, we performed western blot analysis to quantify the expression of total NF-κB, the active phosphorylated format of NF-κB (pNF-κB), and the loading controls GAPDH and β-actin across three experimental groups: wild-type (WT) mice, PBS-treated ALS mice, and CTXD14SkM-EV-treated ALS mice. As expected, both NFκB and pNF-κB protein levels were significantly elevated in the TA muscle of the PBStreated ALS mice compared to the WT group, indicating a heightened inflammatory response in ALS-affected skeletal muscles. Notably, CTXD14SkM-EV treatment markedly downregulated both NF-κB and pNF-κB protein levels in ALS, bringing them closer to baseline levels observed in WT mice (Figure 3.6A, B, C). Meanwhile, the CTXD14SkM-EV-treated group exhibited an increased mRNA expression of key markers associated with M2 macrophage polarization and anti-inflammatory responses, including Interleukin-10 (IL-10), Chitinase-Like Protein 3 (Chil3), and Arginase 1 (Arg1) (Supplement 3.1 A-C). These findings suggest that CTXD14SkM-EV treatment effectively suppresses NF-kB signaling in the skeletal muscle of SOD1<sup>G93A</sup> mice, supporting its potential to mitigate inflammation and muscle atrophy in ALS.



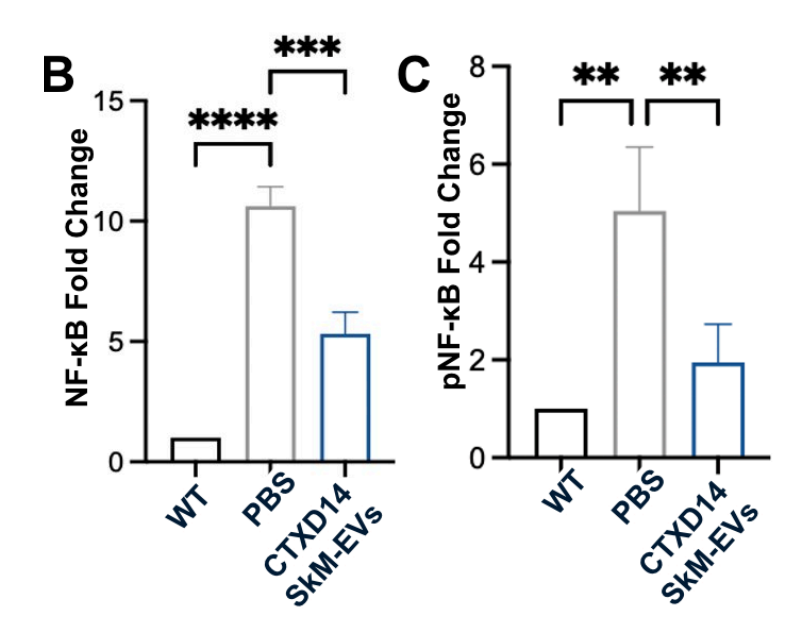
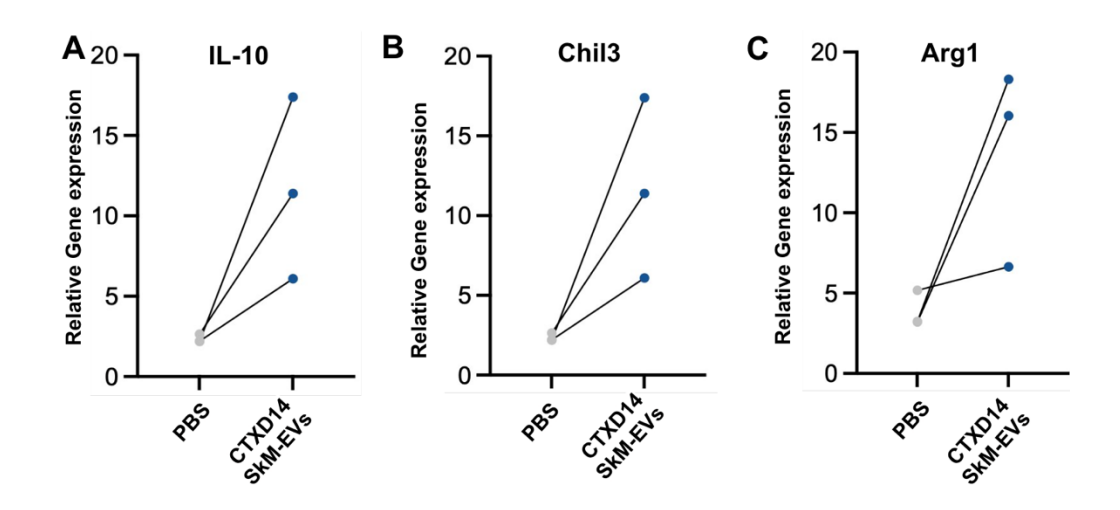


Figure 3.6 CTXD14SkM-EVs Suppress NF-κB Pathway Activation in the Skeletal Muscle of SOD1<sup>G93A</sup> Mice. (A) Western blot analysis of NF-κB, pNF-κB, GAPDH, and β-actin proteins for three groups: WT (n=3), PBS (n=3), and CTXD14SkM-EVs (n=3). (B) Quantification of NF-κB protein levels among the three groups using Image J, statistical analysis by one-way ANOVA. (C) Quantification of pNF-κB protein levels among the three groups using Image J, statistical analysis by one-way ANOVA. \*\*P  $\leq$  0.0001, \*\*\*\* p < 0.0001.



**Supplement 3.1** Transcription levels of M2 macrophage polarization-associated markers. (A–C) mRNA expression levels of IL-10, Chil3, and Arg1 in two groups: WT and CTXD14SkM-EVs (n = 3). Statistical analysis was performed using a paired t-test.

#### 3.3 Discussion

This study explores the therapeutic potential of EVs derived from regenerating skeletal muscle for treating ALS-afflicted muscle atrophy. Most current pharmacological treatments for ALS focus on targeting neuronal deficits, showing limited clinical promise. Given the importance of muscle atrophy in ALS progression and pathogenesis, approaches targeting muscle wasting are of high therapeutic interest. Multiple pathogenic mechanisms are known to be involved in ALS-related motor defects and muscle atrophy, including chronic inflammation, impaired regeneration, proteostasis dysregulation, mitochondrial and metabolic defects. Current therapeutic strategies targeting ALS-afflicted muscle defects often focus on one or few misregulated pathways. Our findings demonstrated that regenerating SkM-derived EVs provide a multifaceted strategy to counter muscle atrophy in an ALS mouse model (SOD1<sup>G93A</sup>) by promoting muscle regeneration, shifting macrophage polarization towards an anti-inflammatory phenotype, and downregulating the pro-inflammatory NF-κB signaling pathway essential for protein

homeostasis. These EVs (CTXD14SkM-EVs) are derived from cells within the regenerating SkM 14 days post-acute injury, the peak phase of regeneration facilitated by the collective activities of residing cells, such as macrophages predominantly in an anti-inflammatory M2 state, activated muscle stem cells, and newly formed muscle fibers. EVs are known to inherit molecular cargos from their sourced cells and mediate regulatory functions in recipient cells. Recently, EVs have been proved to be key mediators of the therapeutic effects of stem cells, instead of stem cell engrafting and differentiation. As expected, the CTXD14SkM-EVs may carry and transfer functional molecules from cells within the regenerating SkM to recipient cells in ALS-afflicted SkM, facilitating an anti-inflammatory and pro-regenerative environment for muscle repair.

In an ALS-like cellular models of muscle wasting, the CTXD14SkM-EVs mitigated the detrimental effects induced by the pro-inflammatory cytokine TNF-α on myoblasts, as evidenced by improved differentiation and fusion indices. Moreover, in vivo, intramuscular administration of CTXD14SkM-EVs alleviated ALS-related muscle atrophy in SOD1<sup>G93A</sup> mice, as indicated by increased muscle mass and muscle fibre size. Meanwhile, a higher percentage of myofibers with centralized nuclei was observed post EV-treatment, suggesting active muscle regeneration. These results suggest that CTXD14SkM-EVs may counteract inflammation-induced muscle wasting by enhancing myoblast function and promoting muscle regeneration.

The anti-inflammatory properties of CTXD14SkM-EVs were further supported by their ability to modulate macrophage polarization and regulate NF-kB signaling. In ALS-affected skeletal muscle, chronic inflammation involves a disrupted transition of macrophages from the pro-inflammatory M1 phenotype, which clears debris and

damaged tissue, to the anti-inflammatory M2 phenotype, which promotes muscle regeneration and tissue repair. This prolonged pro-inflammatory state may not only impair muscle stem cell function for regeneration but also exacerbate muscle protein breakdown, leading to muscle atrophy [57, 58]. CTXD14SkM-EVs effectively promoted a phenotypic shift in macrophages from the M1 to M2 phenotype in ALS-affected SkM. This shift may may alleviate the inflammatory burden and create a more favorable microenvironment for muscle regeneration and repair. As such, CTXD14SkM-EVs hold significant potential as modulators of immune responses in ALS therapy. In addition to modulating macrophage populations, CTXD14SkM-EVs also significantly suppressed the excessive activation of the NF-kB pathway in ALS skeletal muscles. Specifically, they downregulated the expression of both NF-κB and its phosphorylated form (pNF-κB) in the skeletal muscles of SOD1<sup>G93A</sup> mice. Persistent activation of NF-kB in ALS muscle is associated with elevated inflammation, increased proteolytic activity, reduced expression of myogenic regulatory factors, and impaired muscle regeneration, collectively driving muscle atrophy [44, 45]. Thus, targeting NF-kB signaling represents a promising therapeutic strategy to attenuate inflammation and mitigate muscle atrophy in ALS. By downregulating NF-kB signaling, CTXD14SkM-EVs may interrupt these pathogenic cascades, thereby reducing chronic inflammation, enhancing myogenic differentiation, and decreasing protein degradation. Together, these therapeutic effects contribute to muscle repair and functional recovery in ALS.

This study demonstrates that CTXD14SkM-EVs possess therapeutic potential to mitigate ALS-related muscle atrophy, providing valuable insights into leveraging EVs derived from regenerating skeletal tissue to address multiple pathogenic processes

underlying muscle degeneration. These findings lay a strong foundation for developing EV-based therapies targeting muscle atrophy in ALS, which could complement therapeutic strategies focusing on neuroprotection. Future research should prioritize identifying the molecular cargo within CTXD14SkM-EVs responsible for these therapeutic effects, as well as optimizing delivery and dosing strategies to enhance their efficacy in treating ALS and other muscle-wasting diseases.

#### 3.4 Materials and Methods

#### 3.4.1 Animals and treatment

Experiments were conducted using transgenic mice overexpressing human SOD1 with a Gly93-Ala mutation (SOD1<sup>G93A</sup>) (strain designation B6SJL–TgN[SOD1–G93A]1Gur, stock number 002726) and wild-type (WT) B6SJL mice, both obtained from Jackson Laboratories (Bar Harbor, ME, USA). All animals were maintained in a controlled environment under standard laboratory conditions. Five SOD1<sup>G93A</sup> mice received an intramuscular injection of about  $4.4 \times 10^9$  CTXD14SkM-EVs suspended in 20 µL PBS into the tibialis anterior (TA) and gastrocnemius (GAS) muscles of one limb. As a control, 20 µL of PBS was injected into the TA and GAS muscles of the opposite limb. Treatments were administered weekly, beginning at the pre-symptomatic stage (day 66), with muscle tissue collected at the late symptomatic stage (day 119).

#### 3.4.2 CTXD14SkM-EVs Isolation

To isolate CTXSkM-EVs from acutely injured skeletal muscle, cardiotoxin (CTX) (10  $\mu$ M, 20  $\mu$ L) was injected intramuscularly into the TA and GAS muscles of approximately 2-month-old WT mice. Fourteen days post-injury, the TA and GAS muscles were harvested and sectioned into 2-3 mm pieces using a scalpel. The sliced muscles

were then placed in a digestion solution containing 2 mg/mL Collagenase Type II (Worthington-Biochem, Cat#LS004176) in DMEM with 100 U/mL Penicillin/Streptomycin (P-S) (Gibco, Cat#15140122), with 500 μL used for each TA muscle and 1 mL for each GAS muscle. The tissue was rotated in the digestion solution at 37°C for 24 hours. After digestion, the tissue mixture was centrifuged at 1,000 xg for 30 minutes at 4°C, and the supernatant was collected and filtered through a 0.8 μm filter (Millipore, Cat#SLAAR33SS). CTXD14SkM-EVs were then isolated from the filtered supernatant by ultracentrifugation using ultracentrifugation tubes (Fisher Scientific, Cat#45-239) at 100,000 xg for 1 hour at 4°C. The resulting EV pellet was resuspended in PBS and stored at -80°C until use.

#### 3.4.3 MemGlow assessment

The size and concentration of the isolated EVs were assessed using nano-flow cytometry on the Flow NanoAnalyzer (NanoFCM, Xiamen, China). To determine the proportion of particles with a lipid membrane, the EVs (around 2.4 × 10^8 EVs diluted in 1 mL PBS) were stained with 2 nM MemGlow 488 (Cytoskeleton, Denver, CO), a fluorogenic membrane probe, for 10 minutes. Fluorescence was then measured using the Flow NanoAnalyzer. The EV size and concentration were measured at the same dilution using the Flow NanoAnalyzer to ensure consistency. Two mice (both TA and GAS muscles) were used to isolate CTXD14SkM-EVs, with a total yield of approximately 5× 10^11 EVs per mouse.

#### 3.4.4 C2C12 Differentiation

C2C12 myoblast, obtained from XX, were cultured in Dulbecco's Modified Eagle Medium (DMEM; Invitrogen) supplemented with 10% FBS and 100 U/mL P-S. Cells were

maintained at 37°C in a humidified incubator with a 5%  $CO_2/95\%$  air atmosphere. C2C12 cells were seeded at 100,000 cells per well in the 24-well plate with growth medium. After 24 hours, the growth medium was replaced into differentiation medium (DMEM supplemented with 2% horse serum and 100 U/mL P-S) to initiate differentiation. Three treatment conditions were applied: (1) differentiation medium only, (2) differentiation medium with 5 ng/ml TNF- $\alpha$  and PBS, (3) differentiation medium with 5 ng/mL TNF- $\alpha$  and approximately 1.8 × 10^8 CTXD14SkM-EVs. After 3 days of treatment, cells were evaluated for myosin heavy chain (MHC) expression.

#### 3.4.5 Immunostaining of cells

C2C12 were fixed with 4% paraformaldehyde (PFA) for 10 minutes at room temperature, followed by permeabilization with 0.1% Triton X-100 in PBS. Cells were then blocked in 10% FBS in PBS for 1 hour at room temperature. The primary antibody, MF20 (Developmental Studies Hybridoma Bank, DSHB), was diluted in a blocking buffer and applied overnight at 4°C. The following day, cells were washed three times with PBS to remove any excess primary antibody. A secondary antibody, donkey anti-mouse (Abcam, Cat# ab150108) diluted in PBS, was then applied for 1 hour at room temperature. After incubation, cells were washed three additional times with PBS, and DAPI was applied for nuclear counterstaining. Fluorescence images were captured using a fluorescence microscope.

#### 3.4.6 Histology

TA muscle tissues were embedded in OCT compound and frozen. Cryosections (10 µm) were prepared, mounted on glass slides, and air-dried. Sections were fixed in 4% PFA for 10 minutes, rinsed in PBS, and stained with hematoxylin (Harris, Sigma, Cat

No. HHS32) for 1 minute. After rinsing, sections were stained with eosin (Sigma, Cat No. HT110316) for 30 seconds, followed by a brief wash in distilled water. Slides were then dehydrated through graded ethanol concentrations, cleared with xylene, and coverslipped with a permanent mounting medium. Images were captured using a light microscope.

#### 3.4.7 Immunohistochemistry of Skeletal Muscle

TA muscle tissues were embedded in OCT, frozen, and cryosectioned at 10 µm thickness. Sections were mounted on glass slides, air-dried, and fixed with 4% PFA for 10 minutes, followed by PBS rinses. Tissues were permeabilized with 0.1% Triton X-100 in PBS for 10 minutes, then blocked in 10% fetal bovine serum (FBS) in PBS for 1 hour at room temperature. Primary antibody against Laminin (Sigma-Aldrich, Cat# L9393, 1:1000) was applied in the blocking buffer and incubated overnight at 4°C. The next day, sections were washed in PBS and incubated with fluorophore-conjugated secondary antibodies in PBS for 1 hour at room temperature in the dark. After final PBS washes, sections were mounted with an antifade mounting medium containing DAPI for nuclear counterstaining. Images were captured using a fluorescence microscope. For M1/2 macrophage staining, longitudinal section of GAS muscle, 20 µm thick, were collected and fixed in 4% PFA for 10 minutes. Tissues were then permeabilized with 0.1% Triton X-100 in PBS for 10 minutes, followed by blocking in the solution of 10% FBS and 0.1% Triton X-100 in PBS for 1 hour at room temperature. Primary antibodies anti-CD11b (eBioscience, Cat#14-0112-81, 1:100), iNOS (Bio-Techne, Cat#NB300-605SS, 1:200), and anti-mannose receptor (Abcam, Cat#ab64693, 1:1000), were prepared in the blocking buffer and applied to the tissue sections, which were incubated overnight at 4°C. The following day, sections were washed with PBS and incubated with fluorophoreconjugated secondary antibodies: Alex Fluor 488 anti-Rat (Invitrogen, Cat#53-4031-80, 1:1000) and Alex Fluor 594 anti-Rabbit (abcam, Cat#ab150080, 1:1000) for 1 hour at room temperature in the dark. Finally, images were captured using a fluorescence microscope.

#### 3.4.8 Western Blotting

Collected TA muscle samples were lysed in RIPA buffer supplemented with phosphatase and protease inhibitors. Proteins were separated via SDS-PAGE gel, transferred onto PVDF membranes, blocked with 5% FBS in PBST (PBS with 0.1% Tween 20) for 1 hour, and then incubated overnight at 4 °C with primary antibodies: anti-Myogenin (Invitrogen, Cat#PA5-87235, 1:1000), anti-NF-κB p65 (Cell Signaling Technology, Cat#8242, 1:1000), anti-Phospho-NF-κB p65 (Cell Signaling Technology, Cat#3033, 1:1000), anti-beta-actin (Cell Signaling, Cat#4970S, 1:1000), anti-Vinculin (Cell Signaling, Cat#2148S, 1:1000), and anti-GAPDH (Cell Signaling, Cat#97166T, 1:1000). Membranes were then incubated with HRP-conjugated anti-Rabbit IgG (H+L) secondary antibody (Promega, Cat#W4011, 1:10,000) or HRP-conjugated anti-Mouse IgG (Cell Signaling, Cat#7076S, 1:10,000) for 1 hour at room temperature. Protein bands were revealed using an WesternBright enhanced chemiluminescent system (ECL, Fisher Scientific, Cat#NC0930892). Imaged were acquired by using ChemiDoc™ MP imaging system (Bio-Rad) and analysed by ImageJ software.

#### 3.4.9 RNA extraction and real-time PCR

Total RNA was extracted from TA muscle using the TRIzol-chloroform method. Tissue samples were homogenized in 500  $\mu$ L TRIzol until fully lysed, followed by a 5-minute incubation at room temperature. After adding 125  $\mu$ L chloroform and vigorous

shaking, the samples were incubated for 5 minutes and centrifuged at 10,000 rpm for 5 minutes to separate phases. The RNA-containing aqueous layer (~250 µL) was carefully collected and precipitated with 275 µL isopropanol, incubated for 5 minutes, and centrifuged at 14,000 rpm for 20 minutes at 20°C. The RNA pellet was washed twice with 75% ethanol, centrifuged at 9,500 rpm, and air-dried before being resuspended in 30 µL DNase/RNase-free water. Subsequently, 500 ng of total RNA was reverse transcribed into complementary DNA (cDNA) using the GoScript Reverse Transcriptase kit (Promega, Cat#A5003). Quantitative real time-PCR (qRT-PCR) was performed to meaasure messenger RNA (mRNA) expression of IL-10 (forward primer: TGGACAACATACTGCTAACCGAC, reverse primer: CCTGGGGCATCACTTCTACC), Chil3 (forward primer: TTTCTCCAGTGTAGCCATCCTT, reverse primer: TCTGGGTACAAGATCCCTGAA), (forward and Arg1 primer: CTCCAAGCCAAAGTCCTTAGA, reverse primer: AGGAGCTGTCATTAGGGACATC), with GAPDH (forward primer: CACCATCTTCCAGGAGCGAG, reverse primer: CCTTCTCCATGGTGGAAGAC) as the endogenous control. qRT-PCR was conducted on a 7300 Real-Time PCR system (Applied Biosystems) using the Tribo 2x SYBR qPCR Super Mix Lox Rox (Cat#TBS4001LR-20).

#### 3.4.10 Statistical Analysis

Data were analysed using GraphPad Prism version 10.0 (GraphPad Software). A two-tailed, unpaired Student's Paired t-test was used for comparisons between two treatment groups. For comparisons among more than two groups with a single variable, one-way ANOVA followed by Tukey's post-hoc test was applied for multiple comparisons.

All data are presented as mean  $\pm$  standard error of the mean (SEM). Statistical significance was set at \* P  $\leq$  0.05, \*\*P  $\leq$  0.005, \*\*\* p < 0.0001, \*\*\*\* P  $\leq$  0.0001

### **CHAPTER 4**

# SYNERGIZED THERAPEUTIC EFFICACY OF EXTRACELLULAR VESICLES FROM REGENERATING SKELETAL MUSCLE AND NEURAL STEM CELLS IN AN ALS MOUSE MODEL<sup>4</sup>

\_

<sup>&</sup>lt;sup>4</sup>Gao, J., Zheng, Y., Sikal, A., Hankin, R., Sterling, E., Heo, J., Call, J., Chan, K., Rather, K., Yousuf, H., Streleckis, A., Yao, Y. Synergized Therapeutic Efficacy of Extracellular Vesicles from Regenerating Skeletal Muscle and Neural Stem Cells in an ALS Mouse Model. To be submitted to a peer-reviewed journal.

#### **Abstract**

Amyotrophic lateral sclerosis (ALS) is a devastating neuromuscular disease characterized by motor neuron degeneration and muscle atrophy, with no effective treatments currently available. Increasing evidence highlights skeletal muscle actively contributes to ALS progression through retrograde signaling to the central nervous system (CNS). In this study, we establish skeletal muscle as a therapeutic target for ALS and investigate the potential of extracellular vesicles (EVs) derived from regenerating muscle as a novel intervention. Specifically, we examine EVs derived from cardiotoxin (CTXSkM-EVs), (CTX)-induced regenerating skeletal muscle muscle-resident fibro/adipogenic progenitors (CTXFAP-EVs), and neural stem cells-derived EVs (NSC-EVs). Our findings demonstrate that CTXSkM-EVs and CTXFAP-EVs promote myogenesis in atrophic muscle cells, suggesting their broader therapeutic potential for muscle atrophic diseases. Additionally, these EVs enhance cell viability and alleviating mitochondrial dysfunction in ALS-like motor neurons, further supporting their role in muscle and neuronal protection. Furthermore, we introduce a novel mixed EV-based therapeutic strategy that combines NSC-EVs with either CTXSkM-EVs or CTXFAP-EVs, which effectively mitigates muscle atrophy in vivo, likely by promoting muscle regeneration and suppressing NF-kB signaling in ALS-affected skeletal muscle. Notably, this combination strategy also modulates NF-kB signaling in the spinal cord, suggesting a potential neuroprotective effect. These findings provide the first evidence that regenerative muscle-derived EVs offer a viable therapeutic strategy for ALS and propose a dual-targeted EV therapeutic strategy of mitigating both skeletal muscle degeneration

and CNS pathology. This study provides insights for further translational research into EV-based interventions for ALS and other neuromuscular diseases.

#### 4.1 Introduction

Amyotrophic lateral sclerosis (ALS) is a devastating neurodegenerative disease characterized by motor neuron degeneration and muscle atrophy, with no effective treatments currently available. The disease typically leads to death within 2-5 years post-diagnosis [38]. ALS is a multisystem disorder that affects both the central nervous system (CNS) and skeletal muscles, driven by complex pathological mechanisms such as neuroinflammation, mitochondrial dysfunction, and impaired protein homeostasis [5, 59]. These interconnected pathologies create a vicious cycle of motor neuron and skeletal muscle degeneration, accelerating disease progression and posing significant challenges for therapeutic development.

While ALS treatment has traditionally focused on preserving motor neurons, emerging evidence suggests skeletal muscle as an active player in disease progression, including retrograde pathogenic signaling to the CNS. Mitigating skeletal muscle atrophy can effectively slow disease progression and extend survival in ALS animal models, highlighting skeletal muscle as a promising but largely overlooked therapeutic target [60, 61]. Here, we explored extracellular vesicle (EV)-based therapies as a novel and multifaceted strategy to counter skeletal muscle degeneration and modulate neuroinflammatory pathways in the spinal cord for ALS treatment.

EVs are nanosized, lipid bilayer-enclosed vesicles secreted by most cell types, carrying bioactive molecules such as nucleic acids, proteins, and lipids. As key mediators of intercellular communication, EVs participate in a wide range of physiological processes

and have emerged as a promising cell-free therapeutic approach with high bioavailability and low immunotoxicity [62]. In this study, we explored the therapeutic potential of EVs derived from regenerating skeletal muscle cells and neural stem cells (NSCs) in ALS models. NSC-derived EVs (NSC-EVs) were chosen for their well-documented antiinflammatory and neurotrophic properties in preclinical models of neurodegenerative diseases, such as Alzheimer's disease, Parkinson's disease, and Stroke [15, 63, 64]. Meanwhile, EVs derived from cardiotoxin (CTX)-induced regenerating skeletal muscle (CTXSkM-EVs) were selected based on recent findings that early-stage regenerating skeletal muscle secretes EVs enriched with bioactive molecules that modulate gene expression and recipient cell activities, thereby fostering a promising microenvironment for muscle repair [65]. To further evaluate and elucidate the therapeutic effects within this EV pool, we specifically examined both CTXSkM-EVs, representing the total EV population from regenerating skeletal muscle, and CTXFAP-EVs, derived from fibro/adipogenic progenitors (FAPs), a key mesenchymal stem cell population involved in muscle regeneration. During the early phase of skeletal muscle regeneration, FAPs reach peak amount three days post-acute injury and secrete factors that coordinate muscle regeneration by interacting with satellite cells and immune cells [65, 66]. By isolating and investigating CTXFAP-EVs within the broader CTXSkM-EV pool, we aimed to gain deeper insight into the specific contributions of different muscle-derived EV subpopulations to ALS therapy.

The results demonstrated that CTXSkM-EVs and CTXFAP-EVs significantly enhanced myogenic differentiation and fusion in a cellular muscle atrophy model. Furthermore, both EV types improved the viability of ALS-like motor neurons under

oxidative stress in vitro, likely by restoring mitochondrial function. In vivo, intravenous administration of NSC-EVs, along with intramuscular delivery of either CTXSkM-EVs or CTXFAP-EVs, mitigated muscle atrophy and promoted muscle regeneration in an established ALS mouse model. In addition, downregulation of aberrantly activated inflammatory NF-kB signaling was observed in both ALS-affected muscle and spinal cord tissues following EV treatment, suggesting a potential neuroprotective effect that extends beyond skeletal muscles [67, 68]. Collectively, these findings provide the first evidence that EVs derived from early-stage regenerating skeletal muscle, particularly those from FAPs, play a critical role in mitigating ALS-associated muscle atrophy. This study also establishes the feasibility of a dual-targeted EV-based therapeutic strategy that addresses both skeletal muscle degeneration and spinal cord neuroinflammatory, offering a novel treatment for ALS and potentially other neuromuscular diseases.

#### 4.2 Results

#### 4.2.1 Isolation and Characterization of CTXSkM-EVs and CTXFAP-EVs

To isolate and enrich EVs from regenerating skeletal muscle, tibialis anterior (TA) and gastrocnemius (GAS) muscles were dissected from 3-month-old wild-type mice three days after cardiotoxin (CTX)-induced acute injury. CTX, a snake venom toxin commonly used to induce acute muscle damage, triggers the muscle regeneration process [69, 70]. EVs were enriched from these regenerating muscles through using a combination of serial enzymatic digestion and ultracentrifugation (Figure 4.1A). The isolated EVs were observed under transmission electron microscope (TEM) (JEM-1011, JEOL, Japan), providing nanoscale visualization of their morphology (Figure 4.1B). Additionally, the concentration and size distribution of the CTXSkM-EVs were evaluated using nanoflow

cytometry (Figure 4.1C). The purity of the isolated CTXSkM-EVs population was approximately 90%, as determined by treatment with MemGlow dye. This dye labels the lipid bilayer, enabling high-resolution fluorescence-based detection (Figure 4.1D). Within the EV pool from early-stage regenerating skeletal muscle, EVs derived from muscleresident mesenchymal progenitors, known as FAPs, exhibit the potential to contribute to the muscle repair process. This is attributed to the functional interactions of FAPs with muscle stem cells (satellite cells) and inflammatory cells, which collectively drive muscle regeneration following acute injury [71]. Upon activation by acute injury, FAPs release paracrine factors that promote satellite cell-mediated muscle repair [72]. Based on this, we further investigated the effects of EVs from activated FAPs on muscle atrophy in the context of ALS. Firstly, FAPs were collected from the skeletal muscle of wild-type mice three days post-CTX injection (referred to as CTXFAPs), a time point corresponding to their peak proliferation and the critical regenerative window [66]. CTXFAPs were isolated using magnetic-activated cell sorting (MACS), which is a highly selective method for sorting cell populations based on surface markers (Figure 4.1E). Following sorting, the identity and purity of the CTXFAPs were confirmed by immunostaining for platelet-derived growth factor receptor alpha (PDGFRα), a well-established marker for FAPs, and costaining with myosin heavy chain (MHC), the majority muscle myofiber protein present in skeletal muscle. The results showed over 90% purity of the isolated FAPs, confirming the effectiveness of the sorting method (Figure 1F). After expanding the CTXFAPs for around one week, EVs derived from these cells (CTXFAP-EVs) were collected (Figure 4.1E). Their concentration and size distribution were assessed by nanoflow cytometry to ensure consistent EV characteristics (Figure 4.1G). Furthermore, the purity of the CTXFAP-EVs

was validated using MemGlow dye staining, which indicated a highly pure EV population, consistent with the earlier observations (Figure 4.1H).

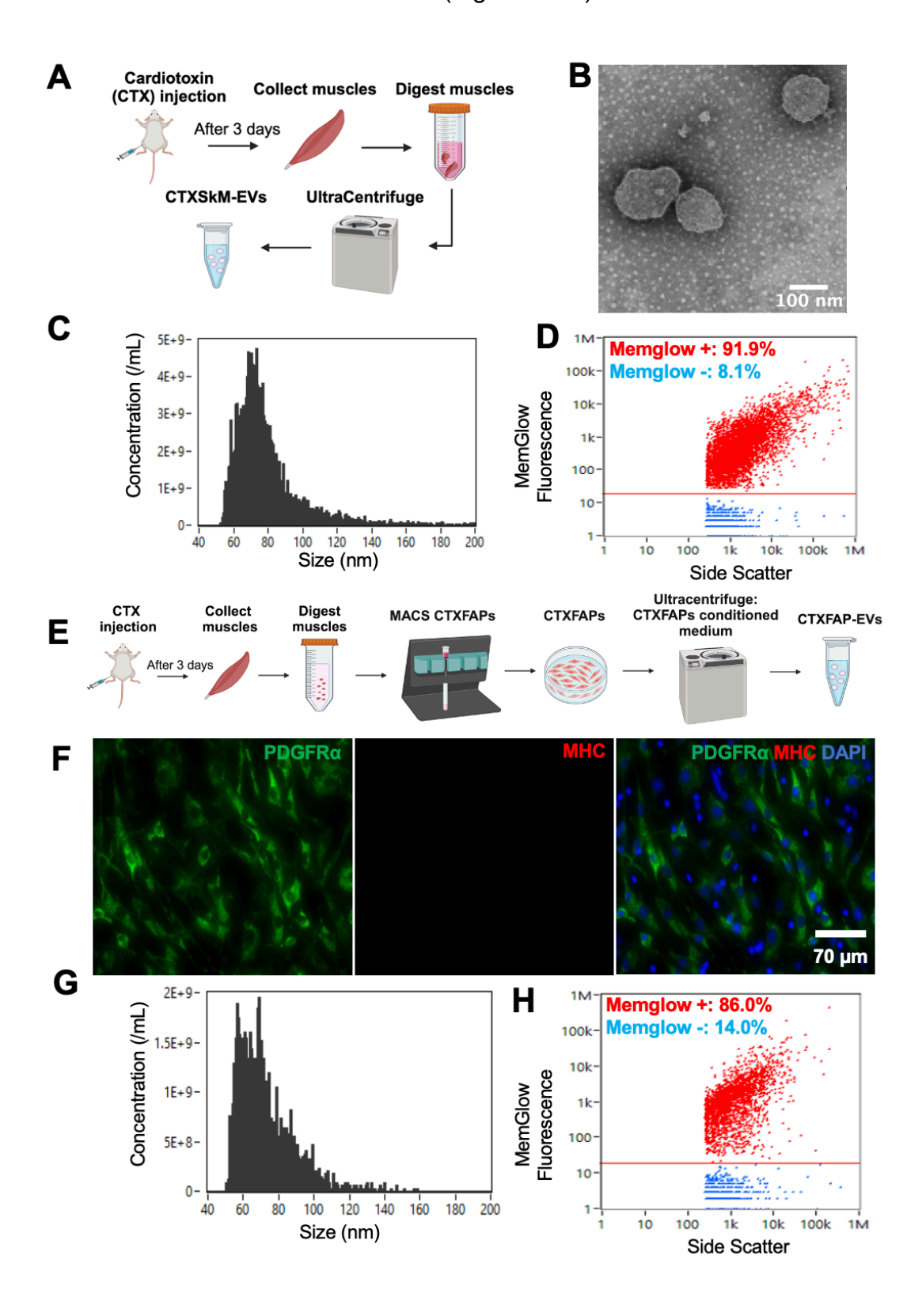
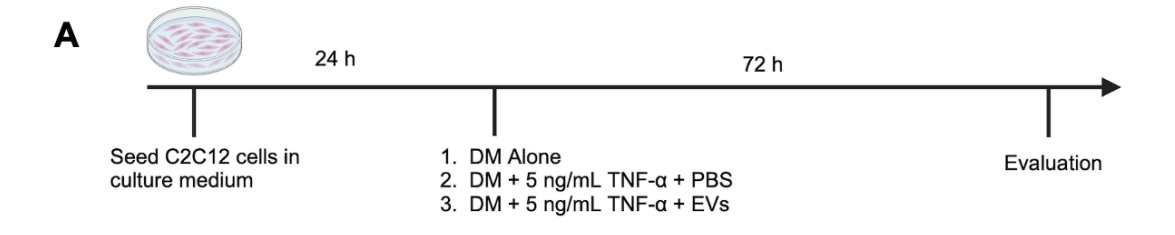


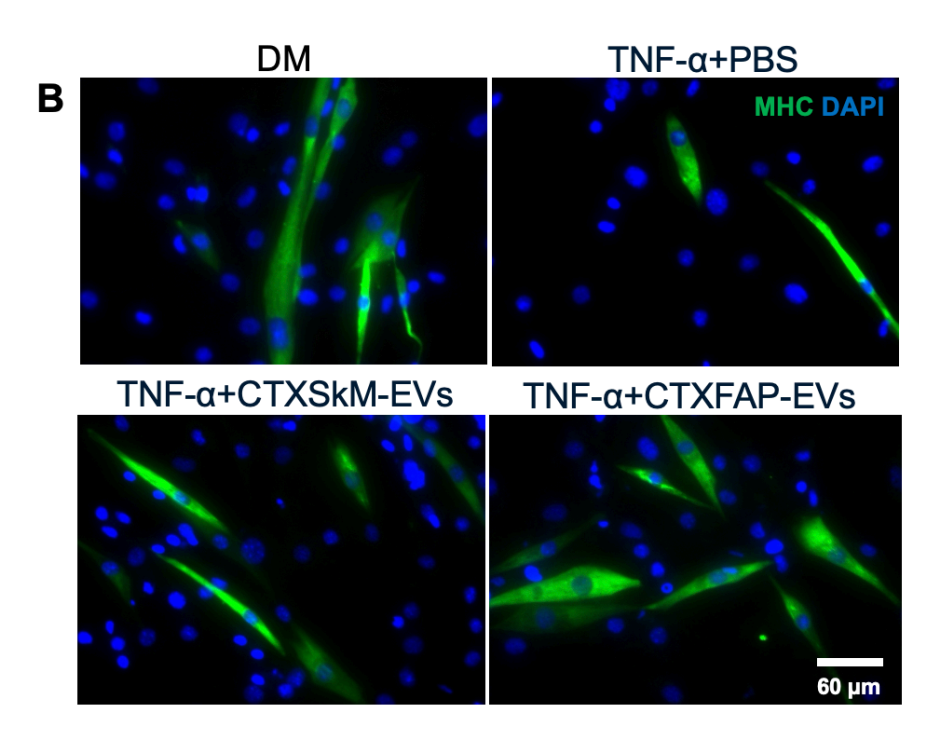
Figure 4.1 Isolation and Characterization of CTXSkM-EVs and CTXFAP-EVs. (A) Schematic overview of the isolation process for CTXSkM-EVs. (B) Contrast image of isolated EVs samples. Scale bar: 100 μm. This test performed by Yaochao Zheng. (C) Size distribution profile of CTXSkM-EVs. This evaluation performed by Rachel Hankin. (D) MemGlow staining of CTXSkM-EVs: red dots indicate MemGlow-positive EVs, blue dots indicate MemGlow-negative EVs. This evaluation performed by Rachel Hankin. (E) Schematic overview of the isolation process for CTXFAP-EVs. (F) Immunostaining of isolated FAPs showing PDGFRα (green), MHC (red) and DAPI (blue) markers. (G) Size distribution profile of CTXFAP-EVs. This evaluation performed by Rachel Hankin. (H) MemGlow staining of CTXFAP-EVs: red dots indicate MemGlow-positive EVs, blue dots indicate MemGlow-negative EVs. This evaluation performed by Rachel Hankin.

# 4.2.2 CTXSkM-EVs and CTXFAP-EVs Enhance C2C12 Differentiation in the Presence of Pro-Inflammatory Cytokine TNF-α

To investigate the therapeutic potential of CTXSkM-EVs and CTXFAP-EVs in mitigating muscle atrophy, we employed a well-established TNF- $\alpha$ -induced myotube atrophy model using C2C12 myoblasts. TNF- $\alpha$ , a pro-inflammatory cytokine elevated in ALS, is known to impair myogenic differentiation and activate catabolic pathways, including the ubiquitin-proteasome system and Nuclear factor kappa B (NF- $\kappa$ B) signalling [73, 74]. These pathways not only suppress essential myogenic markers such as MyoD and myogenin but also promote the degradation of muscle structural proteins, contributing to muscle wasting [75]. As such, TNF- $\alpha$  -induced myotube atrophy models are widely used to study the mechanisms underlying muscle atrophy and to evaluate potential therapeutic interventions. In this study, we assessed the protective effects of CTXSkM-

EVs and CTXFAP-EVs on TNF-α-induced atrophy to determine their capacity to preserve myotube integrity and function (Figure 4.2A). After 72 hours of treatment, myotubes were immunostained for myosin heavy chain (MHC), a key marker of myoblast differentiation into mature muscle fibres (Figure 4.2B). The results demonstrated that TNF-α treatment significantly reduced both the differentiation and fusion indices of myoblasts. Notably, treatment with CTXSkM-EVs and CTXFAP-EVs significantly restored these indices under TNF-α-induced conditions (Figure 4.2C, D). This experiment demonstrates the protective effects of CTXSkM-EVs and CTXFAP-EVs on myogenic differentiation and myotube formation. These findings underscore the potential of these EVs as a promising therapeutic strategy to counteract inflammation-driven muscle atrophy.





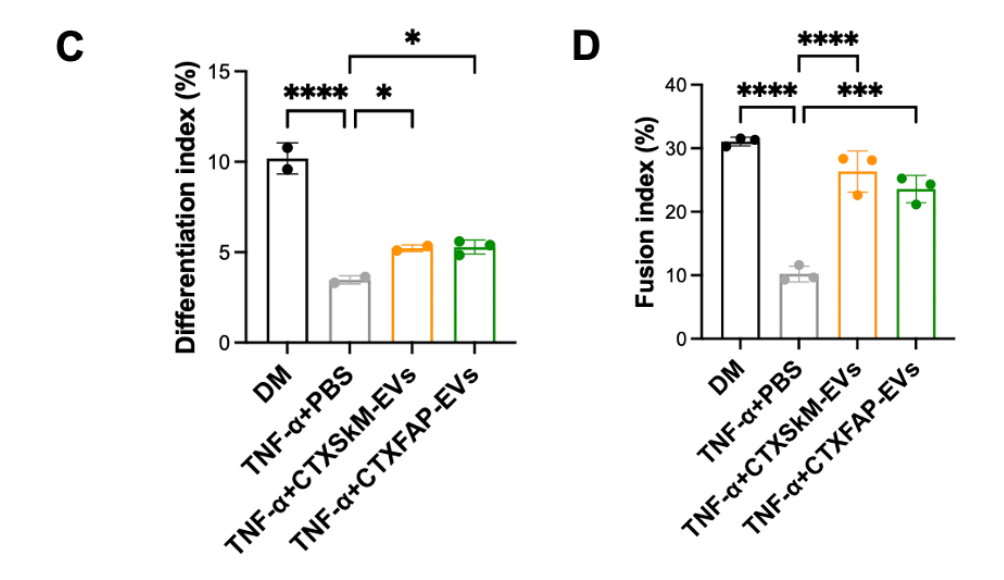


Figure 4.2 CTXSkM-EVs and CTXFAP-EVs Enhance C2C12 Differentiation in the Presence of Pro-Inflammatory Cytokine TNF-α. (A) Schematic overview of C2C12 differentiation. (B) Immunostaining of MHC (green) and DAPI (blue) in four treatment groups: differentiation medium only, differentiation medium with 5 ng/mL TNF-α and PBS, differentiation medium with 5 ng/mL TNF-α and CTXSkM-EVs, and differentiation medium with 5 ng/mL TNF-α and CTXSkM-EVs, and differentiation index, calculated as the ration of MHC+ cells to the total number of nuclei. (D) Fusion index, calculated as the ratio of nuclei in MHC+ cells with ≥2 nuclei to total number of nuclei. Data are reported as means ± SEM. The in vitro experiments were repeated three times. Statistical significance indicated by \* P ≤ 0.05, \*\*\* p < 0.0001, \*\*\*\* p < 0.0001, determined by One-way ANOVA.

# 4.2.3 CTXSkM-EVs and CTXFAP-EVs Alleviate Mitochondrial Dysfunction in an ALS-like Motor Neuron In Vitro Model

To evaluate the therapeutic effects of CTXSkM-EVs and CTXFAP-EVs on motor neuron viability in ALS-like motor neuron cellular model, we utilized the NSC-34

SOD1<sup>G93A</sup> cell line. This cell line, derived from the fusion of motor neuron-enriched embryonic mouse spinal cord cells and neuroblastoma cells [37], is transfected with the G93A mutant SOD1 gene, a hallmark mutation in ALS. NSC-34 SOD1<sup>G93A</sup> cells exhibit key motor neuron characteristics, such as mitochondrial dysfunction, making them a suitable for ALS-related studies [76-78]. Under H<sub>2</sub>O<sub>2</sub>-induced oxidative stress, both CTXSkM-EVs and CTXFAP-EVs significantly improved the viability of NSC-34 SOD1<sup>G93A</sup> cells (Figure 4.3A). NSC-34 cells transfected with wild-type SOD1 (NSC-34 SOD1WT) were used as controls to confirm the specificity of the protective effects. In addition, mitochondrial dysfunction plays a central role in the pathogenesis of both sporadic and familial ALS, leading to impaired energy production in motor neurons and skeletal muscles. This dysfunction contributes to key ALS hallmarks such as motor neuron degeneration and muscle atrophy [79]. Therefore, we evaluated the therapeutic potential of CTXSkM-EVs and CTXFAP-EVs in mitigating mitochondrial dysfunction in NSC-34 SOD1<sup>G93A</sup> cells. Our findings revealed that both CTXSkM-EVs and CTXFAP-EVs provided significant protection for mitochondrial function, as evidenced their effects on mitochondrial membrane potential ( $\Delta \Psi m$ ) under H<sub>2</sub>O<sub>2</sub>-induced oxidative stress.  $\Delta \Psi m$ , a critical indicator of mitochondrial health and ATP production, was assessed using tetramethylrhodamine methyl ester (TMRM) labelling. In NSC-34 SOD1<sup>G93A</sup> cells, ΔΨm was significantly reduced and further compromised under oxidative stress. Treatment with CTXSkM-EVs and CTXFAP-EVs substantially restored ΔΨm in these cells (Figure 4.3B, C). To further assess the therapeutic effects CTXFAP-EVs on mitochondrial function, we measured the mitochondrial oxygen consumption rate (OCR) in NSC-34 SOD1<sup>G93A</sup> cells under oxidative stress. The results demonstrated that treatment with CTXFAP-EVs

significantly enhanced OCR, as indicated by improved responses to both cytochrome C (Cyto C) and carbonyl cyanide-4-(trifluoromethoxy) phenylhydrazone (FCCP), compared to untreated control (Figure 4.3D). These findings suggest that both CTXSkM-EVs and CTXFAP-EVs have the potential to mitigate mitochondrial dysfunction, which likely contributes to their protective effects on the viability of the ALS-like cellular model.

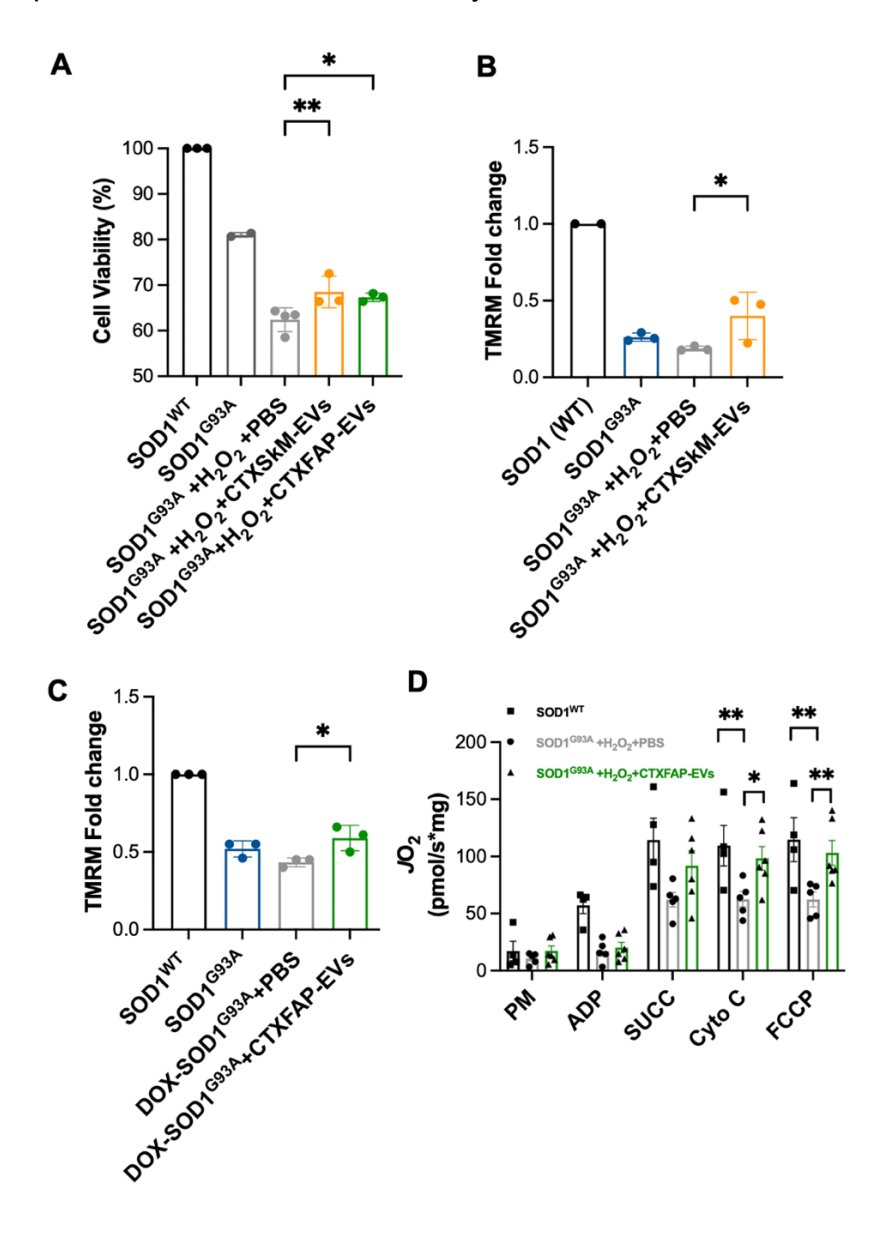


**Figure 4.3** CTXSkM-EVs and CTXFAP-EVs Alleviate Mitochondrial Dysfunction in an ALS-like Motor Neuron In Vitro Model. (A) Cell viability rate of NSC-34 SOD1<sup>WT</sup>,

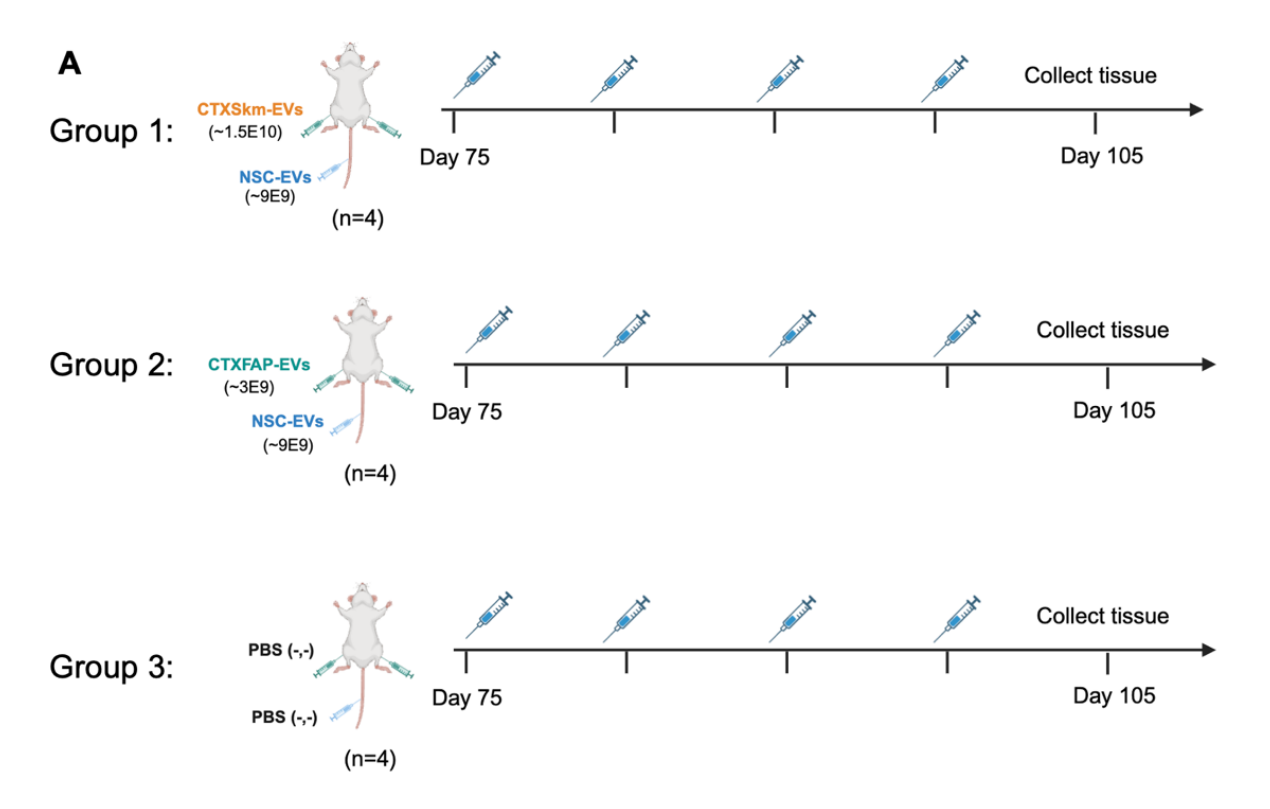
SOD1<sup>G93A</sup> cells, SOD1<sup>G93A</sup> cells treated with H<sub>2</sub>O<sub>2</sub> and PBS, SOD1<sup>G93A</sup> cells treated with H<sub>2</sub>O<sub>2</sub> and CTXSkM-EVs, and SOD1<sup>G93A</sup> cells treated with H<sub>2</sub>O<sub>2</sub> and CTXFAP-EVs. (B) TMRM assay of NSC-34 SOD1<sup>WT</sup>, SOD1<sup>G93A</sup> cells, SOD1<sup>G93A</sup> cells treated with H<sub>2</sub>O<sub>2</sub> and PBS, and SOD1<sup>G93A</sup> cells treated with H<sub>2</sub>O<sub>2</sub> and CTXSkM-EVs. (C) TMRM assay of NSC-34 SOD1<sup>WT</sup>, SOD1<sup>G93A</sup> cells, DOX induced SOD1<sup>G93A</sup> cells with PBS, DOX induced SOD1<sup>G93A</sup> cells with CTXFAP-EVs. (D) Mitochondrial Oxygen Consumption of NSC-34 SOD1<sup>WT</sup>, SOD1<sup>G93A</sup> cells treated with H<sub>2</sub>O<sub>2</sub> and PBS, and SOD1<sup>G93A</sup> cells treated with H<sub>2</sub>O<sub>2</sub> and CTXFAP-EVs. This evaluation was conducted by Junwon Heo from Dr. Jarrod Call's lab. Statistical significance indicated by \* P ≤ 0.05, \*\*P ≤ 0.005, data analysed by One-way ANOVA (A, B, C), by Two-way ANOVA (D).

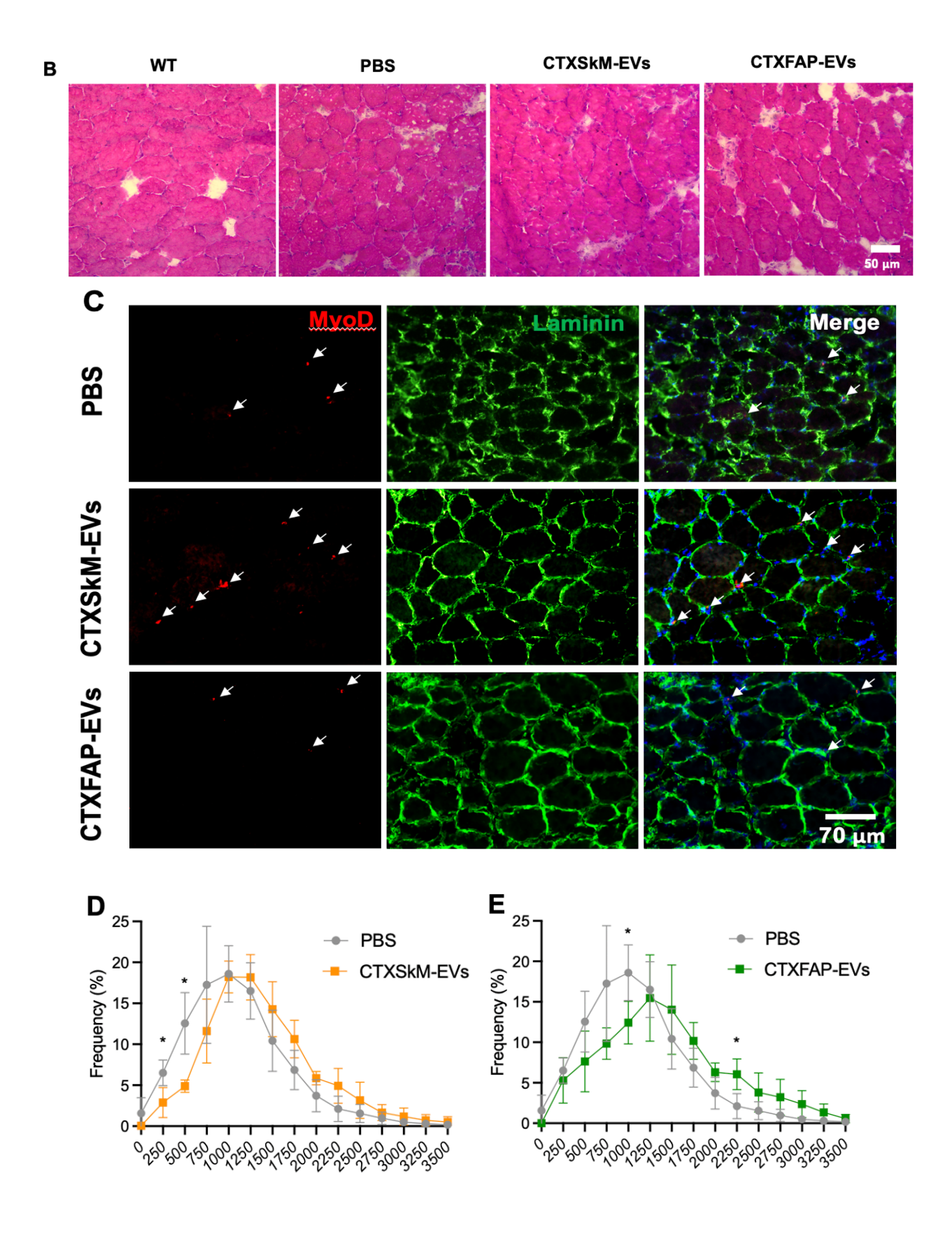
# 4.2.4 CTXSkM-EVs and CTXFAP-EVs Mitigate ALS-related Muscle Atrophy in vivo

To evaluate the effects of these EVs in a preclinical ALS model, we utilized SOD1<sup>G93A</sup> mice, a well-established model exhibiting key ALS-related degenerative characteristics, including skeletal muscle atrophy [30, 31]. CTXSkM-EVs and CTXFAP-EVs were administered intramuscularly into the TA muscle of two separate groups of SOD1<sup>G93A</sup> mice at the early symptomatic stage (day 75). Additionally, NSC-EVs were administered intravenously to both groups. As a control, a separate group of SOD1<sup>G93A</sup> mice received PBS injections both intramuscularly and intravenously. All treatments were delivered weekly until tissue collection at the late symptomatic stage (day 105) (Figure 4.4A). Hematoxylin and eosin (H&E) staining of TA muscle fibers revealed that PBS-treated SOD1<sup>G93A</sup> mice exhibited smaller muscle fiber cross-sectional areas (CSA) compared to wild-type mice. In contrast, mice treated with CTXSkM-EVs and CTXFAP-EVs displayed larger muscle fibers compared to the PBS-treated group, suggesting a

potential protective effect of EV treatments (Figure 4.4B). To further evaluate muscle regeneration and morphology, muscle sections from PBS, CTXSkM-EVs, and CTXFAP-EVs groups were immunostained for Laminin, a marker of the myofiber basement membrane, and MyoD, a marker of differentiating muscle stem cells. Analysis of CSA distribution revealed that the CTXSkM-EVs group had a lower percentage of small myofiber compared to the PBS-treated group (Figure 4.4D), and the average CSA was significantly greater in the CTXSkM-EVs group compared to the PBS-treated group (Figure 4.4F). CSA distribution analysis in the CTXFAP-EVs group revealed a higher percentage of larger myofibers compared to the PBS-treated control group, with a significant greater average CSA (Figure 4.4C, E, F). These findings suggest that EV treatment mitigates the muscle atrophic process. Furthermore, the expression of the myogenic marker MyoD was significantly higher in the CTXSkM-EVs-treated group compared to the PBS-treated group (Figure 4.4G), indicating that CTXSkM-EVs may mitigate muscle atrophy by stimulating muscle regeneration through enhanced satellite cell differentiation. Additionally, the percentage of myofibers with centralized nuclei, a hallmark of active muscle regeneration, was significantly greater in the CTXSkM-EVs group compared to the PBS-treated group (Figure 4.4H). However, no significant difference in centralized nuclei myofibers was observed between the CTXFAP-EVs group and the PBS-treated group myofibers (Figure 4.4H). The differing outcomes between CTXSkM-EVs and CTXFAP-EVs may reflect variations in dosage or intrinsic EV properties, suggesting that optimizing dosages and further characterizing EV types could improve therapeutic efficacy. Overall, our findings demonstrate that both EV treatments provide therapeutic benefits in mitigating muscle atrophy in the SOD1<sup>G93A</sup> mouse model.

These results underscore the potential of EV-based therapies for muscle preservation in ALS and highlight the need for further investigation to optimize EV delivery for clinical applications.





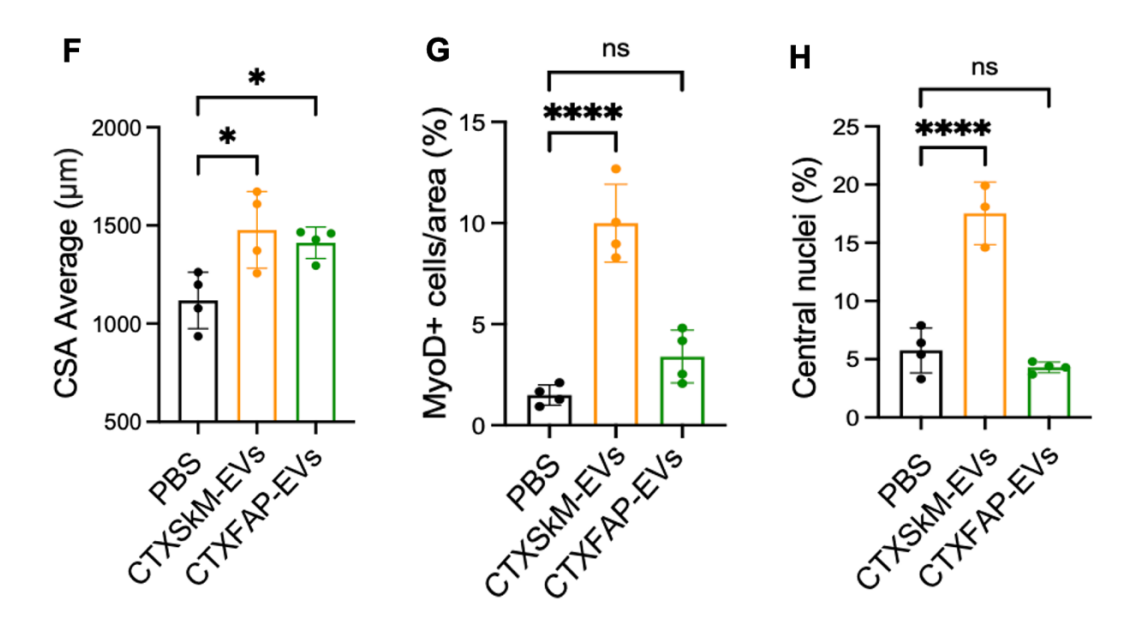


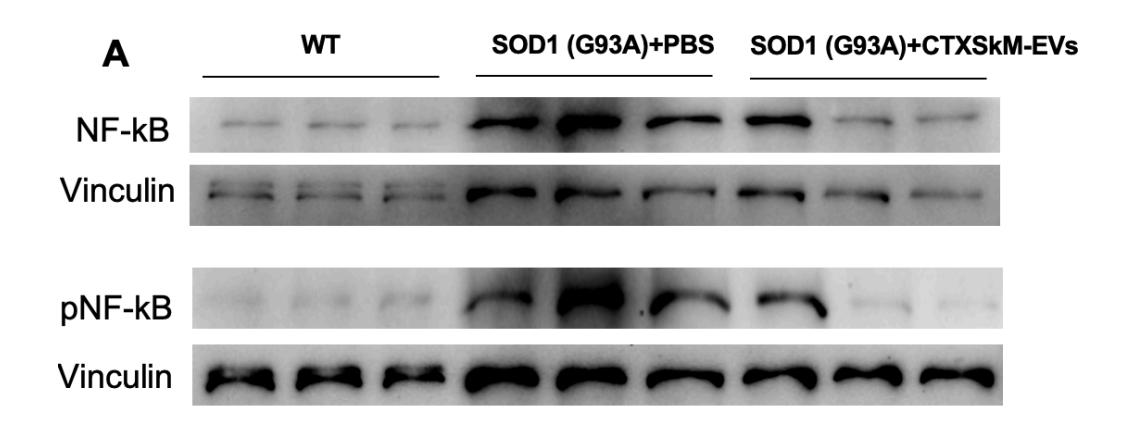
Figure 4.4 CTXSkM-EVs and CTXFAP-EVs Mitigate Muscle Atrophy in SOD1<sup>G93A</sup> Mice. (A) Schematic timeline for EV treatment in the experimental groups. (B) Representative H&E staining of TA muscle sections in four groups: WT, PBS, CTXSkM-EVs, and CTXFAP-EVs. Scale bar: 50 μm. (C) Immunofluorescence staining for MyoD (red), Laminin (green), and DAPI (blue) in TA muscle sections from PBS, CTXSkM-EVs, and CTXFAP-EVs groups. Scale bar: 70 μm. (D) CSA size distribution in TA muscle comparing PBS and CTXSkM-EVs groups. (E) CSA size distribution in TA muscle comparing PBS and CTXFAP-EVs groups. (F) Comparison average of CSA of TA muscle among three groups: PBS, CTXSkM-EVs and CTXFAP-EVs. (G) Comparison of percentage of MyoD+ cells per area among three groups: PBS, CTXSkM-EVs and CTXFAP-EVs. (H) Comparison the percentage of muscle fibers with central nuclei among three groups: PBS, CTXSkM-EVs and CTXFAP-EVs. Statistical significance indicated by \* P ≤ 0.05, \*\*\*\* P < 0.0001, determined by One-way ANOVA.

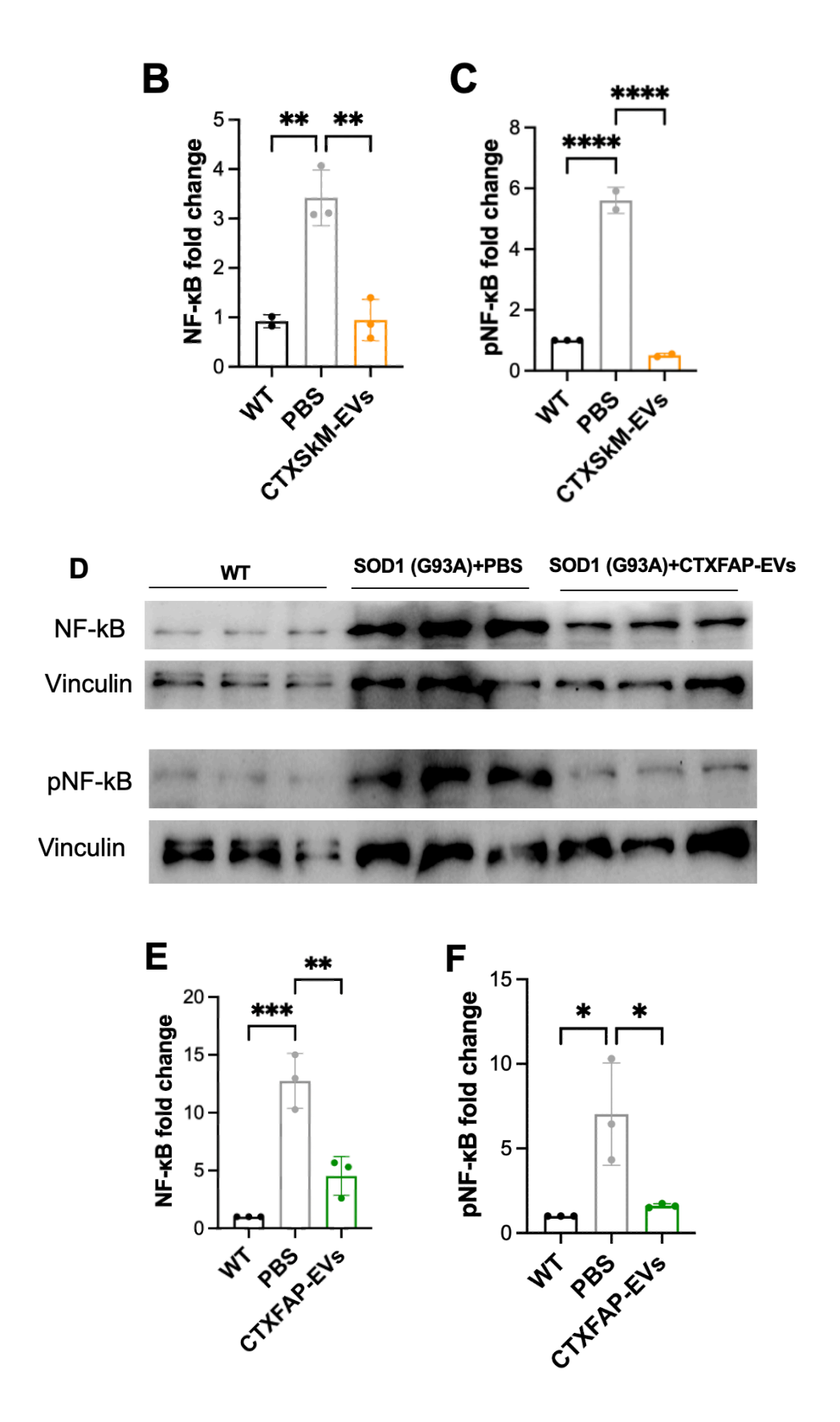
# 4.2.5 CTXSkM-EVs and CTXFAP-EVs Downregulate the Activated NF-κB Pathway in Muscle

Persistent activation of NF-kB signaling in ALS-affected skeletal muscles is a major contributor to muscle degeneration and atrophy, as it drives chronic inflammation, upregulates proteolytic enzymes, and suppresses myogenic regulatory factors like MyoD [67, 80, 81]. NF-κB, activated by elevated pro-inflammatory cytokines such as TNF-α in ALS, promotes catabolic pathways and inhibits myogenic differentiation, further exacerbating muscle wasting [82]. These findings highlight NF-kB signaling as a critical therapeutic target for reducing inflammation and mitigating muscle atrophy in ALS. To determine whether EV treatment affects NF-kB signalling in the TA muscle of SOD1 (G93A) mice, western blot analysis was performed to evaluate the protein levels of NFκB, phosphorylated NF-κB (pNF-κB), and vinculin (as a loading control) across wild-type (WT) mice, PBS-treated mice, CTXSkM-EVs-treated mice, and CTXFAP-EVs-treated mice. The results showed a significant increase in NF-κB and pNF-κB protein levels in the TA muscle of the PBS-treated group compared to the WT group. However, treatment with CTXSkM-EVs significantly reduced both NF-κB and pNF-κB protein levels (Figure 4.5A, B, C). Similarly, the CTXFAP-EVs-treated group demonstrated a significant reduction in NF-κB and pNF-κB levels compared to the PBS-treated group (Figure 4.5D, E, F). The findings suggest that the EV treatment modulates NF-kB signaling, potentially alleviating inflammation and mitigating muscle atrophy in the ALS model.

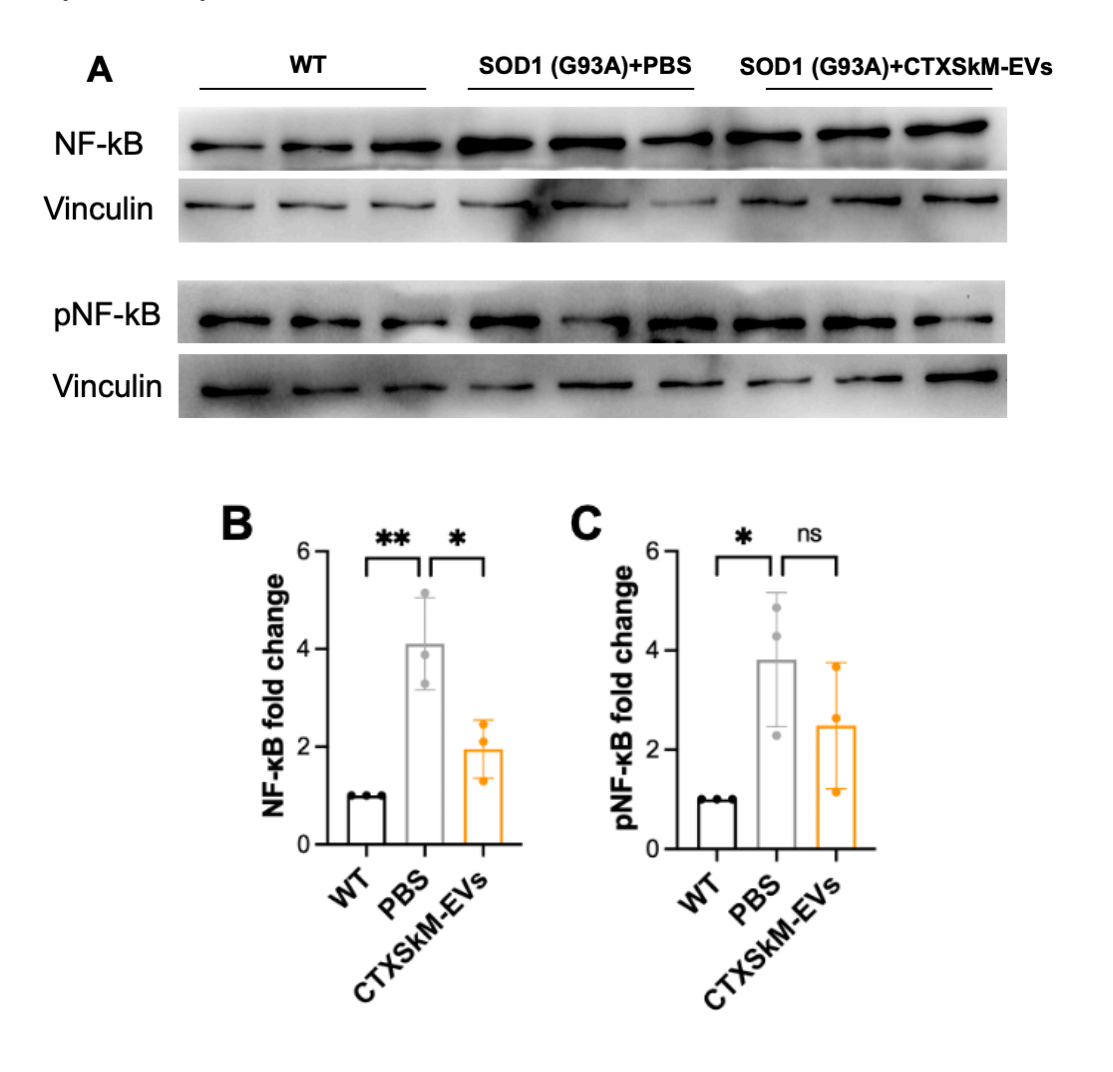
Since both the CTXSkM-EVs and CTXFAP-EVs groups also received intravenous NSC-EVs, which are known to mitigate inflammation in various neurodegenerative diseases, we investigated their effects on the NF-kB signaling pathway in the spinal cord.

Our analysis revealed significantly elevated NF-κB protein levels in the spinal cord of PBS-treated group compared to the WT group. Notably, the CTXSkM-EVs group exhibited a significant reduction in NF-κB protein levels relative to the PBS-treated group (Figure 4.6A, B). While pNF-κB protein levels in the CTXSkM-EVs group did not show a statistically significant difference from the PBS group, a decreasing trend was observed following EV treatment (Figure 4.6C). The CTXFAP-EVs group did not exhibit significant downregulation of NF-κB or pNF-κB protein levels, though a similar downward trend was noted (Figure 4.6D, E, F). These findings suggest that EV treatment, particularly with CTXSkM-EVs, may have therapeutic potential in modulating inflammatory pathways in the spinal cord of ALS models. This highlights their promise as a strategy to mitigate neuroinflammation and support motor neuron health in ALS.





**Figure 4.5** CTXSkM-EVs and CTXFAP-EVs Downregulate the Activated NF-κB Pathway in Muscle. (A) Western blot analysis showing protein levels of NF-κB, pNF-κB, and Vinculin (loading control) in three groups: WT, PBS, and CTXSkM-EVs. (B, C) Quantification of NF-κB and pNF-κB protein levels with statistical comparison across WT, PBS, and CTXSkM-EVs groups. (D) Western blot analysis of NF-κB, pNF-κB, and Vinculin in WT, PBS, and CTXFAP-EVs groups. (E, F) Quantification of NF-κB and pNF-κB protein levels with statistical comparison across WT, PBS, and CTXFAP-EVs groups. Statistical significance indicated by \* P  $\leq$  0.05, \*\*P  $\leq$  0.005, \*\*\* p < 0.0001, \*\*\*\* p < 0.0001, determined by One-way ANOVA.



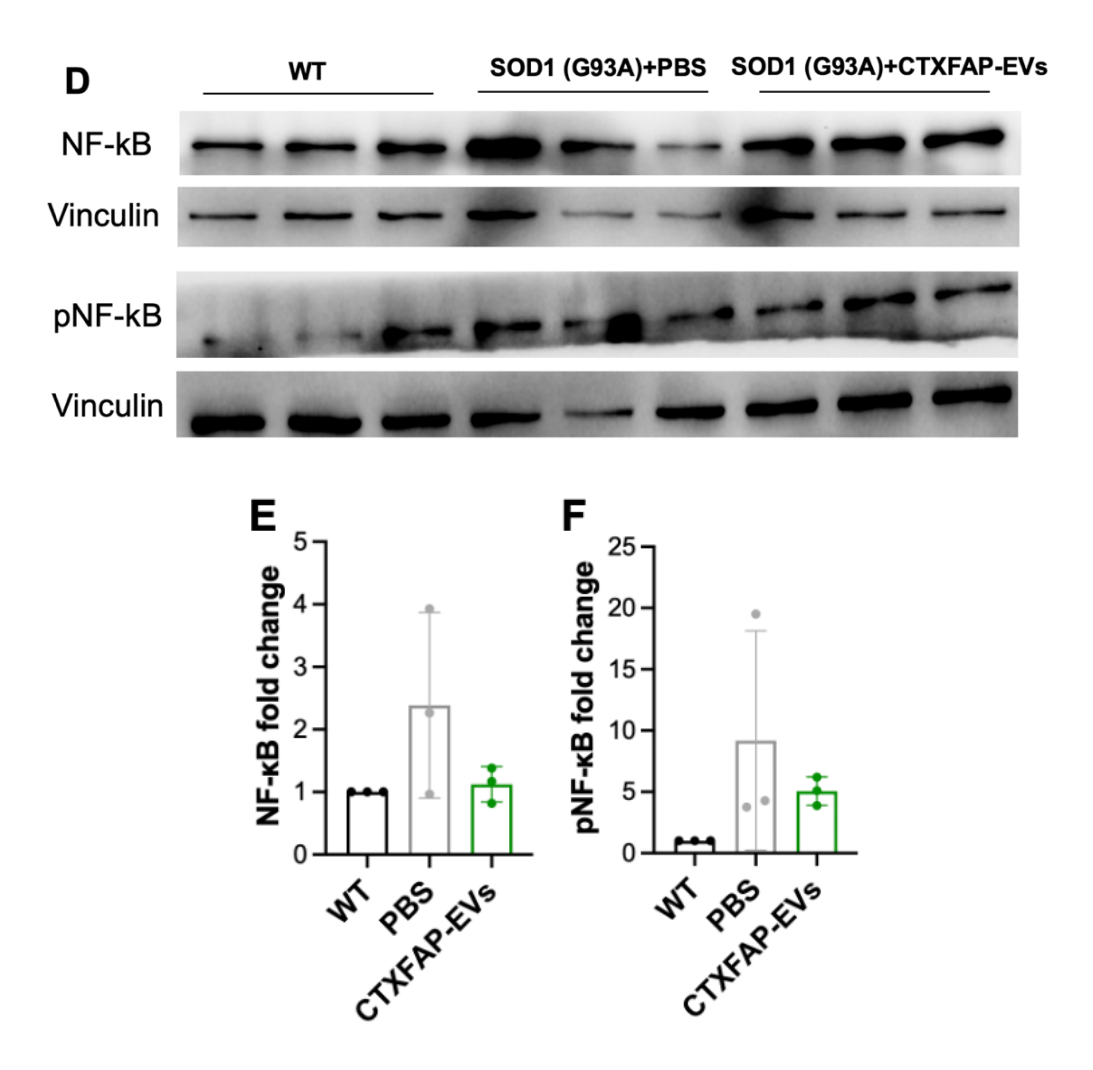


Figure 4.6 Effects of EV Treatment on the Activated NF-κB Pathway in the Spinal Cord (A) Western blot analysis showing protein levels of NF-κB, pNF-κB, and Vinculin (loading control) across three groups: WT, PBS, and CTXSkM-EVs. (B, C) Quantification of NF-κB and pNF-κB protein levels with statistical comparison among WT, PBS, and CTXSkM-EVs groups. (D) Western blot analysis of NF-κB, pNF-κB, and Vinculin in WT, PBS, and CTXFAP-EVs groups. (E, F) Quantification of NF-κB and pNF-κB protein levels with statistical comparison among WT, PBS, and CTXFAP-EVs groups. Data are presented as mean  $\pm$  SEM. Statistical significance was determined by one-way ANOVA and is indicated as follows: \* P  $\leq$  0.005, \*\*P  $\leq$  0.005.

#### 4.3 Discussion

Recent studies highlight skeletal muscle as an increasingly promising therapeutic target for ALS. Traditionally considered a secondary site of ALS pathology, skeletal muscle has garnered attention due to its active involvement in disease progression [83, 84]. Evidence suggests that skeletal muscle degeneration can initiate a "dying-back" process that exacerbates motor neuron degeneration, contributing to ALS progression through retrograde signalling to the central nervous system (CNS) [83, 84]. Given this involvement, interventions targeting skeletal muscle may offer substantial therapeutic benefits in ALS. Previous studies have shown that mesenchymal stem cells (MSCs) transplantation into the skeletal muscle of ALS mouse models reduces muscle atrophy, neuromuscular junction (NMJ) denervation, and motor neuron degeneration [85, 86]. Similarly, the administration of the anti-inflammatory cytokine Interleukin-10 (IL-10) to skeletal muscle has been found to modulate inflammation, delay muscle atrophy, and mitigate motor neuron loss [60]. These findings underscore the potential of muscledirected therapies to enhance muscle integrity, stabilize NMJs, regulate inflammation, and slow ALS progression.

EVs represent a promising, cell-free alternative to traditional cell-based therapies due to their regenerative and anti-inflammatory properties [87]. Unlike stem cell transplantation, EVs offer a targeted and minimally invasive method for delivering bioactive molecules that influence both muscle and neuronal function. Their ability to cross biological barriers and modulate disease mechanisms positions them as a compelling therapeutic tool for ALS. In this study, we explored the application of EVs derived from regenerating skeletal muscle (CTXSkM-EVs) and fibro/adipogenic

progenitors (CTXFAP-EVs) in an atrophic muscle cellular model. Their beneficial effects on myogenesis suggest a broader therapeutic potential for muscle-wasting diseases. By promoting muscle regeneration and enhancing myogenic differentiation, these EVs may aid in restoring muscle integrity and function in conditions characterized by progressive muscle atrophy, such as muscular dystrophy, sarcopenia, and cachexia. Furthermore, CTXSkM-EVs and CTXFAP-EVs enhanced viability and mitigated mitochondrial dysfunction in ALS-like motor neurons, further indicating their beneficial effects on mitochondrial function. This suggests that these EVs may contribute to maintaining cellular energy homeostasis, reducing oxidative stress, and preserving mitochondrial integrity in degenerating motor neurons. By improving mitochondrial function, CTXSkM-EVs and CTXFAP-EVs could help sustain neuronal survival and resilience against ALSassociated metabolic stress, highlighting their potential as a therapeutic strategy for mitigating neurodegeneration in ALS and other neuromuscular disorders. Beyond their regenerative and neuroprotective effects on cellular models, we introduce a novel mixed EV-based therapeutic strategy that combines NSC-EVs with either CTXSkM-EVs or CTXFAP-EVs to simultaneously target both skeletal muscle and the CNS. In vivo, this approach effectively mitigated muscle atrophy, likely by promoting muscle regeneration and suppressing the pro-inflammatory NF-kB signaling pathway in ALS-affected skeletal muscle. Notably, EV treatment also modulated NF-kB signaling in the spinal cord of SOD1<sup>G93A</sup> mice, suggesting a neuroprotective effect that extends beyond the muscle. These findings provide the first evidence that regenerative muscle-derived EVs offer a viable therapeutic strategy for ALS and propose a dual-targeted EV therapy possess the potential to address both muscle degeneration and neuroinflammation.

Future research should focus on optimizing EV dosage, delivery methods, and timing to maximize therapeutic efficacy. Additionally, further investigation into the specific regenerative biomolecules within these EVs may enable the development of refined therapeutic approaches that harness key EV components for enhanced muscle and neuronal repair. These insights could extend EV-based therapies beyond ALS to other neuromuscular diseases characterized by muscle atrophy and neurodegeneration.

#### 4.4 Materials and Methods

#### 4.4.1 Animals and treatment

Experiments were conducted using transgenic mice overexpressing human SOD1 with a Gly93-Ala mutation SOD1<sup>G93A</sup> (strain designation B6SJL–TgN[SOD1–G93A]1Gur, stock number 002726) and wild-type (WT) mice (B6SJL) obtained from Jackson Laboratories (Bar Harbor, ME, USA). Animals were maintained in a controlled environment under standard laboratory conditions. Genotyping of transgenic mice was confirmed via polymerase chain reaction (PCR) targeting the human SOD1 gene using specific primers: SOD1 primers included forward (113)5'gene CATCAGCCCTAATCCATCTGA-3' 5'and reverse (114)CGCGACTAACAATCAAAGTGA-3'; while housekeeping gene primers included forward 5'-CTAGGCCACAGAATTGAAAGATCT-3' 5'-(7338)and (7339)reverse GTAGGTGGAAATTCTAGCATCATCC-3'.

Mice were divided into four groups: WT mice (n=3), SOD1 (G93A) mice treated with phosphate buffered saline (PBS; n=4), SOD1<sup>G93A</sup> mice treated with NSC-EVs and CTXSkM-EVs (n=4), and SOD1<sup>G93A</sup> mice treated with NSC-EVs and CTXFAP-EVs (n=4). Treatments administered weekly, beginning at 75 days of age, with tissue collection at

105 days. CTXSkM-EVs were administered intramuscularly at approximately  $1.5 \times 10^{10}$  EVs per muscle, CTXFAP-EVs were administered intramuscularly at an average dose of  $3 \times 10^9$  EVs per muscle, and NSC-EVs were given intravenously at approximately  $9 \times 10^9$  EVs per mouse.

#### 4.4.2 CTXSkM-EVs Isolation

To isolate CTXSkM-EVs from acutely injured skeletal muscle, cardiotoxin (CTX) (10 µM, 20 µL) was intramuscularly injected into the tiabialis anterior (TA) and gastrocnemius (GAS) muscles of 2-month-old WT mice. At day 3 post-injury, the TA and GAS muscles were harvested and sliced into 2-4 mm sections using a scalpel. The sliced muscles were then placed in a digestion solution containing 2 mg/mL Collagenase Type Ш (Worthington-Biochem, Cat#LS004176) in DMEM with 100 U/mL Penicillin/Streptomycin (P/S) (Gibco, Cat#15140122), using 500 µL for each TA muscle and 1 mL for each GAS muscle. The tissue was rotated in the digestion solution at 37°C for 24 hours. Following digestion, the tissue mixture was centrifuged at 1,000 xg for 30 minutes at 4°C, and the supernatant was collected and filtered through a 0.8 µm filter. CTXSkM-EVs were then isolated from the filtered supernatant by ultracentrifugation at 100,000 xg for 1 hour at 4°C, and the resulting EV pellet was resuspended in PBS.

#### 4.4.3 CTXFAP-EVs Isolation

Acute injury in the TA and GAS muscles of around 2-month-old WT mice was induced with CTX (10  $\mu$ M, 20  $\mu$ L), and muscles were harvested on day 3 post-injury. The tissue was minced to 1–2 mm² pieces and digested in a Collagenase Type II solution (2.433 mg/mL in F-10 medium supplemented with 10% heat-inactivated fetal bovine serum (FBS) and 100 U/mL P-S) at 37°C for 30 minutes, with gentle vertexing after 15

minutes. After centrifugation (150 x g, 5 minutes, 4°C), the pellet was further digested in a Collagenase/Dispase solution (2.5 mg/mL in F-10 medium with 10% FBS and 1% P/S) at 37°C for 15 minutes, followed by gentle trituration using a syringe fitted with an 18G needle. The suspension was filtered through a 40 µm strainer, centrifuged (150 x g, 5 minutes, 4°C), and the pellet resuspended in F10 with 10% FBS and 1% P/S. Cells were stained with biotin-conjugated anti-CD31 (Miltenyi Biotec, Cat#130-119-662), CD45 (Miltenyi Biotec, Cat#130-124-209), and integrin alpha 7 (Miltenyi Biotec, Cat#130-128-938) antibodies, incubated with anti-biotin microbeads (Miltenyi Biotec, Cat#130-090-485), and passed through a magnetic column to enrich FAPs. The isolated FAPs were cultured in DMEM with 20% FBS, 1% P/S, and 2.5 ng/mL fibroblast growth factor 2 (FGF-2) on gelatin-coated plates for expansion over one week. For CTXFAP-EVs collection, FBS was withdrawn from the culture medium for 48 hours, with medium collected every 24 hours. EVs were isolated by sequential centrifugation: 1,000 x g for 30 minutes to remove debris, followed by ultracentrifugation at 130,000 x g for 2 hours at 4°C, a PBS wash, and a final ultracentrifugation at 100,000 x g for 1 hour at 4°C. The final CTXFAP-EVs were resuspended in PBS. The isolated EVs were stored at -80°C until use.

#### 4.4.4 MemGlow assessment

The size and concentration of the isolated EVs were measured using nano-flow cytometry on the Flow NanoAnalyzer (NanoFCM, Xiamen, China). To assess the proportion of particles with lipid membranes, EVs samples were stained with 2 nM MemGlow 488 (Cytoskeleton, Denver, CO), a fluorogenic membrane probe, for 10 minutes. Fluorescence was subsequently detected using the Flow NanoAnalyzer.

#### 4.4.5 Cell Culture

NSC-34 SOD1<sup>WT</sup> cells, NSC-34 SOD1<sup>G93A</sup> cells, and C2C12 myoblast (CRL-1772<sup>TM</sup>, ATCC) were cultured in Dulbecco's Modified Eagle Medium (DMEM; Invitrogen) supplemented with 10% FBS and 100 U/mL P/S. Cells were maintained at 37°C in a humidified incubator with a 5% CO<sub>2</sub>/95% air atmosphere.

# 4.4.6 C2C12 derived atrophic model and treatment

C2C12 cells were seeded at 100,000 cells per well in the 24-well plate with growth medium. After 24 hours, the growth medium was replaced into differentiation medium (DMEM supplemented with 2% horse serum and 100 U/mL P/S) to initiate differentiation. Four treatment conditions were applied: (1) differentiation medium only, (2) differentiation medium with 5 ng/mL TNF- $\alpha$  and PBS, (3) differentiation medium with 5 ng/mL TNF- $\alpha$  and approximately 5 × 10 $^8$  CTXSkM-EVs and CTXFAP-EVs. After 3 days of treatment, cells were evaluated for myosin heavy chain (MHC) expression.

#### 4.4.7 Immunostaining of cells

FAPs were fixed with 4% paraformaldehyde (PFA) for 10 minutes at room temperature, followed by permeabilization with 0.1% Triton X-100 in PBS. Cells were then blocked in 10% FBS in PBS for 1 hour at room temperature. Primary antibodies, anti-PDGFRα (R&D Systems, Cat#AF1062) and MF20 (Developmental Studies Hybridoma Bank, DSHB), were diluted in a blocking buffer and applied overnight at 4°C. The following day, cells were washed three times with PBS to remove excess primary antibody. Secondary antibodies, donkey anti-mouse (Abcam, Cat# ab150108) and anti-rabbit (Abcam, Cat# ab150073), diluted in PBS, were applied for 1 hour at room temperature. After incubation, cells were washed three additional times with PBS. Applied DAPI for

nuclear counterstaining. Fluorescence images were captured using a fluorescence microscope.

# 4.4.8 Mitochondrial Membrane Potential Assay

NSC-34 SOD1<sup>WT</sup> and NSC-34 SOD1<sup>G93A</sup> cells were seeded at 15,000 cells per well in a 96-well plate. After 24 hours, the culture medium was replaced with a medium containing 2 μg/mL doxycycline (DOX) to induce SOD1 protein expression. Following another 24-hour incubation, the medium was replaced with 30 ng/mL H<sub>2</sub>O<sub>2</sub> along with ~6 × 10<sup>8</sup> to 2 × 10<sup>9</sup> CTXSkM-EVs or CTXFAP-EVs, respectively. After 4 hours of H<sub>2</sub>O<sub>2</sub> treatment, tetramethylrhodamine methyl ester (TMRM) (AAT Bioquest, Cat#22221) was applied to label mitochondrial membrane potentials. According to the manufacturer's instructions, cells were incubated with 100 nM TMRM for 30 minutes at 37°C, then detached for fluorescence analysis using a CytoFLEX Flow Cytometer (Beckman Coulter).

# 4.4.9 Mitochondrial Oxygen Respiration Assay

NSC-34 SOD1<sup>WT</sup> and NSC-34 SOD1<sup>G93A</sup> cells were seeded at a density of 80,000 cells per well in a 48-well plate. After 24 hours, the medium was replaced with fresh medium containing 2  $\mu$ g/mL DOX to induce SOD1 protein expression. Following an additional 24-hour incubation, the medium was replaced with 30 ng/mL H<sub>2</sub>O<sub>2</sub> along with approximately 3 × 10<sup>9</sup> CTXFAP-EVs. After 6 hours of H<sub>2</sub>O<sub>2</sub> treatment, high-resolution respirometry was conducted using an Oroboros Oxygraph-2K (Oroboros Instruments, Innsbruck, Austria) as previously described (PMID: 34888943) in permeabilized cells with a slight modification. Experiments were carried out at 37°C in 500  $\mu$ L of Buffer Z (105 mM K-MES, 30 mM KCl, 1 mM EGTA, 10 mM K2HPO4, 5 mM MgCl, 0.5 mg/mL bovine serum

albumin; pH 7.1) supplemented with creatine (5 mM). Following counting the cells, the cells were transferred to the chambers and were permeabilized with Digitonin (20  $\mu$ g/ml). After recording the basal rate, the assay began by adding pyruvate/malate (PM; 1 mM/2 mM), followed by ADP (500  $\mu$ M). Succinate (10 mM) was added to fuel complex II-mediated mitochondrial respiration, followed by Cytochrome c (10  $\mu$ M) to check the mitochondrial integrity. Finally, respiratory stimulation was conducted via a respiratory uncoupler (FCCP; 1  $\mu$ M).

#### 4.4.10 Cellular Viability Assay

NSC-34 SOD1<sup>WT</sup> and NSC-34 SOD1<sup>G93A</sup> cells were seeded at 80,000 cells per well in a 48-well plate. After 24 hours, the medium was replaced with the fresh medium containing 2 μg/mL DOX to induce SOD1 protein expression. Following an additional 24-hour incubation, the medium was replaced with 30 ng/mL H<sub>2</sub>O<sub>2</sub> along with around 3 × 10<sup>9</sup> CTXSkM-EVs or CTXFAP-EVs, respectively. After 6 hours of H<sub>2</sub>O<sub>2</sub> treatment, cell proliferation was assessed using the Cell Counting Kit-8 (CCK8) (DOJINDO, Cat# CK04) according to the manufacturer's instructions. A 10% CCK8 solution in culture medium was added to each well and incubated for 1 hour at 37°C. Absorbance was measured using a SpectraMax iD3 plate reader (MOLECULAR DEVICES).

#### 4.4.11 Histology

TA muscle tissues were embedded in OCT and frozen. Cryosections (10 μm) were prepared, mounted on glass slides, and air-dried. Sections were fixed in 4% PFA for 10 minutes, rinsed in PBS, and stained with hematoxylin (HARRIS, SIGMA, Cat No. HHS32) for 1 minute. After rinsing, sections were stained with eosin (SIGMA HT110316) for 30 seconds, washed briefly in distilled water. Slides were dehydrated through ascending

ethanol concentrations, cleared with xylene, and coverslipped using a permanent mounting medium. Images were acquired with a light microscope.

# 4.4.12 Immunohistochemistry of Skeletal Muscle

TA muscle tissues were embedded in OCT, frozen, and cryosectioned at 10 μm thickness. Sections were mounted on glass slides, air-dried, and fixed with 4% PFA for 10 minutes, followed by PBS rinses. Tissues were permeabilized with 0.1% Triton X-100 in PBS for 10 minutes, then blocked in 10% fetal bovine serum (FBS) in PBS for 1 hour at room temperature. Primary antibodies against Laminin (Sigma-Aldrich, Cat# L9393) and MyoD (Santa Cruz, Cat# sc-377460) were applied in the blocking buffer and incubated overnight at 4°C. The next day, sections were washed in PBS and incubated with fluorophore-conjugated secondary antibodies in PBS for 1 hour at room temperature in the dark. After final PBS washes, sections were mounted with an antifade mounting medium containing DAPI for nuclear counterstaining. Images were captured using a fluorescence microscope.

### 4.4.13 Western Blotting

Tissue samples were lysed in RIPA buffer (Millipore Sigma, Cat#20-188) containing phosphatase and protease inhibitors. Proteins were separated on an SDS-PAGE gel, transferred to PVDF membranes, then blocked with 5% FBS in PBST (PBS with 0.1% Tween 20) for 1 hour at room temperature. The membranes incubated overnight at 4 °C with primary antibodies: anti-NF-κB p65 (Cell Signaling Technology, Cat#8242), anti-phospho-NF-κB p65 (Cell Signaling Technology, Cat#3033), and anti-Vinculin (Cell Signaling Technology, Cat#13901). Membranes were then incubated with HRP-conjugated anti-Rabbit IgG (H+L) secondary antibody (Promega, Cat#W4011) for 1

hour at room temperature. Protein bands were visualized under ChemiDoc™ MP imaging system (Bio-Rad) with WesternBright ECL chemiluminescent substrate (Fisher Scientific, Cat#NC0930892).

# 4.4.14 Statistical Analysis

Data were analyzed using GraphPad Prism version 10.0 (GraphPad Software). A two-tailed, unpaired Student's t-test was used for comparisons between two treatment groups. For comparisons among more than two groups with a single variable, one-way ANOVA followed by Tukey's post-hoc test was applied for multiple comparisons. Mitochondrial oxygen respiration data were analyzed using two-way ANOVA. All data are presented as mean  $\pm$  standard error of the mean (SEM). Statistical significance was set at \* P  $\leq$  0.05, \*\*P  $\leq$  0.005, \*\*\* p < 0.0001, \*\*\*\* P < 0.0001.

### **CHAPTER 5**

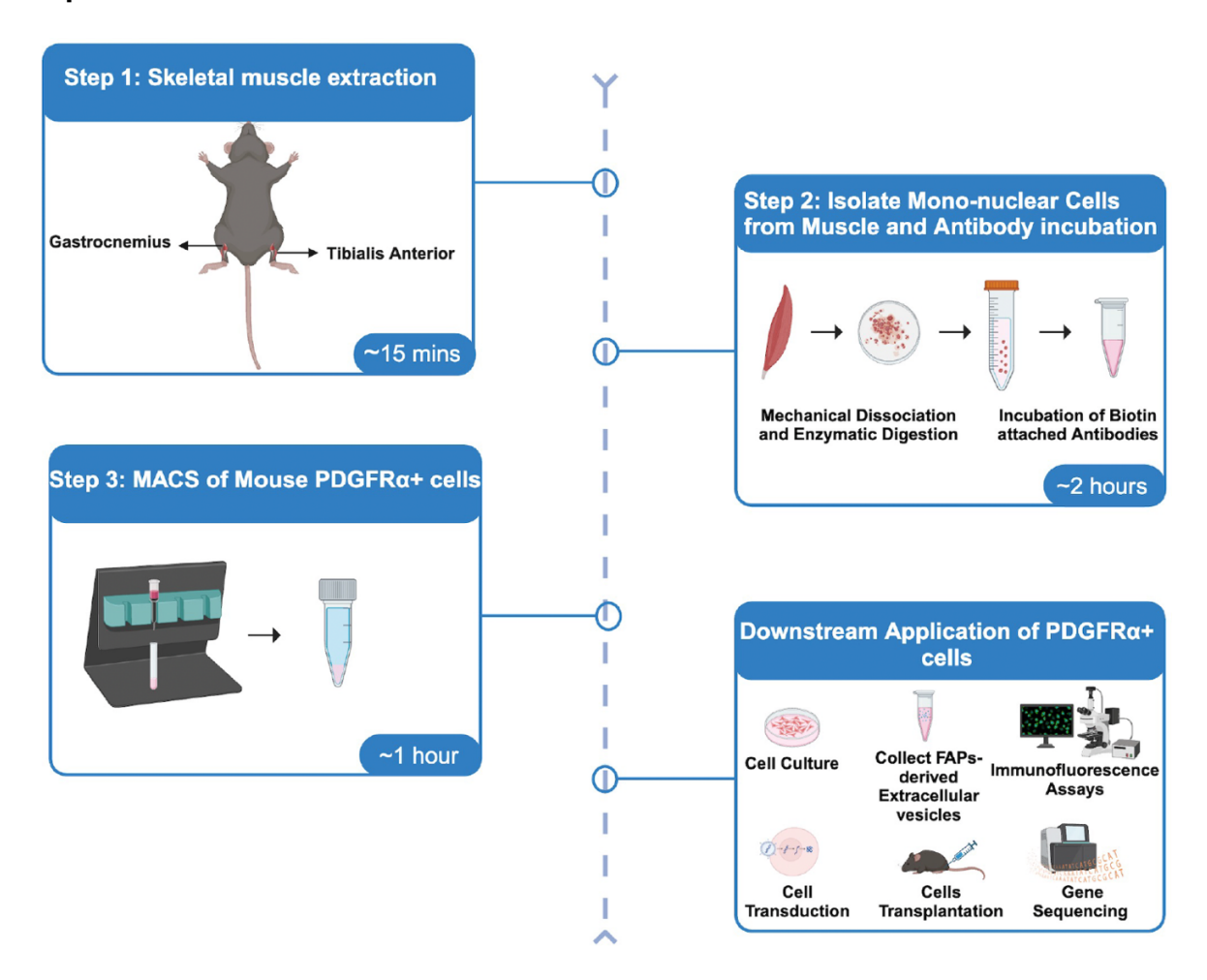
# PROTOCOL FOR THE ISOLATION OF MOUSE FIBRO/ADIPOGENIC PROGENITORS USING MAGNETIC ACTIVATED CELL SORTING<sup>5</sup>

<sup>5</sup> Gao, J., Zheng, Y., Sikal, A., Sterling, E., Hankin, R., Yao, Y. Protocol for the Isolation of Mouse Fibro/Adipogenic Progenitors using Magnetic Activated Cell Sorting. Accepted by *STAR Protocols*. Reprinted here with permission of publisher, March 2024.

# Summary

Fibro/adipogenic progenitors (FAPs) are mesenchymal progenitors that activate muscle stem cells and remodel the extracellular matrix to support muscle regeneration. This protocol outlines the isolation of FAPs from mouse skeletal muscle using enzymatic digestion, mechanical dissociation, and magnetic-activated cell sorting (MACS). It provides a high yield of FAPs with substantial purity, suitable for downstream applications such as cell culture, immunofluorescence staining, and gene expression analysis. This approach advances our understanding of muscle disorders and aids in developing muscle regeneration strategies.

# **Graphical abstract**



### 5.1 Background

FAPs play a pivotal role in muscle regeneration and hemostasis[71]. Following muscle acute injury, FAPs secrete cytokines and growth factors that promote the activation and differentiation of muscle stem cells (satellite cells), while also modulating immune response to facilitate efficient tissue repair [71, 72]. Furthermore, FAPs are essential in remodelling the extracellular matrix (ECM), providing the necessary structural and environmental support required for optimal muscle function and repair [71]. However, under pathogenic conditions, FAPs can differentiate into adipocytes and fibroblasts, contributing to fat infiltration and fibrosis in muscle disorders and aging [88, 89]. These dual roles of FAPs-supporting regeneration under normal conditions but contributing to degeneration in disease states-highlight the need for a deeper understanding of their molecular and functional properties. To address this, we present a protocol for the isolation of mouse FAPs through MACS from wild-type mice. This approach has also been successfully applied to isolating FAPs from acutely injured skeletal muscle. Given the importance of FAPs in muscle regeneration and degeneration, this refined FAP isolation method will contribute to advancing research on muscle disorders and facilitate the development of improved strategies for effective muscle regeneration and repair.

# 5.2 Preparation of muscle digestion media, FAPs growth media and gelatin-coated plate

Timing: ~15 min

Freshly prepare Digest 1 mix and Digest 2 mix, keep them on ice prior to use.
 Prepare PBS for collecting dissected skeletal muscle and keep it on ice.

2. Freshly prepare the growth media for culturing FAPs. Prewarm the media in 37°C

water bath for 5-10 min just before use.

3. Precoat wells for cell culture with enough gelatin to cover the entire bottom of the

well and incubate the plates for approximately 2-3 h in a 37°C incubator before

seeding isolated cells.

5.3 Step-by-Step method details

5.3.1 Extraction of mice skeletal muscle

Timing: ~15 min per mouse

1. Sanitization and Setup:

a. Clean and sanitize the dissection area thoroughly to maintain a sterile environment

with 70% ethanol.

b. Arrange all the necessary dissection tools (e.g., scissors, forceps, scalpel) and

have them sterilized.

Confirmation of Euthanasia:

a. Euthanize mice according to your approved IACUC protocol.

3. Positioning the Mouse:

a. Lay the mouse on its back on a clean, sterile surface.

b. To stabilize the body, you can pin down the limbs using needles or similar tools

designed for dissection purposes. This immobilization is crucial for precise

incisions and manipulations during the dissection process.

4. Skin Incision and Exposure:

a. Spray down mouse limb with 70% ethanol (Figure 5.1A).

97

- b. Make a transverse incision at the terminal part of the hindlimb using sterilized scissors or a scalpel and carefully peel back the skin to expose the underlying skeletal muscle tissue. It's important to make this initial incision as clean and precise as possible to facilitate easy access to the muscle tissue while minimizing potential damage to the underlying structures. Additionally, ensure minimal to no hair contact with the exposed muscle to reduce the risk of contamination (Figure 5.1B, C).
- 5. Dissection of Skeletal Muscles:
- a. Carefully remove the fascia on top of the tibialis anterior (TA) muscle with microdissection tweezer, then gently isolate the skeletal muscle tissue, such as extensor digitalis longus, soleus, and gastrocnemius (GAS), ensuring to avoid pulling too forcefully on the muscle during removal from the hindlimb. Carefully remove surrounding connective tissues, such as tendons, without damaging the muscles to ensure sample purity and to maximize the yield of viable FAPs (Figure 5.1D, E, F).
- b. Place dissected skeletal muscles into the pre-cold PBS.

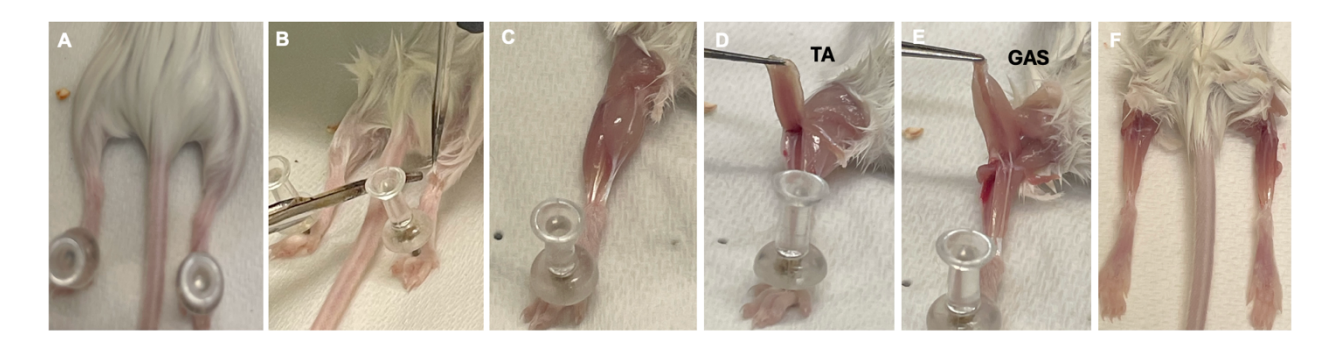


**Figure 5.1** Extraction of hindlimb skeletal muscles from adult mice. Mouse skeletal muscle dissection. (A) Spray the hindlimb of the mice with 70% ethanol. (B, C) Make a

transverse incision along the terminal part of the hindlimb and peel back the skin to expose the skeletal muscle. (D, E, F) Dissect the TA and GAS muscles.

# 5.3.2 Enzymatic and mechanical dissociation of skeletal muscle to release mononuclear muscle cells

Timing: ~ 2 h for 1 mouse. Add 15-30 min for each additional mouse.

- 6. Mince Muscle Tissue in the Hood:
- a. Place the isolated muscle tissues on a sterile plate inside the hood and rinse them twice with PBS to remove any remaining fur from their surface (Figure 5.2A).
- b. Mince the muscle tissue using sterile scissors into small pieces, approximately 2-3 mm³ in size (Figure 5.2B).
- 7. First Digestion Step:
- a. Transfer the minced muscle into the Digest 1 Mix solution, using 1 mL per GAS and 500 µL per TA (Figure 5.2C).
- b. Seal the tube with parafilm to prevent leakage and contamination.
- c. Incubate the tubes in a 37°C water bath for 30 minutes. Vortex gently after 15 minutes to enhance digestion efficiency (Figure 5.2D).
- d. Centrifuge at 150 x g for 5 min at 4°C (Figure 5.2E).
- e. Transfer the supernatant to a 15 mL tube, add an equal volume of pre-cooled Wash Solution (WS), and keep it on ice for subsequent filtration.
- 8. Second Digestion Step:
- a. Resuspend the pellet from the first centrifugation in Digest 2 Mix using 1 mL per GAS and 500 μL per TA, seal the tube with parafilm, and incubate in a 37°C water bath for 15 minutes (Figure 5.2F).

- b. Following incubation, dilute the mixture 1:1 with WS, then gently mince it three times using a 5 mL syringe equipped with an 18G needle to further dissociate the tissue (Figure 5.2G).
- c. Filter the suspension through a 40  $\mu$ m cell strainer into a 50 mL tube, combining it with the previously set aside supernatant.
- 9. Final Centrifugation and Cell Resuspension:
- a. Centrifuge the combined filtrate at 150 x g for 5 min at 4°C.
- b. Carefully aspirate the supernatant, ensuring minimal disturbance to the cell pellet.
- c. Resuspend the cell pellet in WS ( $10^6$  cells per 50  $\mu$ L) for downstream applications. Notes:
- Ensure all instruments and solutions are sterile to prevent contamination.
- Handle sharp instruments with care to prevent injury.
- Monitor the status of tissue throughout each digestion step to optimize digestion conditions for different muscle types or conditions.

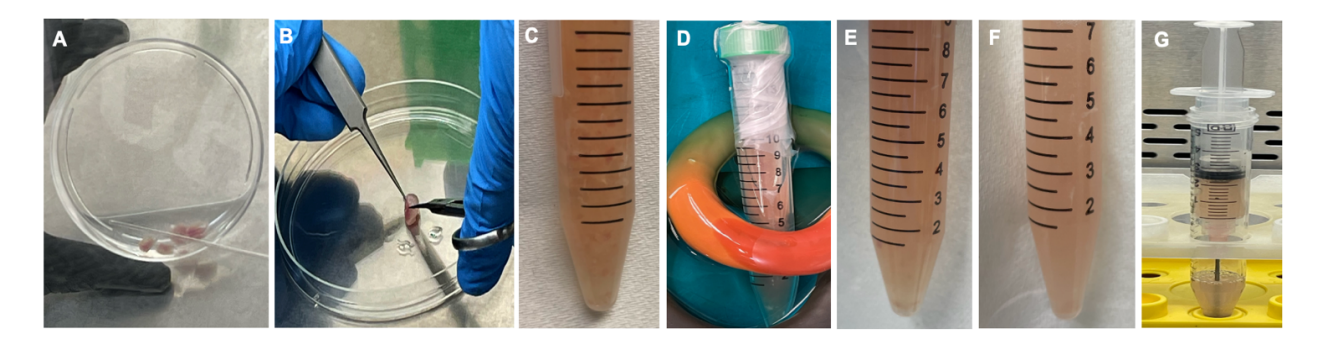


Figure 5.2 Mechanical and enzymatic dissociation of skeletal muscle to release single cells. Trituration of skeletal muscle TA and GAS to release myofibers. (A) Wash the muscles with PBS to remove any remaining fur on the muscles. (B) Mince the muscle with scissors into pieces of approximately 2-3 mm³ in size. (C) Transfer the minced muscles into Digest 1 mix solution in a 15mL tube and seal it. (D)Transfer the tube into a

37°C water bath. (E) After 30 min of water bath incubation of the minced muscle in Digest

1. (F) After 15 min of water bath incubation in Digest 2. (G) Gently mince the tissue mixture by passing through a 5 mL syringe fitted with an 18G needle three times.

# 5.3.3 Antibody staining of mono-nuclear cells associated with skeletal muscle

Timing: ~1 h for 1 mouse. Add 15-30 min for each additional mouse.

In this step, stain the cells with antibodies to negatively exclude hematopoietic cells (anti-CD45 antibody), endothelial cells (anti-CD31 antibody), and muscle satellite cells (anti-integrin alpha 7 antibody).

- 10. Label MACS tubes (1.5 mL tube) for each experimental sample.
- 11. Transfer the cells suspension from the 50 mL tube into their respective MACS tubes.
- 12. Stain cell samples with biotin-conjugated anti-CD31, CD45, integrin alpha 7 antibodies at a 1:50 dilution for 15 min in a 4°C refrigerator.
- 13. Centrifuge the cells at 150 x g for 5 min at room temperature (RT).
- 14. Aspirate the supernatant and resuspend the cell pellet in WS (10<sup>6</sup> cells per 50 μL), gently pipetting up and down to fully dissociate into a single-cell suspension.
- 15. Add Anti-Biotin microbeads at a 1:5 dilution and incubate for 15 min in a 4°C refrigerator.
- 16. While incubating, prepare the magnetic and rinsing columns by rinsing each column with 3 mL of WS (Figure 5.3).
- 17. Transfer the cell suspension into the column and collect the flow-through containing unlabelled cells.

- 18. Wash the column twice with 1 mL of WS, collecting the pass-through cells and combining them with the previous flow-through.
- 19. Centrifuge the combined cells at 150 x g for 4 min at RT.
- 20. During centrifugation, aspirate gelatin from the coating plate, rinse the plate with PBS and add FAPs pre-warmed culture medium.
- 21. After centrifugation, carefully aspirate the supernatant and resuspend the cell pellet with 1 mL FAPs culture medium.
- 22. Determine the cell concentration using a cell counter.
- 23. Seed the cells at a density of 10,000 per cm<sup>2</sup> in wells pre-filled with FAP cultural medium. Change the medium every other day until cells reach 80% confluency.



**Figure 5.3** MACS isolation of FAPs. The mixed cells flow through the MACS column, with PDGFR $\alpha^+$  cells being sorted out after negative selection using anti-Biotin microbeads, which bind to Biotin-conjugated cells.

# 5.3.4 Downstream ex vivo analysis of sorted FAPs

In this section we discuss downstream applications including cell culture, immunofluorescence (IF), isolation of FAPs derived extracellular vesicles.

### Passaging of FAPs:

- 1. Precoat wells for cell culture with gelatin 2-3 h prior to seeding cells.
- 2. Remove the growth medium (GM) and rinse the cells with PBS.
- 3. Add warmed Accutase to cover the cells and incubate wells for 5 min at 37°C.
- 4. Confirm under a microscope that >90% of the cells have detached from the well.
- 5. Gently add an equal volume of warmed GM to dilute the Accutase and transfer the cell suspension into a 15 mL tube.
- 6. Centrifuge the cell suspension at 300 x g for 4 min at RT.
- 7. Aspirate the supernatant and resuspend the cell pellet in GM for cell counting.
- 8. Seed cells at the appropriate density (such as 10,000 per cm<sup>2</sup>) and continue culturing in GM.

Note: Passage the isolated FAPs when they reach approximately 80% confluent to prevent differentiation. After 3-4 days of culturing, the isolated FAPs are usually ready for passage. Refresh the GM every other day to maintain optimal conditions.

# Immunofluorescence staining of the FAPs:

- Remove the GM from each well. Rinse the cells with PBS to remove any residual GM.
- Add enough 4% paraformaldehyde (PFA) to cover the cells and incubate at RT for
   15 min to fix them.
- Remove the 4% PFA solution and wash the cells with PBS three times.
- 4. Permeabilize cells with 0.1% Triton-X solution for 10 min at RT.
- 5. Wash the cells with PBS three times to remove the Triton-x solution.

- Add blocking buffer (5% Normal Donkey Serum, 5% BSA in PBS) for 1 hour at RT to block non-specific binding sites.
- 7. Aspirate the blocking buffer, add the primary antibody diluted in blocking buffer to each well and incubate overnight (~12 h) at 4°C.
- 8. Remove the primary antibody solution and wash the cells four times for 15 min with PBS at RT to ensure thorough removal of unbound primary antibody.
- Add the secondary antibody diluted in PBS to cover the cells and incubate for 1 hour at RT.
- 10. Remove the secondary antibody solution from the well and wash the cells with PBS our times for 15 min each at RT.
- 11. Add DAPI solution (1  $\mu$ g/mL DAPI in PBS) to the cells and incubate for 5 min at RT to stain the nuclei.
- 12. Remove the DAPI staining solution and wash the cells with PBS for 5 min to remove excess DAPI.
- 13. After the final wash, the cells are ready for imaging. Cover the wells to prevent any contamination or drying out of the cells.

#### Collect EVs derived from the FAPs:

- 1. Culture FAPs in GM until they reach 70-80% confluency.
- 2. Replace the GM without FBS to avoid contamination with exogenous vesicles from the serum and incubate for 24 h to allow the cells to release EVs into the media.
- After 24 h incubation, collect the conditioned media from the cell culture and refeed
  the cells with GM without FBS for another 24 h (The conditioned medium was
  collected twice, each after 24 h of incubation).

- 4. Centrifuge the collected media at 300 x g for 10 min to remove cells and large debris.
- 5. Transfer the supernatant to a new tube and centrifuge again at 1,000 xg for 30 min to remove smaller debris and apoptotic bodies.
- 6. Transfer the supernatant to ultracentrifuge tubes.
- 7. Ultracentrifuge at 100,000 x g for 2 h at 4°C to pellet the EVs.
- 8. Carefully remove the supernatant without disturbing the EV pellet.
- 9. Washing the EV pellet in pre-cold PBS.
- 10. Ultracentrifuge again at 100,000 x g for 1h at 4°C to pellet the EVs.
- 11. Remove the supernatant and resuspend the EV pellet in a small volume of PBS.
- 12. Store the isolated EVs at -80°C for long-term storage. Avoid repeated freeze-thaw cycles.

# 5.3.5 Expected outcomes

After completing the detailed isolation procedure outlined above, muscle-resident endothelial cells, hematopoietic cells, and muscle satellite cells are effectively removed through negative selection, while FAPs are enriched through positive selection. Utilizing a combination of two-step enzymatic and mechanical dissociation of skeletal muscle along with the MACS protocol, we typically obtain approximately 600,000 FAPs from two TA and two GAS muscles from healthy adult mice aged 12-16 weeks. FAPs were immunostained for PDGFRα, a cytoplasmic marker of FAPs, immediately after MACS isolation (Figure 5.4A). Despite the sorted cells not fully spreading out, the immunostaining results demonstrated high purity. Upon culturing, the isolated FAPs typically reached confluency within three days. Their identity and purity were further

validated by assessing the cytoplasmic markers PDGFRα and Myosin Heavy Chain (MHC), the latter being a marker expressed in muscle myofibers (Figure 5.4B). Furthermore, co-immunofluorescence staining for PDGFRα and Sca1 confirmed a purity level exceeding 90% (Figure 5.4C).

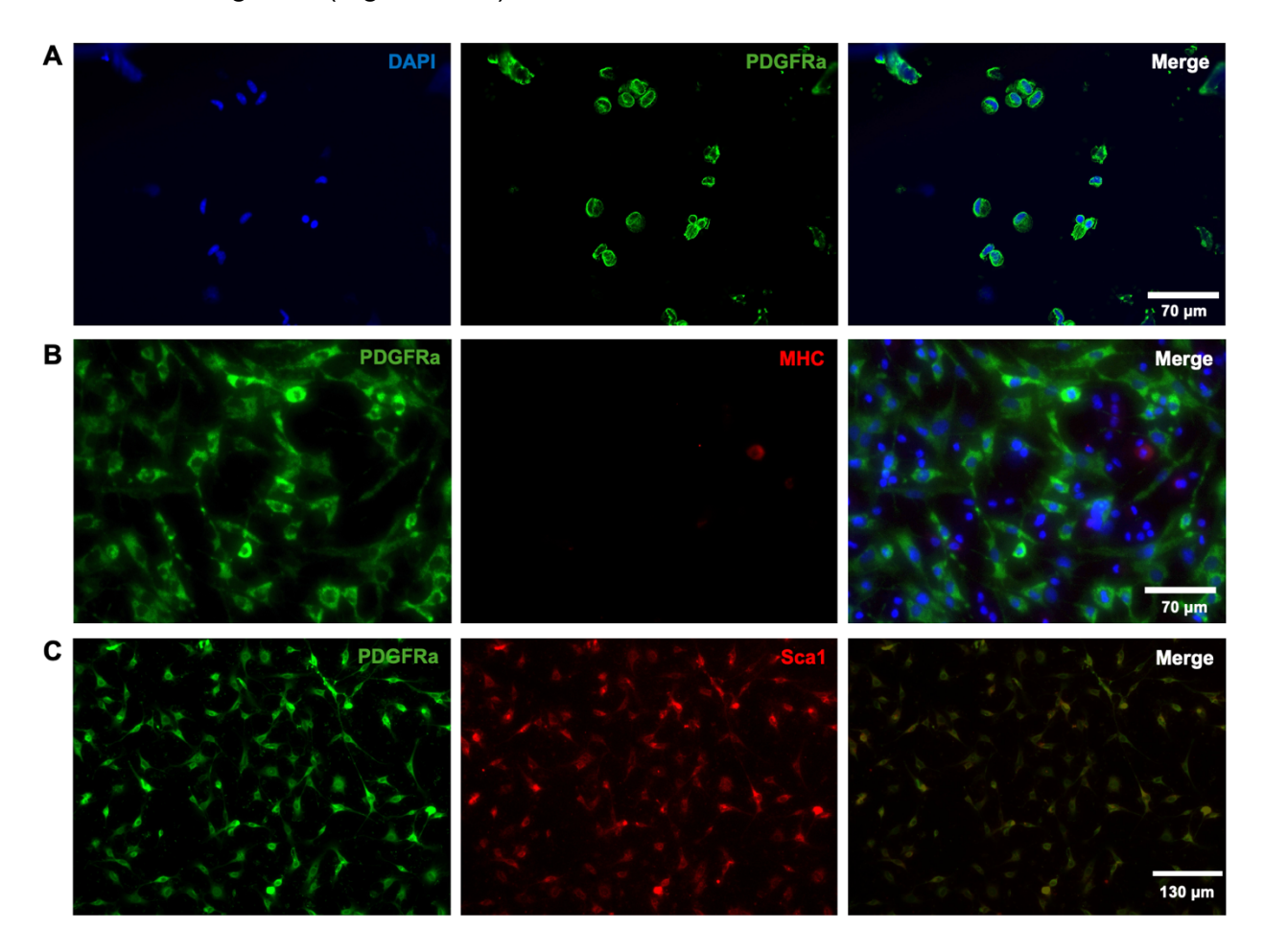


**Figure 5.4** Immunofluorescent staining of MACS-sorted FAPs. (A) FAPs immediately after MACS were immunostained for nuclei (DAPI, blue) and PDGFRα (green). Scale bar: 70 μm. (B) FAPs cultured for two days were immunostained for nuclei (DAPI, blue), PDGFRα (green), and MHC (red). Scale bar: 70 μm. (C) FAPs cultured for two days were immunostained for nuclei (DAPI, blue), PDGFRα (green), and Sca1 (red). Scale bar: 130 μm.

#### 5.3.6 Limitations

This method predominantly yields FAPs, however, the isolation process may alter their cellular status. Additionally, ex vivo culturing could further modify FAP characteristics. It is crucial to acknowledge that both the isolation process and subsequent ex vivo culturing can potentially affect the intrinsic properties of FAPs. Further studies are necessary to investigate these effects, as they are essential for refining the isolation technique and ensuring the reliability and validity of subsequent experimental outcomes.

#### 5.3.7 Troubleshooting

#### **Problem 1**

Low purity of isolated FAPs.

#### Potential solution

- 1. Gently resuspend cell pellets thoroughly before adding biotin-conjugated antibodies and Anti-Biotin microbeads to make sure they can access all the single cells. Additionally, optimizing dilution of these antibodies and microbeads according to the cell amounts specified in the product sheet. Finally, apply the appropriate column based on the number of cells to isolate them effectively.
- 2. Add the FcR Blocking Reagent (Miltenyi Biotec, Cat# 130-092-575) to the wash buffer when resuspending cell pellets collected from muscle tissue. Mix the buffer with the cells and incubate for 10 min in a 4°C refrigerator. Subsequently, incubate the cells with biotin-conjugated antibodies. This step may enhance the specificity of labelling with MACS antibodies or MACS microbeads, improving the purity of isolated FAPs.

#### Problem 2

Low yield of MACS-sorted FAPs.

#### Potential solution

- Increase the quantity of extracted skeletal muscle. Carefully and thoroughly dissect the skeletal muscles of interest to maximize cell yield.
- Avoid over-digestion of skeletal muscle, be cautious with digestion times. Overdigestion during incubation in Digest mix 1 and 2 can potentially decrease the viability of the cells. Optimize digestion times to balance between effective tissue dissociation and cell viability

#### Problem 3

Too many blood cells in the final isolated cells.

#### Potential solution

1. Resuspend the cell pellet in 1 mL of Red Blood Cell Lysis solution to remove erythrocytes after isolating the cells from muscle tissue. Incubate at room temperature for no more than 2 min. Centrifuge at 150 x g for 10 min and aspirate the supernatant completely. Next, resuspend the cells in an appropriate amount of wash medium containing biotin-conjugated antibodies, continuing step 12.

#### Problem 4

Primary FAPs do not attach well after first passage.

### Potential solution

 To detach FAPs from the plate, apply Accutase instead of Trypsin to incubate the cells at 37°C for 5 min. Gently tap the plate to ensure the cells are fully detached.
 Dilute the accutase-cell mixture with freshly prepared pre-warmed culture medium, then collect the cell pellets by centrifuging at 300 x g for 4 min. Gently resuspend the cell pellets in the pre-warmed culture medium and seed them onto a gelatin-coated plate.

# **5.4 Key Resource Tables**

Table 1. Key Resource

REAGENT or	SOURCE	IDENTIFIER
RESOURCE		
CD45-Biotin, mouse	Miltenyi Biotec	Cat#130-124-209
CD31-Biotin, mouse	Miltenyi Biotec	Cat#130-119-662
Anti-integrin alpha 7- Biotin, mouse	Miltenyi Biotec	Cat#130-128-938
Anti-Biotin Microbeads	Miltenyi Biotec	Cat#130-090-485
anti-mPDGFRα	R&D systems	Cat#AF1062
anti-mouse Ly-6A/E	BD Biosciences	Cat#557403
Anti-mouse Myosin heavy chain	DSHB	MF 20
Human basic fibroblast growth factor (bFGF)	EMD Millipore	Cat#GF003
DMEM, high glucose	Gibco	Cat#11-995-065
Collagenase type II,	Worthington-	Cat#LS004176 (1
powder	Biochem	gm)
Collagenase/Dispase,	Millipore Sigma	Cat#10269638001

Fetal bovine serum (FBS)	Neuromics	Cat#FBS002
Ham's F-10 nutrient mix (F10)	Gibco	Cat#11550043
Gelatin, 0.1%	STEMCELL Technology	Cat#07903
PBS, without calcium and magnesium	Corning	Cat#21-040-CV
Triton X-100	ThermoFisher Scientific	Cat#J66624.AP
Penicillin-Streptomycin (P-S), 10,000 U/mL	Gibco	Cat#15140122
Typan Blue	Corning	Cat#25-900-CI
Mouse: C57BL/6J, male, approximately 8 weeks old	The Jackson Laboratory	Cat#000664
40 μm cell strainers, sterile	Corning	Cat#07-201-430
Glass Pasteur pipette	Fisher Scientific	Cat#13-678-20D
5 mL Syringe	Fisher Scientific	Cat#14955452

# Table 2. Wash Solution (WS)

Reagent	Final	Amount
	concentration	

FBS	10%	5 mL
Penicillin/Streptomycin (P-S),	1%	500 μL
10,000 U/mL		
F10	n/a	44.5 mL
Total	n/a	50 mL

Table 3. Digest Mix Solutions

Digest Mix	Composition	Instructions
Digest 1 mix	WS with 2.433 mg/mL Collagenase Type II	Keep on ice
Digest 2 mix	WS with 2.5 mg/mL Collagenase/Dispase	Keep on ice

Table 4. Growth Media (GM)

Reagent	Final	Amount
	concentration	
Heat-inactivated Fetal Bovine Serum (FBS)	20%	4 mL
Human basic fibroblast growth factor (bFGF)	2.5	1 μL
(50 μg/mL aliquot)	ng/mL	
Penicillin/Streptomycin (P-S), 10,000 U/mL	1%	200 µL
Dulbecco's modified Eagle's medium	n/a	15.8 mL
(DMEM), high glucose		
Total	n/a	20 mL

#### **CHAPTER 6**

#### SUMMARY AND CONCLUSIONS

### 6.1 NPC-EV Mitigate the ALS's Pathological Phenotypes

ALS is a fatal neurodegenerative disease characterized by progressive motor neuron degeneration, oxidative stress, and neuroinflammation. Transplantation of human NPCs has demonstrated neuroprotective and regenerative effects in ALS models. However, their clinical application remains limited due to ethical and safety concerns. To address these challenges, we explored NPC-EVs as a potential cell-free therapeutic alternative in ALS models, focusing on their neuroprotective, antioxidative, and anti-inflammatory properties.

Our **in vitro** findings demonstrated the neuroprotective effects of NPC-EVs, as they significantly enhanced the survival and proliferation of ALS-like motor neurons (NSC-34 SOD1<sup>G93A</sup> cells) under oxidative stress. Additionally, NPC-EVs exhibited antioxidative effects by reducing reactive oxygen species (ROS) levels, which may help counteract mitochondrial dysfunction-a key contributor to ALS pathology. Beyond their neuroprotective and antioxidative properties, NPC-EVs also demonstrated anti-inflammatory effects, as evidenced by their ability to attenuate TNF-α-induced morphological changes in microglia, highlighting their potential role in modulating neuroinflammation. Notably, at the same concentration, NPC-EVs exhibited greater efficacy than EVs derived from a non-neuronal cell source (HEK-EVs) in promoting motor neuron viability, proliferation and antioxidative defense. This suggests that NPC-EVs may

contain specific biomolecules that provide enhanced benefits to motor neurons or that they are more efficiently taken up by motor neurons compared to HEK-EVs. Further investigation into these mechanisms could optimize the therapeutic potential of NPC-EVs for ALS treatment. In **in vivo** studies, NPC-EVs demonstrated superior uptake efficiency in the central nervous system (CNS) compared to HEK-EVs, suggesting enhanced bioavailability and targeted delivery. Notably, following intravenous administration in an ALS mouse model (SOD1<sup>G93A</sup> mice), NPC-EVs modulated NF-κB signaling in the spinal cord, a key inflammatory pathway implicated in ALS progression. Given the critical role of chronic neuroinflammation in exacerbating motor neuron degeneration, the ability of NPC-EVs to influence this pathway highlights their potential as a multifaceted therapeutic strategy.

#### **Conclusion and Future Directions:**

The findings presented in this dissertation provide compelling evidence that NPC-EVs exhibit therapeutic potential in ALS by exerting neuroprotective, antioxidative, and anti-inflammatory effects, which suggests NPC-EVs could serve as a promising alternative to stem cell-based therapies while overcoming safety and ethical concerns.

Despite these promising results, further studies are necessary to optimize the clinical translation of NPC-EVs. Future research should focus on:

- Determining optimal dosing, administration timing, and treatment duration to maximize therapeutic benefits.
- Elucidating the molecular mechanisms by which NPC-EVs exert their neuroprotective effects, particularly their interactions with recipient cells in the CNS.

- 3. Identifying and optimizing the key biomolecules within NPC-EVs that contribute to their neuroprotective, antioxidative, and anti-inflammatory effects to enhance their therapeutic potential for ALS greater and other neurodegenerative diseases.
- Evaluating long-term efficacy and safety in preclinical ALS models, including assessments of disease onset, lifespan extension, and motor function improvement.
- 5. Comparing NPC-EVs with other EV-based and pharmacological therapies to determine their relative efficacy and potential for combination treatments.

By addressing these aspects, NPC-EVs could be further developed into a viable therapeutic strategy for ALS, potentially paving the way for clinical trials. This research contributes valuable insights into EV-based therapeutics and underscores the potential of NPC-EVs in tackling the multifaceted pathology of ALS, ultimately advancing the field of neurodegenerative disease treatment.

# 6.2 Regenerating Skeletal Muscle-derived EVs at the Anti-Inflammatory Stage Mitigate ALS-Associated Muscle Atrophy

ALS is a progressive neuromuscular disease characterized by motor neuron degeneration and severe muscle atrophy, with no effective treatments currently available. Emerging studies indicate that skeletal muscle is a promising therapeutic target for ALS, as defects in skeletal muscle can retrogradely impact the central nervous system. Chronic inflammation, impaired muscle regeneration, and proteostasis dysregulation are key contributors to ALS-related muscle atrophy, highlighting the need for novel therapeutic approaches that directly target muscle pathology. This dissertation investigates the therapeutic potential of EVs derived from regenerating skeletal muscle 14 days post-

acute injury (CTXD14SkM-EVs), which originate from an anti-inflammatory microenvironment within regenerating muscle, as a strategy to combat ALS-associated muscle atrophy.

Our findings demonstrate that CTXD14SkM-EVs effectively mitigate musclewasting processes through multiple mechanisms. In vitro, CTXD14SkM-EVs promoted myogenesis in a muscle-wasting model induced by the pro-inflammatory cytokine TNF-α by enhancing myoblast differentiation and fusion indices. This suggests their ability to counteract inflammation-driven muscle degeneration. In vivo, intramuscular administration of CTXD14SkM-EVs in an ALS mouse model (SOD1<sup>G93A</sup> mice) resulted in significant improvements in muscle mass and myofiber size. An increased percentage of myofibers with centralized nuclei in treated muscles, along with upward trend in the expression of the muscle differentiation marker MyoD, further suggests enhanced muscle regeneration. Chronic inflammation in ALS is characterized by an imbalance in macrophage polarization, where a sustained pro-inflammatory M1 phenotype contributes to muscle degeneration by impairing muscle stem cell function and exacerbating protein degradation. CTXD14SkM-EVs facilitated a shift from the pro-inflammatory M1 phenotype to the anti-inflammatory M2 phenotype in ALS skeletal muscle, creating a more favourable environment for tissue repair. Additionally, CTXD14SkM-EVs significantly suppressed excessive activation of the NF-kB pathway, a major driver of muscle inflammation, proteolysis, and impaired regeneration in ALS. By downregulating NF-κB and its phosphorylated form (pNF-κB), CTXD14SkM-EVs reduced inflammatory signaling and proteolytic activity, thereby preserving muscle integrity and function.

#### **Conclusion and Future Directions**

This study is the first to provide strong evidence that EVs derived from regenerating skeletal muscle possess significant therapeutic potential in mitigating ALS-associated muscle atrophy. By promoting muscle regeneration, modulating immune responses, and suppressing inflammation-driven proteolysis, CTXD14SkM-EVs address multiple pathological aspects of ALS-related muscle degeneration. These findings establish a foundation for further exploration of regenerating muscle-derived EVs as a novel therapeutic approach for ALS and other muscle atrophy-related diseases.

To advance the clinical translation of CTXD14SkM-EVs, future research should focus on:

- Elucidating the molecular cargo of CTXD14SkM-EVs responsible for their therapeutic effects, including proteins, microRNAs, and lipids that mediate muscle regeneration and inflammation resolution.
- Optimizing EV delivery and dosing strategies to enhance their therapeutic efficacy and ensure reproducibility in preclinical models.
- Investigating long-term effects and safety of CTXD14SkM-EV administration in ALS and other muscle-wasting diseases to assess their feasibility for clinical applications.
- Exploring combination therapies where CTXD14SkM-EVs could be used alongside neuroprotective interventions to provide a comprehensive approach for ALS treatment.

Overall, this study highlights the potential of regenerating muscle-derived EVs as a novel and promising therapeutic approach for ALS-related muscle atrophy. With further

refinement and validation, CTXD14SkM-EVs could pave the way for innovative muscletargeted therapies, ultimately improving patient outcomes and addressing a critical gap in ALS treatment strategies.

# 6.3 Synergistic Effects of Regenerating Skeletal Muscle-Derived EVs, FAP-Derived EVs, and NSC-Derived EVs in Mitigating ALS-Associated Muscle Atrophy

Skeletal muscle was traditionally considered a secondary consequence of motor neuron loss in ALS; however, emerging evidence has revealed that skeletal muscle actively contributes to ALS progression through retrograde signaling to the CNS. This dissertation establishes skeletal muscle as a viable therapeutic target for ALS and investigates the potential of EVs derived from regenerating skeletal muscle and NSCs as a novel intervention. Specifically, we examined EVs derived from day 3 post-cardiotoxin (CTX)-induced regenerating skeletal (CTXSkM-EVs), fibro/adipogenic muscle progenitors (CTXFAP-EVs), and neural stem cells (NSC-EVs) to evaluate their therapeutic effects on ALS-associated muscle and neuronal dysfunction. During the early stage of skeletal muscle regeneration, muscle tissue actively secretes EVs to facilitate repair. To further elucidate the therapeutic mechanisms within this EV pool, we specifically examined both CTXSkM-EVs, representing the total EV population from regenerating skeletal muscle, and CTXFAP-EVs, derived from FAPs, a key mesenchymal stem cell population involved in muscle regeneration. FAPs reach peak activity three days post-acute injury and secrete factors that coordinate muscle repair by interacting with satellite cells and immune cells.

Given their regenerative potential, FAP-derived EVs may play a crucial role in mediating intercellular communication and promoting skeletal muscle regeneration.

Our in vitro findings demonstrate that CTXSkM-EVs and CTXFAP-EVs promote myogenesis in atrophic muscle cells, enhancing myoblast differentiation and fusion in a TNF-α-induced muscle-wasting model. This suggests their broader therapeutic potential for muscle atrophic diseases beyond ALS. Furthermore, these EVs improved cell viability and mitochondrial function in ALS-like motor neurons, indicating their role in mitigating oxidative stress and preserving cellular energy homeostasis in degenerating motor neurons. These results highlight the capacity of regenerating muscle-derived EVs to address both muscle and neuronal pathology in ALS. Beyond individual EV applications, we introduced a novel mixed EV-based therapeutic strategy, combining NSC-EVs with either CTXSkM-EVs or CTXFAP-EVs to simultaneously target skeletal muscle degeneration and CNS pathology. In vivo, this combination therapy effectively mitigated muscle atrophy, likely by promoting muscle regeneration and suppressing NF-κB signaling in ALS-affected skeletal muscle. Notably, EV treatment also modulated NF-κB signaling in the spinal cord of SOD1<sup>G93A</sup> mice, suggesting a potential neuroprotective effect that extends beyond skeletal muscle. These findings provide the first evidence that regenerative muscle-derived EVs, particularly when combined with NSC-EVs, offer a promising dual-targeted therapeutic strategy for ALS.

#### **Conclusion and Future Directions**

This dissertation provides strong evidence that regenerating skeletal musclederived EVs, alone or in combination with NSC-EVs, offer a novel and multifaceted therapeutic approach for ALS. By addressing muscle atrophy, mitochondrial dysfunction, inflammation, and neurodegeneration, these EVs hold significant potential as a cell-free, regenerative therapy that complements existing neuroprotective strategies. To facilitate the clinical translation of this EV-based approach, future research should focus on:

- Optimizing EV dosage, administration routes, and treatment timing to maximize therapeutic efficacy.
- 2. Characterizing the molecular cargo of CTXSkM-EVs and CTXFAP-EVs to identify key bioactive components responsible for their therapeutic effects.
- Independently assess the therapeutic efficacy of CTXSkM-EVs and CTXFAP-EVs
  in ALS preclinical animal models to determine their distinct contributions to muscle
  regeneration and disease modifications.
- 4. Assessing long-term safety and efficacy in preclinical ALS models to evaluate disease progression, lifespan extension, and functional recovery.
- Expanding investigations to other neuromuscular diseases characterized by muscle atrophy and neurodegeneration, such as muscular dystrophy, sarcopenia, and cachexia.

These findings establish a foundation for the further development of EV-based interventions that target both muscle degeneration and CNS pathology in ALS. By refining EV therapies, we may move closer to a clinically viable, multi-targeted treatment that offers meaningful benefits for ALS patients and other neuromuscular disorders.

#### REFERENCES

- 1. Byrne, S., et al., *Rate of familial amyotrophic lateral sclerosis: a systematic review and meta-analysis.* J Neurol Neurosurg Psychiatry, 2011. **82**(6): p. 623-7.
- Watanabe, T., et al., Protective effects of MCI-186 on cerebral ischemia: possible involvement of free radical scavenging and antioxidant actions. J Pharmacol Exp Ther, 1994. 268(3): p. 1597-604.
- Miller, T.M., et al., Trial of Antisense Oligonucleotide Tofersen for SOD1 ALS. N
   Engl J Med, 2022. 387(12): p. 1099-1110.
- Tzeplaeff, L., et al., Current State and Future Directions in the Therapy of ALS.
   Cells, 2023. 12(11).
- 5. Bradford, D. and K.E. Rodgers, *Advancements and challenges in amyotrophic lateral sclerosis*. Front Neurosci, 2024. **18**: p. 1401706.
- 6. Liu, J. and F. Wang, *Role of Neuroinflammation in Amyotrophic Lateral Sclerosis:*Cellular Mechanisms and Therapeutic Implications. Front Immunol, 2017. 8: p. 1005.
- 7. Goutman, S.A., et al., Stem cell treatments for amyotrophic lateral sclerosis: a critical overview of early phase trials. Expert Opin Investig Drugs, 2019. **28**(6): p. 525-543.
- 8. Ferraiuolo, L., A. Frakes, and B.K. Kaspar, *Neural stem cells as a therapeutic approach for amyotrophic lateral sclerosis.* Mol Ther, 2013. **21**(3): p. 503-5.

- 9. Corti, S., et al., Systemic transplantation of c-kit+ cells exerts a therapeutic effect in a model of amyotrophic lateral sclerosis. Hum Mol Genet, 2010. **19**(19): p. 3782-96.
- 10. Yan, J., et al., Combined immunosuppressive agents or CD4 antibodies prolong survival of human neural stem cell grafts and improve disease outcomes in amyotrophic lateral sclerosis transgenic mice. Stem Cells, 2006. **24**(8): p. 1976-85.
- 11. Zalfa, C., et al., *Transplantation of clinical-grade human neural stem cells reduces* neuroinflammation, prolongs survival and delays disease progression in the SOD1 rats. Cell Death Dis, 2019. **10**(5): p. 345.
- 12. Volarevic, V., et al., *Ethical and Safety Issues of Stem Cell-Based Therapy.* Int J Med Sci, 2018. **15**(1): p. 36-45.
- Pitt, J.M., G. Kroemer, and L. Zitvogel, Extracellular vesicles: masters of intercellular communication and potential clinical interventions. J Clin Invest, 2016.
   126(4): p. 1139-43.
- 14. Apodaca, L.A., et al., *Human neural stem cell-derived extracellular vesicles mitigate hallmarks of Alzheimer's disease.* Alzheimers Res Ther, 2021. **13**(1): p. 57.
- 15. Lee, E.J., et al., *Human neural stem cell-derived extracellular vesicles protect against Parkinson's disease pathologies.* J Nanobiotechnology, 2022. **20**(1): p. 198.

- 16. Vogel, A.D., R. Upadhya, and A.K. Shetty, *Neural stem cell derived extracellular vesicles: Attributes and prospects for treating neurodegenerative disorders.*EBioMedicine, 2018. **38**: p. 273-282.
- 17. Webb, R.L., et al., *Human Neural Stem Cell Extracellular Vesicles Improve Tissue* and Functional Recovery in the Murine Thromboembolic Stroke Model. Transl Stroke Res, 2018. **9**(5): p. 530-539.
- 18. Cookson, M.R., P.G. Ince, and P.J. Shaw, *Peroxynitrite and hydrogen peroxide induced cell death in the NSC34 neuroblastoma x spinal cord cell line: role of poly (ADP-ribose) polymerase.* J Neurochem, 1998. **70**(2): p. 501-8.
- 19. Richardson, K., et al., *The effect of SOD1 mutation on cellular bioenergetic profile*and viability in response to oxidative stress and influence of mutation-type. PLoS
  One, 2013. **8**(6): p. e68256.
- 20. Sanghai, N. and G.K. Tranmer, *Hydrogen Peroxide and Amyotrophic Lateral Sclerosis: From Biochemistry to Pathophysiology.* Antioxidants (Basel), 2021. **11**(1).
- 21. Rosen, D.R., et al., *Mutations in Cu/Zn superoxide dismutase gene are associated* with familial amyotrophic lateral sclerosis. Nature, 1993. **362**(6415): p. 59-62.
- 22. Muyderman, H. and T. Chen, *Mitochondrial dysfunction in amyotrophic lateral sclerosis a valid pharmacological target?* Br J Pharmacol, 2014. **171**(8): p. 2191-205.
- 23. Hooten, K.G., et al., *Protective and Toxic Neuroinflammation in Amyotrophic Lateral Sclerosis*. Neurotherapeutics, 2015. **12**(2): p. 364-75.

- 24. Liu, Z., et al., *Peripheral and Central Nervous System Immune Response Crosstalk in Amyotrophic Lateral Sclerosis.* Front Neurosci, 2020. **14**: p. 575.
- 25. Beland, L.C., et al., *Immunity in amyotrophic lateral sclerosis: blurred lines between excessive inflammation and inefficient immune responses.* Brain Commun, 2020. **2**(2): p. fcaa124.
- 26. Mantovani, S., et al., *Immune system alterations in sporadic amyotrophic lateral sclerosis patients suggest an ongoing neuroinflammatory process.* J Neuroimmunol, 2009. **210**(1-2): p. 73-9.
- 27. Frakes, A.E., et al., *Microglia induce motor neuron death via the classical NF-kappaB pathway in amyotrophic lateral sclerosis.* Neuron, 2014. **81**(5): p. 1009-1023.
- 28. Daga, K.R., et al., *Microglia morphological response to mesenchymal stromal cell* extracellular vesicles demonstrates EV therapeutic potential for modulating neuroinflammation. J Biol Eng, 2024. **18**(1): p. 58.
- 29. Dutta, K., et al., *Mitigation of ALS Pathology by Neuron-Specific Inhibition of Nuclear Factor Kappa B Signaling.* J Neurosci, 2020. **40**(26): p. 5137-5154.
- 30. Gurney, M.E., et al., *Motor neuron degeneration in mice that express a human Cu,Zn superoxide dismutase mutation.* Science, 1994. **264**(5166): p. 1772-5.
- 31. Vinsant, S., et al., Characterization of early pathogenesis in the SOD1(G93A) mouse model of ALS: part I, background and methods. Brain Behav, 2013. **3**(4): p. 335-50.
- 32. Teng, Y.D., et al., Multimodal actions of neural stem cells in a mouse model of ALS: a meta-analysis. Sci Transl Med, 2012. **4**(165): p. 165ra164.

- 33. Hwang, D.H., et al., Intrathecal transplantation of human neural stem cells overexpressing VEGF provide behavioral improvement, disease onset delay and survival extension in transgenic ALS mice. Gene Ther, 2009. **16**(10): p. 1234-44.
- 34. Glass, J.D., et al., *Transplantation of spinal cord-derived neural stem cells for ALS:*Analysis of phase 1 and 2 trials. Neurology, 2016. **87**(4): p. 392-400.
- 35. Baloh, R.H., et al., *Transplantation of human neural progenitor cells secreting GDNF into the spinal cord of patients with ALS: a phase 1/2a trial.* Nat Med, 2022. **28**(9): p. 1813-1822.
- 36. Knippenberg, S., et al., Intraspinal administration of human spinal cord-derived neural progenitor cells in the G93A-SOD1 mouse model of ALS delays symptom progression, prolongs survival and increases expression of endogenous neurotrophic factors. J Tissue Eng Regen Med, 2017. **11**(3): p. 751-764.
- 37. Cashman, N.R., et al., *Neuroblastoma x spinal cord (NSC) hybrid cell lines* resemble developing motor neurons. Dev Dyn, 1992. **194**(3): p. 209-21.
- 38. Masrori, P. and P. Van Damme, *Amyotrophic lateral sclerosis: a clinical review.*Eur J Neurol, 2020. **27**(10): p. 1918-1929.
- 39. E O Talbott, A.M.M., D Lacomis *The epidemiology of amyotrophic lateral sclerosis.*Handb Clin Neurol, 2016.
- 40. Christina Wolfson, D.E.G., Foluso Ishola, Maryam Oskoui, *Global Prevalence and Incidence of Amyotrophic Lateral Sclerosis*. Neurology, 2023.
- 41. Gokhan Burcin Kubat, P.P., Skeletal muscle dysfunction in amyotrophic lateral sclerosis: a mitochondrial perspective and therapeutic approaches. Neurological Sciences, 2024.

- 42. Safa Al-Sarraj, A.K., Matt Cleveland, Pierre-François Pradat, Andrea Corse, Jeffrey D Rothstein, Peter Nigel Leigh, Bams Abila, Stewart Bates, Jens Wurthner, Vincent Meininger, *Mitochondrial abnormalities and low grade inflammation are present in the skeletal muscle of a minority of patients with amyotrophic lateral sclerosis; an observational myopathology study.* Acta Neuropathologica Communications, 2014.
- 43. Yanan Ji, M.L., Mengyuan Chang, Ruiqi Liu, Jiayi Qiu, Kexin Wang, Chunyan Deng, Yuntian Shen, Jianwei Zhu, Wei Wang, Lingchi Xu, Hualin Sun, Inflammation: Roles in Skeletal Muscle Atrophy. Antioxidants, 2022.
- 44. Emma Källstig, B.D.M., Bernard L Schneider, *The Links between ALS and NF-κB*.
  International Journal of Molecular Sciences, 2021.
- 45. Dongsheng Cai, J.D.F., Nicholas E. Tawa, Jr., Peter A. Melendez, Byung-Chul Oh, Hart G.W. Lidov, Per-Olof Hasselgren, Walter R. Frontera, Jongsoon Lee, David J. Glass, and Steven E. Shoelson, IKKβ/NF-κB Activation Causes Severe Muscle Wasting in Mice. Cell, 2004.
- 46. Elise Duchesne, S.S.D., Nicolas A. Dumont, *Impact of Inflammation and Anti- inflammatory Modalities on Skeletal Muscle Healing: From Fundamental Research to the Clinic.* Physical Therapy & Rehabilitation Journal, 2017.
- 47. Paola Fabbrizio, C.M., Jessica D'Agostino, Giuseppe Suanno, Lorenzo Quetti, Caterina Bendotti and Giovanni Nardo, *Intramuscular IL-10 Administration Enhances the Activity of Myogenic Precursor Cells and Improves Motor Function in ALS Mouse Model.* cells, 2023.

- 48. Yanjie Wang, J.L.a.Y.L., *Skeletal Muscle Regeneration in Cardiotoxin-Induced Muscle Injury Models.* International Journal of Molecular Sciences, 2022.
- 49. Zhaohong Liao, H.L., Xiaoting Jian, Jingwen Huang, Han Wang, Jijie Hu3 and Hua Liao, *Myofiber directs macrophages IL-10-Vav1-Rac1 efferocytosis pathway in inflamed muscle following CTX myoinjury by activating the intrinsic TGF-β signaling.* Cell Communication and Signaling, 2023.
- 50. Zhou, X.W.a.L., *The Many Roles of Macrophages in Skeletal Muscle Injury and Repair.* Frontiers in Cell and Developmental Biology, 2022.
- 51. Edwards, D.M.M.a.J.P., *Exploring the full spectrum of macrophage activation*. Nat Rev Immunol, 2008.
- Marı´a Ya´ nˇ ez-Mo´, P.R.-M.S., Zoraida Andreu, Apolonija Bedina Zavec, Francesc E. Borra's, Edit I. Buzas, Krisztina Buzas, Enriqueta Casal, Francesco Cappello, Joana Carvalho, Eva Cola´s, Anabela Cordeiro-da Silva, Stefano Fais, Juan M. Falcon-Perez, Irene M. Ghobrial, Bernd Giebel, Mario Gimona, Michael Graner, Ihsan Gursel, Mayda Gursel, Niels H. H. Heegaard, An Hendrix, Peter Kierulf, Katsutoshi Kokubun, Maja Kosanovic, Veronika Kralj-Iglic, Eva-Maria Kra¨ mer-Albers, Saara Laitinen, Cecilia La¨sser, Thomas Lener, Erzse´ bet Ligeti, Aija Line⁻, Georg Lipps, Alicia Llorente, Jan Lo¨tvall, Mateja Mancˇ ek-Keber, Antonio Marcilla, Maria Mittelbrunn, Irina Nazarenko, Esther N.M. Nolte-'t Hoen, Tuula A. Nyman, Lorraine O'Driscoll, Mireia Olivan, Carla Oliveira, E´ va Pa´ Ilinger, Hernando A. del Portillo, Jaume Revento´ s, Marina Rigau, Eva Rohde, Marei Sammar, Francisco Sa´ nchez-Madrid, N. Santare´m, Katharina Schallmoser, Marie Stampe Ostenfeld, Willem Stoorvogel, Roman Stukelj, Susanne G. Van der

- Grein, M. Helena Vasconcelos, Marca H. M. Wauben and Olivier De Weve, Biological properties of extracellular vesicles and their physiological functions. Journal of Extracellular Vesicles, 2015.
- 53. Tomasz Powrózek, D.P.-Z., Marcin Mazurek, Michael Ochieng Otieno, Mansur Rahnama-Hezavah, Teresa Małecka-Massalska, *TNF-α Induced Myotube Atrophy in C2C12 Cell Line Uncovers Putative Inflammatory-Related IncRNAs Mediating Muscle Wasting.* Int J Mol Sci, 2022.
- 54. Q Zhao, S.T.Y., J J Wang, J Zhou, S S Xing, C C Shen, X X Wang, Y X Yue, J Song, M Chen, Y Y Wei, Q P Zhou, T Dai, Y H Song *TNF alpha inhibits myogenic differentiation of C2C12 cells through NF-κB activation and impairment of IGF-1 signaling pathway.* Biochem Biophys Res Commun, 2015.
- 55. Ravi Chandran, T.J.K., Mirela Anghelina, Sudha Agarwal, *Biomechanical signals* upregulate myogenic gene induction in the presence or absence of inflammation.

  Am J Physiol Cell Physiol, 2007.
- Mark E. Gurney, H.P., Arlene Y. Chiu, Mauro C. Dal Canto, Cynthia Y. Polchow, Denise D. Alexander, Jan Caliendo, Afif Hentati, Young W. Kwon, Han-Xiang Deng, Wenje Chen, Ping Zhai, Robert L. Sufit, and Teepu Siddique, Motor Neuron Degeneration in Mice that Express a Human Cu, Zn Superoxide Dismutase Mutation. Science, 1995.
- 57. Elisabetta Carata, M.M., Simona Di Giulio, Stefania Mariano, Elisa Panzarini,

  Looking to the Future of the Role of Macrophages and Extracellular Vesicles in

  Neuroinflammation in ALS. International Journal of Molecular Sciences, 2023.

- 58. Jonathan M Van Dyke, I.M.S.-O., Corey Macrander, Dan Krakora, Michael G Meyer, Masatoshi Suzuki, *Macrophage-mediated inflammation and glial response in the skeletal muscle of a rat model of familial amyotrophic lateral sclerosis (ALS).*Exp Neurol, 2016.
- 59. Zhao, J., et al., *The Impact of Mitochondrial Dysfunction in Amyotrophic Lateral Sclerosis*. Cells, 2022. **11**(13).
- Fabbrizio, P., et al., Intramuscular IL-10 Administration Enhances the Activity of Myogenic Precursor Cells and Improves Motor Function in ALS Mouse Model.
   Cells, 2023. 12(7).
- 61. Gao, J., et al., *Therapeutics Targeting Skeletal Muscle in Amyotrophic Lateral Sclerosis*. Biomolecules, 2024. **14**(7).
- 62. Yanez-Mo, M., et al., *Biological properties of extracellular vesicles and their physiological functions.* J Extracell Vesicles, 2015. **4**: p. 27066.
- 63. Gao, G., et al., Neural stem cell-derived extracellular vesicles mitigate Alzheimer's disease-like phenotypes in a preclinical mouse model. Signal Transduct Target Ther, 2023. **8**(1): p. 228.
- 64. Webb, R.L., et al., *Human Neural Stem Cell Extracellular Vesicles Improve Recovery in a Porcine Model of Ischemic Stroke*. Stroke, 2018. **49**(5): p. 1248-1256.
- 65. Porcu, C., G. Dobrowolny, and B.M. Scicchitano, *Exploring the Role of Extracellular Vesicles in Skeletal Muscle Regeneration*. Int J Mol Sci, 2024. **25**(11).

- 66. Madaro, L., et al., *Denervation-activated STAT3-IL-6 signalling in fibro-adipogenic progenitors promotes myofibres atrophy and fibrosis.* Nat Cell Biol, 2018. **20**(8): p. 917-927.
- 67. Kallstig, E., B.D. McCabe, and B.L. Schneider, *The Links between ALS and NF-kappaB*. Int J Mol Sci, 2021. **22**(8).
- 68. Cai, D., et al., IKKbeta/NF-kappaB activation causes severe muscle wasting in mice. Cell, 2004. **119**(2): p. 285-98.
- 69. Wang, Y., J. Lu, and Y. Liu, *Skeletal Muscle Regeneration in Cardiotoxin-Induced Muscle Injury Models.* Int J Mol Sci, 2022. **23**(21).
- 70. Guardiola, O., et al., Induction of Acute Skeletal Muscle Regeneration by Cardiotoxin Injection. J Vis Exp, 2017(119).
- 71. Molina, T., P. Fabre, and N.A. Dumont, *Fibro-adipogenic progenitors in skeletal muscle homeostasis, regeneration and diseases.* Open Biol, 2021. **11**(12): p. 210110.
- 72. Biferali, B., et al., *Fibro-Adipogenic Progenitors Cross-Talk in Skeletal Muscle: The Social Network.* Front Physiol, 2019. **10**: p. 1074.
- 73. Tomasz Powrózek, D.P.-Z., Marcin Mazurek, Michael Ochieng Otieno, Mansur Rahnama-Hezavah, Teresa Małecka-Massalska TNF-α Induced Myotube Atrophy in C2C12 Cell Line Uncovers Putative Inflammatory-Related IncRNAs Mediating Muscle Wasting. International journal of molecular sciences, 2022.
- 74. Zhao, Q., Yang, S. T., Wang, J. J., Zhou, J., Xing, S. S., Shen, C. C., Wang, X. X., Yue, Y. X., Song, J., Chen, M., Wei, Y. Y., Zhou, Q. P., Dai, T., & Song, Y. H., TNF alpha inhibits myogenic differentiation of C2C12 cells through NF-κΒ

- activation and impairment of IGF-1 signaling pathway. Biochem Biophys Res Commun, 2015.
- 75. Ravi Chandran, T.J.K., Mirela Anghelina, and Sudha Agarwal, *Biomechanical signals upregulate myogenic gene induction in the presence or absence of inflammation*. American journal of physiology Cell physiology, 2007.
- 76. Madji Hounoum, B., et al., *NSC-34 Motor Neuron-Like Cells Are Unsuitable as Experimental Model for Glutamate-Mediated Excitotoxicity.* Front Cell Neurosci, 2016. **10**: p. 118.
- 77. Nango, H., et al., *Highly Efficient Conversion of Motor Neuron-Like NSC-34 Cells into Functional Motor Neurons by Prostaglandin E(2)*. Cells, 2020. **9**(7).
- 78. Menzies, F.M., et al., *Mitochondrial dysfunction in a cell culture model of familial amyotrophic lateral sclerosis*. Brain, 2002. **125**(Pt 7): p. 1522-33.
- 79. Crugnola, V., et al., *Mitochondrial respiratory chain dysfunction in muscle from patients with amyotrophic lateral sclerosis*. Arch Neurol, 2010. **67**(7): p. 849-54.
- 80. Li, H., S. Malhotra, and A. Kumar, *Nuclear factor-kappa B signaling in skeletal muscle atrophy.* J Mol Med (Berl), 2008. **86**(10): p. 1113-26.
- 81. Capitanio, D., et al., *Molecular signatures of amyotrophic lateral sclerosis disease* progression in hind and forelimb muscles of an SOD1(G93A) mouse model.

  Antioxid Redox Signal, 2012. **17**(10): p. 1333-50.
- 82. Guidotti, G., et al., *Tumor Necrosis Factor Alpha in Amyotrophic Lateral Sclerosis:*Friend or Foe? Cells, 2021. **10**(3).

- 83. Wong, M. and L.J. Martin, *Skeletal muscle-restricted expression of human SOD1* causes motor neuron degeneration in transgenic mice. Hum Mol Genet, 2010. **19**(11): p. 2284-302.
- 84. Martin, L.J. and M. Wong, *Skeletal Muscle-Restricted Expression of Human SOD1*in Transgenic Mice Causes a Fatal ALS-Like Syndrome. Front Neurol, 2020. **11**:
  p. 592851.
- 85. Kook, M.G., et al., Repeated intramuscular transplantations of hUCB-MSCs improves motor function and survival in the SOD1 G(93)A mice through activation of AMPK. Sci Rep, 2020. **10**(1): p. 1572.
- 86. Rando, A., et al., Intramuscular transplantation of bone marrow cells prolongs the lifespan of SOD1(G93A) mice and modulates expression of prognosis biomarkers of the disease. Stem Cell Res Ther, 2018. **9**(1): p. 90.
- 87. Zhou, B., et al., *Therapeutic potential of adipose-derived stem cell extracellular vesicles: from inflammation regulation to tissue repair.* Stem Cell Res Ther, 2024. **15**(1): p. 249.
- 88. Chen, W., et al., *Bidirectional roles of skeletal muscle fibro-adipogenic progenitors*in homeostasis and disease. Ageing Res Rev, 2022. **80**: p. 101682.
- 89. Theret, M., F.M.V. Rossi, and O. Contreras, *Evolving Roles of Muscle-Resident Fibro-Adipogenic Progenitors in Health, Regeneration, Neuromuscular Disorders, and Aging.* Front Physiol, 2021. **12**: p. 673404.